Západočeská univerzita v Plzni
Fakulta aplikovaných věd

MONITOROVÁNÍ KOMPOZITNÍCH KONSTRUKCÍ ZA POUŽITÍ PIEZOELEKTRICKÝCH SENZORŮ A AKTUÁTORŮ

Ing. Petr Sadílek

disertační práce
k získání akademického titulu doktor
v oboru Aplikovaná mechanika

Školitel: Ing. Robert Zemčík Ph.D.

Katedra: Katedra mechaniky

Plzeň 2013

University of West Bohemia in Pilsen
Faculty of Applied Sciences

STRUCTURAL HEALTH MONITORING OF COMPOSITES USING PIEZOELECTRIC PATCHES

Ing. Petr Sadílek

Dissertation thesis
submitted in candidacy for degree of Ph.D. in the field of
Applied Mechanics

Supervisor: Ing. Robert Zemčík Ph.D.

Department: Department of Mechanics

Pilsen 2013

Declaration

I certify that the work presented in this thesis is, to the best of my knowledge and belief, original, except as acknowledged in the text, and that the material has not been submitted, either in whole or in part, for a degree at this or any other university.

In Pilsen 20.2.2013

Acknowledgements

The author would like to acknowledge the people involved in completion of this work. This is to be done in his mother tongue for obvious reasons.

Na prvním místě bych chtěl poděkovat všem svým nejbližším a to zejména svým rodičům a mé přítelkyni Tereze, za dlouholetou a bezvýhradnou podporu při studiu. Další velké poděkování patří mému školiteli Ing. Robertu Zemčíkovi Ph.D. za příkladné vedení mého studia, věcným připomínkám v průběhu let a za notnou dávku trpělivosti. V neposlední řadě patří můj dík všem kolegům, kteří svými radami a náměty přispěli ke zkvalitnění této práce.

Petr Sadílek

Abstract

The aim of this thesis is to propose a methodology that is able to identify a damage on a composite structure using change of spectral characteristics. Use of such methodology may reveal damage of the structure without a need of visual inspection. Removal of inspection reduces costs and, moreover, the structure may be monitored continually. Use of piezoelectric materials was chosen for this approach, as they respond in real time.

In the first step, for deeper understanding of behavior of piezoelectric materials, one dimensional finite element with piezoelectric effect was developed. The mathematical model was implemented in MATLAB environment and compared on adequate problems to analytical solution.

Afterwards, experiments on undamaged and damaged structures were performed using two piezoelectric patches (one sensor and one actuator). Firstly, an aluminium grid structure was investigated for eigenfrequencies. An adequate finite element model was created to evaluate eigenfrequencies of the structure. Values from the experiments and FEM analysis differ in maximum 10% in the tracked values. Following experiments were performed on the same aluminium structure with predefined damages. Change of eigenfrequencies was clearly independent of the excitation signal, but localization of the damage was not possible without a deeper research.

After the experiments with isotropic structure, the behaviour of composite structures was tester during series of impact using chirp signal. Firstly, spectrum of eigenfrequencies was measured on undamaged unidirectional composite plate and then after each impact. Measurements of the plate with different level of damage were compared. Change of eigenfrequency spectrum corresponded with the growth of the crack. Following experiments were performed on sandwich materials where more different types of failures may occur. Set of sandwich beams (cut out from one plate made of two outer composite layers and a foam core) was investigated. Several samples were impacted in the same manner to get comparable results. All monitored samples showed similar change of frequency spectrum up to certain frequency.

Tested methodology was able to reveal the damage without a need of additional computations, but for identification of type of damage or its localization more extensive research beyond the scope of this work is necessary.

Abstrakt

Cílem této práce je navrhnout metodiku, s jejíž pomocí je možné identifikovat poškození na kompozitní struktuře v závislosti na změně spektrální charakteristiky. Použití takové metodologie může odhalit poškození konstrukce bez nutnosti vizuální kontroly. Odstranění kontroly snižuje náklady a navíc umožňuje nepřetržité monitorování dané konstrukce. Uvedený přístup využí- vá piezoelektrické materiály a jejich okamžitou odezvu. Pro detailnější poro- zumění chování piezoelektrických materiálů je nejprve vytvořen jednorozměr- ný konečněprvkový model s piezoelektrickým jevem. Numerický model je implementován do prostředí Matlabu a porovnán na odpovídajících problémech s analytickým řešením.

Následně jsou provedeny experimenty na nepoškozených konstrukcích za pomoci piezoelektrického senzoru a aktuátoru. Nejprve jsou zjištěny vlastní frekvence hliníkové sítě. Následně je vytvořen odpovídající konečněprvkový model. Hodnoty získané z experimentů a MKP modelu se liší maximálně o 10% u sledovaných hodnot. Následující experimenty jsou provedeny na stejné hliníkové konstrukci, s předdefinovanými místy poškození. Změna vlastních frekvencí je nezávislá na budícím signálu, ale místo poškození není možné bez hlubšího výzkumu identifikovat.

Po experimentech s isotropní konstrukcí je zkoumáno chování kompozitních struktur během rázových zkoušek. Za použití chirp signálu je nejprve změřeno spektrum vlastních frekvencí na nepoškozené jednosměrové kompo- zitové desce a následně po každém rázu. Měření z jednotlivých poškození jsou porovnána. Změna spektra vlastních frekvencí odpovídá růstu trhliny. Následující experimenty probíhají na sendvičových vzorcích, kde jsou možné různé druhy poškození. Sada sendvičových nosníků (vyříznutých z jedné desky) je podrobena stejné sekvenci rázů, pro dosažení porovnatelných výsled- ků. Všechny sledované vzorky vykazují do určité frekvence srovnatelnou změnu frekvenčního spektra.

Testovaná metodika dokáže odhalit poškození bez dalších přidaných výpočtů, ale pro identifikaci druhu poškození kompozitní konstrukce je nutný hlubší výzkum, který přesahuje rámec této práce.

Contents

Chapter 1

Introduction

As the demands on the ratio of stiffness and strength to weight of structures are rising, light-weight structures are nowadays necessary components in modern state-of-the-art products in all sorts of industries. Light modern superalloys are expensive and like conventional materials can sustain the same loading in all directions, even though the main loading may take effect in only one direction. To provide cheaper light-weight structure, new approach has to be applied. One of the solutions is usage of composite materials. Composite materials are mostly man-made materials made from one or more hard non-continuous component materials imbedded in a less hard continuous material with significantly different physical or chemical properties(at least 5% of each material in final product has to be present). The connection creates a new structure. The two categories of constituent materials are called matrix and reinforcement (at least one portion of each type is required). The matrix material surrounds and supports the reinforcement materials by maintaining their relative positions. The reinforcements transfer their special mechanical and physical properties to enhance the matrix properties. Together they produce material properties unavailable from the individual constituent materials. The wide combination of matrix and strengthening materials allows the designer of the product or structure to choose an optimum combination. By orienting the reinforcement most suitable design of composite material can be found. The physical properties of the new structure are generally not isotropic, but rather are typically orthotropic and therefore can be altered according to the assumed type and direction of loading unlike the isotropic materials.

Due to wide variety of materials to combine, their ratio or orientation of reinforcement, the diversity of composite materials is endless. Despite using same materials for the new composite material, each product can be manufactured in a different way and products therefore may have slightly different

properties. Therefore new approach has to be applied in processing, forming, controlling, maintenance and connecting. As composite materials are generally orthotropic, prediction of failure of material is more complicated then for isotropic materials (fiber and matrix failure as well as delamination may occur). Similar problems may be encountered when connecting composite parts to metal parts. This is done by gluing or screw connection. This results in more frequent check-ups or overdesigning of the whole part.

As both of mentioned solutions of keeping safety result in higher costs, alternative approach was needed to be implemented. Instead of frequent human check-ups an automated, computer based operated system has been developed.

The process of implementing a damage identification strategy is called structural health monitoring (SHM). This process consists of observation of a structure or mechanical system over a period of time using time-spaced measurements of specific features. Results from these measurements are analyzed to determine the current state of health. This is mainly used in aircraft industry ([29] or [6]) for necessary check-ups and in civil engineering ([9] or [13]) for monitoring bridges, dams and tall buildings as well as offshore installations.

For the first SHM in the industry may be considered check-ups that were realized on trains in the beginning of the 19th century. Railroad wheel-tappers have used the sound of a hammer striking the train wheel to evaluate if damage was present. Since than many techniques have been investigated for the purpose of detecting or even locating a failure. Most of them involve probing the system with a specific signal and searching for changes in the structure as that signal propagates through. Different approaches were developed using X-rays, strain gauges, displacement transducers, optic fiber sensors or lasers. Another approach to use is sending a signal, and observation of vibrational response such as eigenfrequencies. These responses may be compared to results predicted from a mathematical model and a damage may be predicted. Observation of a structure can be performed by different sensors, one of possible design are sensors made of piezoelectric materials. Piezoelectric materials change their shape in dependence to a voltage applied to their surface and this effect may be also used in finite element modelling. The first finite element implementation of the piezoelectric phenomenon came in 1970 by Allik and Hughes [2]. After that, many researches have 'equipped' the standard structural finite elements with the piezoelectric capability to simulate the piezoelectric effect. To simulate it, the similarity to the theory of thermo-elasticity was used in some cases. These early models concerned mainly 3D-solid elements, which are not suited for efficient analysis of laminated shell structures. For this reason,the approach changed

8

and in the recent years, the piezoelectric, beam, plate and shell elements are used more frequently. Cen et al. [5], for example, developed a four-node plate element for laminated structures based on first-order shear deformation theory while Lee et al. [12] introduced a nine-node assumed strain element allowing variable thickness, which is not possible for other elements. Hybrid laminated piezo plates are studied by Mitchell and Reddy [19] using higher-order shear deformation theory and layerwise approach for electric potential. Dynamic behavior of smart laminated plates using the layerwise approach are studied by Saravanos et al. [25]. Tzou et al. [31] investigate the control of smart conical shells using triangular finite elements. Kögl and Bucalem [11] introduced a MITC based element suitable for modelling of moderately thick sandwich smart structures. They stress the importance of quadratic variation of electric potential across the layer thickness to accurately model the electric field. There are more various finite element approaches summarized for example in the survey by Benjeddou [3]. Piefort and Preumont [16, 17] use piezoelectric materials for sensing and actuation in vibration and vibroacoustic control of plates modelled by Mindlin shell elements. Zhou et al. [32] study free vibrations of piezoelectric bimorphs by means of analytical solution. Heyliger [7] and later Heyliger and Wu [8] present exact analytical solution for laminated piezoelectric cylinder and sphere, respectively. Zemčík et al. [34] developed four-noded piezoelectric shell element and implemented into commercial code ANSYS.

There are only few research workplaces in the Czech Republic concentrated on piezoelectric materials, e.g. Czech Technical University in Prague [27], Technical University of Liberec [4] or University of West Bohemia in Pilsen [10]. They are mainly focused on mechatronic approach or identification of material properties.

The presented work is divided into several chapters. In the first part, fundamental problem of piezoelectricity is defined and a finite element model is composed for future analysis. The element proposed in this work is two-noded element and has two structural degrees of freedom (DOFs) at each node plus two DOFs for electric potential. Elements are considered as beams. The piezoelectric coupling is full and direct (i.e. non-iterative), and it is intended for the simulation of applied piezoelectric layers – patches. Equation of motion is derived in this work. On the basis of this equation a simulation of modal analysis is carried out. Work then focuses on an approach to piezoelectric bimorphs. Following work focuses on a model of aluminium beam with two piezoelectric patches, one on each side. Three types of testing are carried out. Matlab solution is compared to an experiment and to a MSC.Marc solution based on a similarity to thermal expansion problem.

The dissertation sets its goal to design and perform SHM of a compos-

ite structure with piezoelectric components for the identification of damage of the structure. To realize this, it was necessary to first verify a method of using piezoelectric patches on a simple structure. The second part of presented work therefore starts with investigation of a structure made of aluminium beams. Different approaches were examined using impact hammer and an accelerometer as well as piezoelectric actuator and sensor. The structure was also modelled in finite element method software MSC.Marc. Number of different failures was modelled in MSC.Marc and simulated and examined using piezoelectric patches on the structure. Results were mutually compared again, the method of testing was verified and prepared for further experiments. After verification of the isotropic aluminium structure, the same approach was applied to a composite plate. The actuating method used in previous experiments returned unsatisfactory results, modification of the method was not successful, therefore a different method of actuation was applied. Three composite plates of same geometric and material properties, with different range of damage were compared.

Afterwards a spectrum of eigenfrequencies of a new unidirectional composite plate was investigated. Series of impacts were performed, with measurement of the spectrum after each impact. The plate was gradually damaged, the crack was growing with repeated impacts, until the matrix was divided in two parts. Shifts of spectrum of eigenfrequencies was recorded and compared. Lastly a sandwich beam was subjected to series of impacts with parallel measurement of spectrum of eigenfrequencies. The beam was impacted with growing impacting energy, different types of damage occurred on the beam. Four similar specimens were tested in comparable manner. Shifts of spectrum of eigenfrequencies was recorded and compared.

Chapter 2

Piezoelectricity and SHM

The increasing requirements on structural performance call for the usage of embedded sensors and actuators, resulting in the construction of so-called smart or adaptive structures that can thus respond to loading conditions in real time. Each individual type of smart material has a different property which can be significantly altered, such as viscosity, volume, and conductivity. The property that can be altered influences what types of applications the smart material can be used for. One type of smart materials are piezoelectric materials. The piezoelectric effect describes the relation between mechanical stress and electrical voltage in solids. It is reversible: applied mechanical stress will generate voltage and applied voltage will change the shape of the solid by a small amount (see fig. 2.1). The big advantage of piezoelectric materials is that they may be controlled and they respond in real time. That is fundamental for controlling vibrations of a part. This enables for instance to suppress vibrations or to move frequency of a structure out of the range of eigenfrequencies. Piezoelectric materials also allow us to adapt the desired shape, provided that proper electronic control circuits are applied. Piezoelectric properties may also be used for i.e. structural health monitoring (SHM) of composite parts and failure prediction. That may eliminate scheduled inspections and improve efficiency and accuracy of maintenance. Using piezoelectric sensors also means continuous monitoring of structure, therefore it can predict failure before a scheduled inspection.

The first experimental demonstration of a connection between macroscopic piezoelectric phenomena and crystallographic structure was published in 1880 by Pierre and Jacques Curie. In the scientific society of that time, this effect was absolutely unique. In order to distinguish it form contact electricity and pyroelectricity, it was decided to call it as "piezoelectricity". But the Curie brothers did not predict that crystals would also exhibit the converse piezoelectric effect (stress in response to applied electric field). This

property was mathematically deduced by Lippmann in 1881. After only two years of interactive work in the European scientific community, the core of piezoelectric applications science was established. In the following 25 years (leading up to 1910), more work was done. The 20 natural crystal classes in which piezoelectric effects occur, and all 18 possible macroscopic piezo-electric coefficients were defined. However, no publicly visible or popular applications had been found for any of the piezoelectric crystals. First serious applications work on piezoelectric devices took place during World War I, when an ultrasonic submarine detector was improved. During World War II isolated national research groups worked on improved capacitor materials and a discovery of easily manufactured piezoelectric ceramics with astonishing performance characteristics was made. This started intense research and development into piezoelectric devices.

The reversibility enables us to divide piezo elements into two groups. In most cases, the same element can be used to perform either task.

- **Sensors** The first group - sensors - operates on the principle, that when piezoelectric material is deformed it induces a voltage across the material. Depending on the design of a sensor, different "modes" to load the piezoelectric element can be used: longitudinal, transversal and shear. As they convert mechanical energy into electrical energy, they are referred to as "generators". This can be used for example for sensing vibrations in real time.

- **Actuators** The second group are actuators. Voltage change corresponds to changes in the width of the crystal. In other words they convert electrical energy to mechanical energy. This is why they are referred to as "motors". Therefore mechanical or geometrical properties can be controlled in real time trough electrical circuit.

Thin piezo plates are called piezoelectric patches. When two piezoelectric patches are coupled, they create a biomorph. Piezoelectric bimorphs can produce flexural deformation significantly larger than the length or thickness deformation of the individual piezoelectric layers. Mostly, two basic possible arrangements of the piezoelectric elements are used. The first, called parallel, is coupled in a way that two piezoelectric elements are glued to a center conductor in an orientation that have the same poling direction, and the outer faces are coated with two conductive electrodes. The second order is known as series. In series two piezoelectric elements with opposite poling directions are directly bonded, and then covered by two surface electrodes. The application of an electric field across the two layers of the bimorph causes
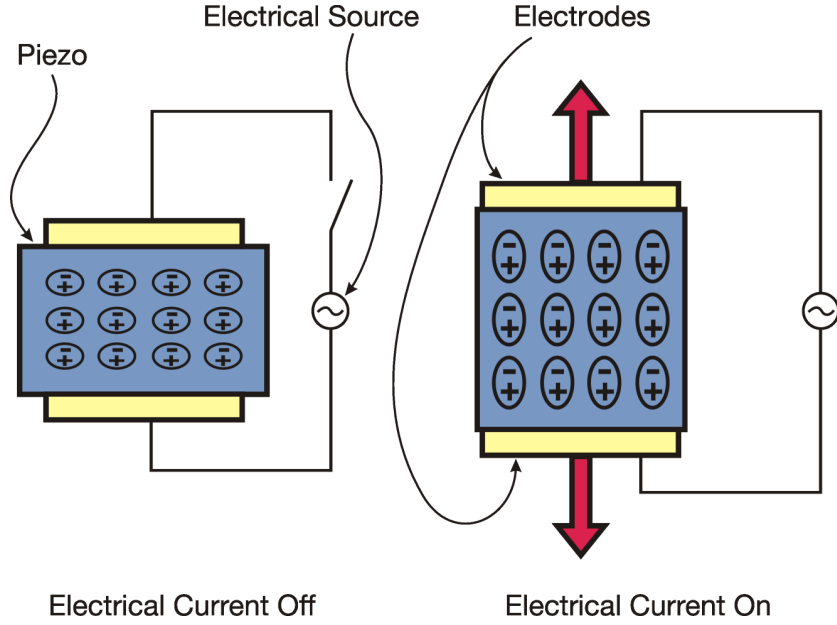
Fig. 2.1: Piezoeffect. Applying electric charge results in change of shape.

one layer to expand, while the other layer contracts. This is the working principle of bimorphs.

To design and use such connection of electrical and mechanical energy rationally, it is crucial to understand to the coupled electromechanical behaviors through effective modelling. Even though the research of piezoelectric bimorphs went though fast growth many of the existing models are either inaccurate or overcomplicated.

2.1   Constitutive equations

The theory of piezoelectric materials used in this work assumes symmetrical hexagonal piezoelectric structure – class $6mm$ (C_{6v}). Only the laminar piezoelectric effect (so-called d_{31} effect [30]) is considered, i.e., the material is polarized in the thickness direction.

The pure mechanical stress-strain law for each piezoelectric element is extended with piezoelectric coupling [33]. This can be then rewritten as

$$
\begin{aligned}
\boldsymbol{\sigma} &= \mathbf{C}\boldsymbol{\varepsilon} - \mathbf{e}^{\mathrm{T}}\mathbf{E}, \\
\mathbf{D} &= \mathbf{e}\boldsymbol{\varepsilon} + \boldsymbol{\epsilon}\mathbf{E},
\end{aligned}
\tag{2.1}
$$

where $\mathbf{D}$ is the vector of electric flux density, $\boldsymbol{\epsilon}$ is the dielectric permittivity matrix, $\mathbf{e}$ is the piezoelectric coefficient matrix and $\mathbf{E}$ is the electric field

vector.

The first of the two equations above is the well-known Hooke's relation between stress and strain extended by piezoelectric coupling.

The permittivity matrix $\boldsymbol{\epsilon}$ is defined as

$$\boldsymbol{\epsilon} = \begin{bmatrix} \epsilon_{11} & 0 & 0 \\ 0 & \epsilon_{22} & 0 \\ 0 & 0 & \epsilon_{33} \end{bmatrix} \tag{2.2}$$

and the piezoelectric matrix $\mathbf{e}$ as

$$\mathbf{e} = \begin{bmatrix} 0 & 0 & 0 & 0 & e_{15} & 0 \\ 0 & 0 & 0 & e_{24} & 0 & 0 \\ e_{31} & e_{32} & e_{33} & 0 & 0 & 0 \end{bmatrix} . \tag{2.3}$$

Chapter 3

Mathematical model of a beam element

3.1 Finite element definition

A beam element was defined and mathematically described in MATLAB software for purposes of finite element analysis. Loading only in one plane was considered and so was the deformation. Not only mechanical coupling is considered, but also piezoelectric coupling was taken in account for piezoelectric element. To a simple mechanical element one layer of piezomaterial on each side of the beam may be defined.

3.1.1 Simple mechanical element

The simple beam element is based on Euler-Bernoulli theory. It has two nodes with one deflection w_i and one rotational φ_i DOF at each node (see fig. 3.1). Let the deflection $w(x)$ across the length be approximated by the polynomial:

$$w(x) = a_0 + a_1 x + a_2 x^2 + a_3 x^3 = \mathbf{N}\mathbf{w} \ , \tag{3.1}$$

where $\mathbf{N}$ is matrix of approximation functions and the structural DOF vector is ordered as

$$\mathbf{w} = [w_n, \varphi_n, w_{n+1}, \varphi_{n+1}]^\mathrm{T} \ . \tag{3.2}$$

Then, the axial displacement can be written as

$$u(x, z) = z\varphi(x) = z\frac{\partial w}{\partial x} \tag{3.3}$$

and, consequently, the axial strain is

$$\varepsilon(x, z) = \frac{\partial u}{\partial x} = z\frac{\partial^2 w}{\partial x^2} = \mathbf{B}\mathbf{w} \ , \tag{3.4}$$

where $\mathbf{B}$ is strain-displacement matrix consisting of shape functions derivatives.
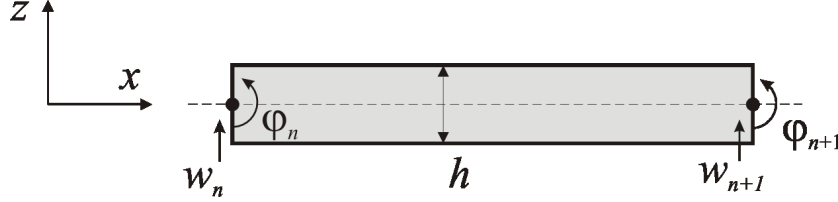
Fig. 3.1: Element geometry example. Supporting structure with its mechanical degrees of freedom).

3.1.2 Element with one piezoelectric layer

When a piezoelectric coupling is considered, electric field has to be taken into account. Let the electric field potential $\phi(x, z)$ be approximated by bi-linear function

$$\phi(x, z) = a_4 + a_5 x + a_6 z + a_7 xz . \tag{3.5}$$

Hence, the electric field intensity vector $\mathbf{E}$ is

$$\mathbf{E} = -\nabla\phi = \mathbf{\Phi}\boldsymbol{\phi} , \tag{3.6}$$

where $\mathbf{\Phi}$ is the electric field intensity-potential matrix and the electrical DOF vector is ordered as

$$\boldsymbol{\phi} = [\phi_n, \psi_n, \phi_{n+1}, \psi_{n+1}]^{\mathrm{T}} \tag{3.7}$$

with ϕ_i and ψ_i being the potential values on the lower and upper surfaces, respectively (see fig. 3.2).
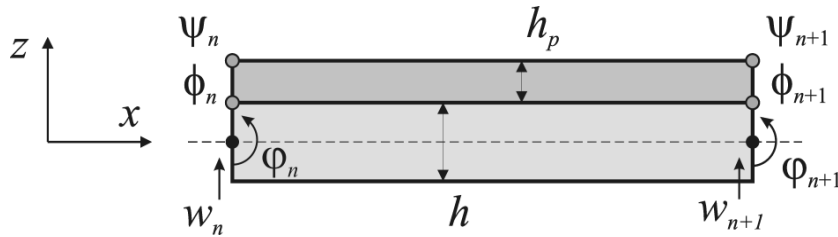
Fig. 3.2: Element geometry example. Piezo material (dark grey) and its supporting structure (light grey) sharing common nodes (degrees of freedom).

3.1.3 Element with two piezoelectric layers

To fully cover one-dimensional element two layers of piezo material were considered, one on each side. Electric field orientation of the second layer was considered with the respect to the first layer to reduce the amount of calculations (see fig. 3.3).
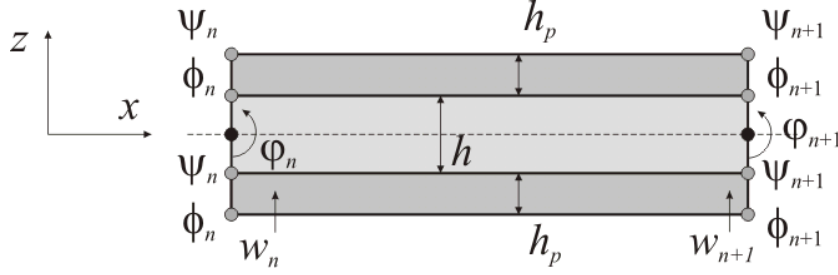
Fig. 3.3: Element geometry example. Piezo material on both sides (dark grey) and its supporting structure (light grey) sharing common nodes (degrees of freedom).

3.2 Variational principle

The equations of motion of a piezoelectric structure can be derived from the Lagrangian and the virtual work which must include both the mechanical and the electrical contributions. The potential energy density P of a piezoelectric material includes contributions from the strain energy and from the electrostatic energy, hence

$$P = \tfrac{1}{2}\boldsymbol{\sigma}^{\mathrm{T}}\boldsymbol{\varepsilon} - \tfrac{1}{2}\mathbf{D}^{\mathrm{T}}\mathbf{E} = \tfrac{1}{2}\boldsymbol{\varepsilon}^{\mathrm{T}}\mathbf{C}\boldsymbol{\varepsilon} - \mathbf{E}^{\mathrm{T}}\mathbf{e}\boldsymbol{\varepsilon} - \tfrac{1}{2}\mathbf{E}^{\mathrm{T}}\boldsymbol{\epsilon}\mathbf{E} \qquad (3.8)$$

while the kinetic energy density is simply

$$K = \tfrac{1}{2}\rho(\dot{w})^2 \ . \qquad (3.9)$$

Let us confine to case without external mechanical forces and electric charge. The Lagrangian can then be written in the form

$$L = \int_V (K - P)\,\mathrm{d}V \ . \qquad (3.10)$$

Using the variation principle, the condition

$$\delta L = 0 \qquad (3.11)$$

must be satisfied for any arbitrary variation of the displacements and electrical potentials, thus the resulting equations of motion with the assumptions made above are assembled as

$$
\begin{bmatrix} \mathbf{M}_{uu} & \mathbf{0} \\ \mathbf{0} & \mathbf{0} \end{bmatrix} \begin{bmatrix} \ddot{\mathbf{w}} \\ \ddot{\boldsymbol{\phi}} \end{bmatrix} + \begin{bmatrix} \mathbf{K}_{uu} & \mathbf{K}_{u\phi} \\ \mathbf{K}_{u\phi}^{\mathrm{T}} & \mathbf{K}_{\phi\phi} \end{bmatrix} \begin{bmatrix} \mathbf{w} \\ \boldsymbol{\phi} \end{bmatrix} = \begin{bmatrix} \mathbf{0} \\ \mathbf{0} \end{bmatrix} , \tag{3.12}
$$

for modal analysis, where the submatrices (element stiffness, piezoelectric coupling, capacitance and mass matrix) are

$$
\begin{aligned}
\mathbf{K}_{uu} &= \int_V \mathbf{B}^{\mathrm{T}} \mathbf{C} \mathbf{B} \, \mathrm{d}V & [4 \times 4] , \\
\mathbf{K}_{u\phi} &= -\int_V \mathbf{B}^{\mathrm{T}} \mathbf{e} \boldsymbol{\Phi} \, \mathrm{d}V & [4 \times 4] , \\
\mathbf{K}_{\phi\phi} &= -\int_V \boldsymbol{\Phi}^{\mathrm{T}} \boldsymbol{\epsilon} \boldsymbol{\Phi} \, \mathrm{d}V & [4 \times 4] , \\
\mathbf{M}_{uu} &= \int_V \rho \mathbf{N}^{\mathrm{T}} \mathbf{N} \, \mathrm{d}V & [4 \times 4] .
\end{aligned} \tag{3.13}
$$

For a case with external mechanical forces and electric charge the equation changes slightly to

$$
\begin{bmatrix} \mathbf{M}_{uu} & \mathbf{0} \\ \mathbf{0} & \mathbf{0} \end{bmatrix} \begin{bmatrix} \ddot{\mathbf{w}} \\ \ddot{\boldsymbol{\phi}} \end{bmatrix} + \begin{bmatrix} \mathbf{K}_{uu} & \mathbf{K}_{u\phi} \\ \mathbf{K}_{u\phi}^{\mathrm{T}} & \mathbf{K}_{\phi\phi} \end{bmatrix} \begin{bmatrix} \mathbf{w} \\ \boldsymbol{\phi} \end{bmatrix} = \begin{bmatrix} \mathbf{F} \\ \mathbf{Q} \end{bmatrix} , \tag{3.14}
$$

where the right-hand side vector consists of a vector of external forces $\mathbf{F}$ and of a vector of electrode electric charges $\mathbf{Q}$ [28].

Equation (3.14) may be for simplicity of the notation for all elements and nodes expressed as

$$
\mathbf{M}\ddot{\mathbf{x}} + \mathbf{K}\mathbf{x} = \overline{\mathbf{F}}, \tag{3.15}
$$

where $\mathbf{x}$ is vector of deflections, rotations and potential values on the lower and upper surfaces. Vector $\overline{\mathbf{F}}$ is vector of forces, moments and charges.

3.3 Modal analysis

In order to perform the modal analysis the system must be statically condensed. By expanding (3.12), two equations can be obtained in the following manner:

$$
\mathbf{M}_{uu}\ddot{\mathbf{w}} + \mathbf{K}_{uu}\mathbf{w} + \mathbf{K}_{u\phi}\boldsymbol{\phi} = \mathbf{0} \tag{3.16}
$$

$$\mathbf{K}_{u\phi}^{\mathrm{T}}\mathbf{w} + \mathbf{K}_{\phi\phi}\boldsymbol{\phi} = \mathbf{0}. \tag{3.17}$$

From (3.17) we can express ϕ as

$$\boldsymbol{\phi} = -\mathbf{K}_{\phi\phi}^{-1}\mathbf{K}_{u\phi}^{\mathrm{T}}\,\mathbf{w}. \tag{3.18}$$

Inserting (3.18) into (3.16) following equation is obtained:

$$\mathbf{M}_{uu}\ddot{\mathbf{w}} + \mathbf{K}_{uu}\mathbf{w} + \mathbf{K}_{u\phi} - \mathbf{K}_{\phi\phi}^{-1}\mathbf{K}_{u\phi}^{\mathrm{T}}\,\mathbf{w} = \mathbf{0}, \tag{3.19}$$

which can be simplified to

$$\mathbf{M}_{uu}\ddot{\mathbf{w}} + \left(\mathbf{K}_{uu} - \mathbf{K}_{u\phi}\mathbf{K}_{\phi\phi}^{-1}\mathbf{K}_{u\phi}^{\mathrm{T}}\right)\mathbf{w} = \mathbf{0} \tag{3.20}$$

Assumed solution can be expressed as

$$\mathbf{w} = \mathbf{W}\mathrm{e}^{-i\omega t} \tag{3.21}$$

which, when inserted into (3.20) leads to

$$\left(\lambda\mathbf{I} - \mathbf{A}\right)\mathbf{W} = \mathbf{0}. \tag{3.22}$$

The problem then reduces to the eigenvalue analysis of the matrix

$$\mathbf{A} = \mathbf{M}_{uu}^{-1}\left(\mathbf{K}_{uu} - \mathbf{K}_{u\phi}\mathbf{K}_{\phi\phi}^{-1}\mathbf{K}_{u\phi}^{\mathrm{T}}\right)\,. \tag{3.23}$$

Eigenfrequencies ω can be gained as a root of eigenvalues λ. Eigenvectors $\mathbf{W}$ represent deflections and rotations of particular nodes.

In the model of a simple beam (without piezo material), the expression $\mathbf{K}_{u\phi}\mathbf{K}_{\phi\phi}^{-1}\mathbf{K}_{u\phi}^{\mathrm{T}}$ is a zero matrix.

The corresponding values for electrical DOFs can be retrieved using (3.18). The set of equations in (3.12) for single element is expanded accordingly in finite element analysis when joining element with common nodes (see fig. 3.3).

3.4 Static analysis

Let us consider piezoelectric patch with static loading and with two faces with applied voltage. Then (3.14) simplifies to

$$\begin{bmatrix} \mathbf{K}_{uu} & \mathbf{K}_{u\phi} \\ \mathbf{K}_{u\phi}^{\mathrm{T}} & \mathbf{K}_{\phi\phi} \end{bmatrix} \begin{bmatrix} \mathbf{w} \\ \boldsymbol{\phi} \end{bmatrix} = \begin{bmatrix} \mathbf{F} \\ \mathbf{Q} \end{bmatrix}, \tag{3.24}$$

where ϕ and $\mathbf{F}$ are known. But it makes (3.24) equation with unknowns in different vectors. Therefore (3.24) has to be rewritten into an equation with

unknown variables in one vector. Expanding (3.24) two equations can be obtained in the same way as (3.16) and (3.17) were gained:

$$\mathbf{K}_{uu}\mathbf{w} + \mathbf{K}_{u\phi}\boldsymbol{\phi} = \mathbf{F}. \tag{3.25}$$

$$\mathbf{K}_{u\phi}^{\mathrm{T}}\mathbf{w} + \mathbf{K}_{\phi\phi}\boldsymbol{\phi} = \mathbf{Q}. \tag{3.26}$$

It arises from (3.26) that

$$\boldsymbol{\phi} = -\mathbf{K}_{\phi\phi}^{-1}\mathbf{K}_{u\phi}^{\mathrm{T}}\ \mathbf{w} + \mathbf{K}_{\phi\phi}^{-1}\mathbf{Q}. \tag{3.27}$$

Inserting (3.27) into (3.25) implies

$$\mathbf{F} = \left(\mathbf{K}_{uu} - \mathbf{K}_{u\phi}\mathbf{K}_{\phi\phi}^{-1}\mathbf{K}_{u\phi}^{\mathrm{T}}\right)\mathbf{w} + \mathbf{K}_{u\phi}\mathbf{K}_{\phi\phi}^{-1}\mathbf{Q}. \tag{3.28}$$

This can be expressed as

$$\begin{bmatrix} \mathbf{K}_{uu} - \mathbf{K}_{u\phi}\mathbf{K}_{\phi\phi}^{-1}\mathbf{K}_{u\phi}^{\mathrm{T}} & \mathbf{K}_{u\phi}\mathbf{K}_{\phi\phi}^{-1} \\ -\mathbf{K}_{\phi\phi}^{-1}\mathbf{K}_{u\phi}^{\mathrm{T}} & \mathbf{K}_{\phi\phi}^{-1} \end{bmatrix} \begin{bmatrix} \mathbf{w} \\ \mathbf{Q} \end{bmatrix} = \begin{bmatrix} \mathbf{F} \\ \boldsymbol{\phi} \end{bmatrix}, \tag{3.29}$$

which, when we search for deflections and charges, leads to

$$\begin{bmatrix} \mathbf{w} \\ \mathbf{Q} \end{bmatrix} = \begin{bmatrix} \mathbf{K}_{uu} - \mathbf{K}_{u\phi}\mathbf{K}_{\phi\phi}^{-1}\mathbf{K}_{u\phi}^{\mathrm{T}} & \mathbf{K}_{u\phi}\mathbf{K}_{\phi\phi}^{-1} \\ -\mathbf{K}_{\phi\phi}^{-1}\mathbf{K}_{u\phi}^{\mathrm{T}} & \mathbf{K}_{\phi\phi}^{-1} \end{bmatrix}^{-1} \begin{bmatrix} \mathbf{F} \\ \boldsymbol{\phi} \end{bmatrix}, \tag{3.30}$$

For other combination of known and unknown inputs the set of equations must be solved out with matrix operations such as Gaussian elimination and redistributing unknowns into one vector in order to create a vector of unknowns on one side of the equation.

3.5 Transient analysis

In the text above (section 3.4) all assumptions were made regardless of time behavior. Transient analysis is a technique used to determine the response of a structure under a time-varying load. When taking force dependent on time, then regarding (3.14) we can write

$$\mathbf{M}_{uu}\ddot{\mathbf{w}} + \mathbf{K}_{uu}\mathbf{w} + \mathbf{K}_{u\phi}\boldsymbol{\phi} = \mathbf{F}. \tag{3.31}$$

This can be rewritten as

$$\ddot{\mathbf{w}} = \mathbf{M}_{uu}^{-1}\left(\mathbf{F} - \mathbf{K}_{uu}\mathbf{w} - \mathbf{K}_{u\phi}\boldsymbol{\phi}\right). \tag{3.32}$$

Different methods need to be used to solve eq. (3.32), for example the shooting method, multiple shooting or global methods like finite differences or collocation methods. Let us show solution through finite-difference method. These are numerical methods for approximating the solutions to differential equations using finite difference equations to approximate derivatives. Finite-difference methods approximate the solutions of differential equations by replacing derivative expressions with approximately equivalent difference quotients. Because the first derivative of a function f is, by definition,

$$f'(x) = \lim_{h \to 0} \frac{f(x+h) - f(x)}{h} \tag{3.33}$$

then a approximation for that derivative would be

$$f'(x) \approx \frac{f(x+h) - f(x)}{h} \tag{3.34}$$

For our case the variable is time and the derivative is structural DOF vector. Hence central differences may be used as

$$\dot{\mathbf{w}}(t_{n+1}) = \frac{\mathbf{w}(t_{n+1}) - \mathbf{w}(t_n)}{\triangle t} \tag{3.35}$$

and

$$\dot{\mathbf{w}}(t_{n+2}) = \frac{\mathbf{w}(t_{n+2}) - \mathbf{w}(t_{n+1})}{\triangle t}, \tag{3.36}$$

where $\mathbf{w}(t_n)$ is a vector of deflections and rotations of nodes in the time step n and $\triangle t$ is a difference between time step n and time step $n+1$.

Using central differences, eq. (3.32) can be derived into following:

$$\ddot{\mathbf{w}}(t_{n+2}) = \frac{\dot{\mathbf{w}}(t_{n+2}) - \dot{\mathbf{w}}(t_{n+1})}{\triangle t} = \mathbf{M}_{uu}^{-1} \left(\mathbf{F}(t_n) - \mathbf{K}_{uu}\mathbf{w}(t_n) - \mathbf{K}_{u\phi}\boldsymbol{\phi}(t_n) \right) \tag{3.37}$$

$$\ddot{\mathbf{w}}(t_{n+2}) = \frac{\mathbf{w}(t_{n+2}) - \mathbf{w}(t_{n+1})}{\triangle t} - \frac{\mathbf{w}(t_{n+1}) - \mathbf{w}(t_n)}{\triangle t} = \\ = \triangle t \mathbf{M}_{uu}^{-1} \left(\mathbf{F}(t_n) - \mathbf{K}_{uu}\mathbf{w}(t_n) - \mathbf{K}_{u\phi}\boldsymbol{\phi}(t_n) \right) \tag{3.38}$$

$$\mathbf{w}(t_{n+2}) = 2\mathbf{w}(t_{n+1}) - \mathbf{w}(t_n) - \triangle t^2 \mathbf{M}_{uu}^{-1} \left(\mathbf{F}(t_n) - \mathbf{K}_{uu}\mathbf{w}(t_n) - \mathbf{K}_{u\phi}\boldsymbol{\phi}(t_n) \right). \tag{3.39}$$

Equation (3.39) serves the purpose of finding $\mathbf{w}(t_{n+2})$ when $\phi(t)$ and $\mathbf{F}(t)$ progressions are known. It is necessary ti know boundary values $\mathbf{w}(t_0)$ and $\mathbf{w}(t_1)$.

Chapter 4

Numerical tests of a beam element

Several types of analyses were carried out using Matlab code and different types of loading were concerned. A finite element model was created in the software. For simplifying of the problem, only two piezolayers may be defined in the programme. They may be of a different thickness or a different position, but all tests with two piezolayers were computed for collocated piezolayers with same geometric properties and opposite polarization. The matrices for each element are solved out and added to the global mass matrix $\mathbf{M}$ and stiffness matrix $\mathbf{K}$ in the main programme. For elements without piezolayer the zero rows and columns of the stiffness matrix and the adequate elements of the derived vector of displacement has to be taken out to prevent singularity.

Different problems were modelled and examined

- **Modal analysis of a beam**

  Static condensation is performed in the same manner as shown in section 3.3. Eigenvalues and eigenvectors (see eq. (3.22)) are gained in this step, consequently eigenfrequencies are solved out from eigenvalues.

- **Static bimorph test**

  For bimorph test only static problems were solved, therefore the mass matrix was not taken into account. Depending on type of the task two approaches were used, clamping at one end is considered in both cases.

  - *Actuator test*

    Voltage is applied, deflections, rotations and charges are solved out.

- *Sensor test*

    In this case only deflection of a free end was defined and induced voltage was computed.

- **Hybrid beam with two piezoelectric patches**

    Three types of analyses of aluminium beam were carried out using Matlab code.

    Modal analysis was performed in the same way as modal analysis described above through static condensation.

    According to the actuator test above, analysis with statical loading induced by change of voltage was performed.

    For the third case of harmonic loading a new subroutine was created. This subroutine uses central differences in the time domain (as in eq. (3.39)). Voltage changes in time in this subroutine. Two outputs are shown in this work, namely the oscillation of a free end through time and the oscillation of the whole beam through time.

All models were based on equations described in text above. All test were based on (3.14) with changes depending on geometry or boundary conditions.

4.1 Modal analysis of a beam

Firstly a basic beam model was created to verify behavior of proposed element through a modal analysis of a simple clamped cantilever beam [35]. The test concerned simple steel cantilever beam clamped at $x = 0$. Equation (3.23) was used to find eigenvalues and eigenvectors. As deflections and rotations of nodes in the clamping are zero, this was used for the first node as a zero rotation $\varphi(0) = \varphi_1 = 0$ and deflection $w(0) = w_1 = 0$ for boundary condition.

Up to three lowest eigenfrequencies were obtained for total length $l = 1\,\mathrm{m}$. The thickness was $h = 0.01\,\mathrm{m}$, width $b = 0.1\,\mathrm{m}$ and material properties are shown in tab. 4.1. Arrangement of the test is shown in fig. 4.1.

Afterwards a sensitivity analysis of the Matlab solution was performed, modelled with 1, 2, 4, 8 and 16 elements, respectively. The resulting values of obtained eigenfrequencies are summarized in tab. 4.2.

Very good convergence is obvious from the results. The shapes for the first three eigenmodes are shown in fig. 4.2.

As the model showed good convergence, similar analysis was performed with a piezoelectric patch of thickness $h_p = 1\,\mathrm{mm}$ through the whole length of the steel beam. The lower surface of the patch was grounded, i.e. $\phi_i = 0\,\mathrm{V}$,
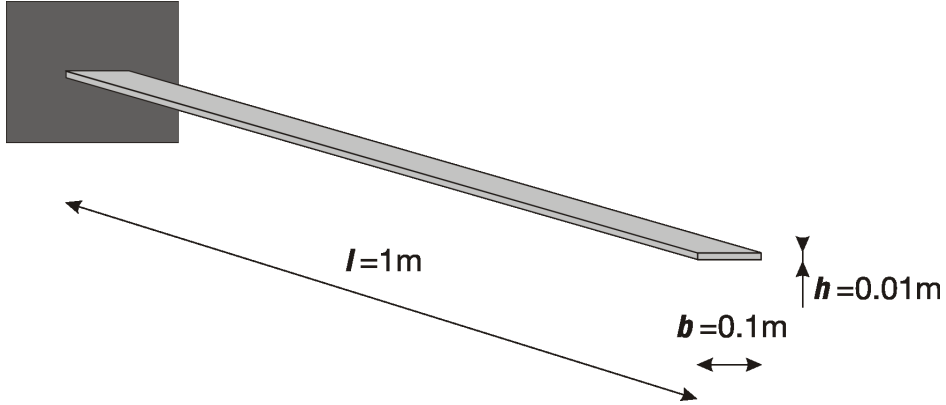
Fig. 4.1: Model for modal analysis.

Tab. 4.1: Material properties.

Material property	Steel	Piezo
E [GPa]	210	2
ρ [kg/m^3]	7850	1800
e_{31} [C/m^2]	-	0.044
$\epsilon_{11} = \epsilon_{33}$ [nF/m]	-	1.062

while the upper surface ψ_i was left open (for details see eq. (3.7)). The piezoelectric properties are again in tab. 4.1. Similar results were obtained, again with a very good convergence. (See tab. 4.3.)

The shapes for the first three eigenmodes are shown in fig. 4.3 – fig. 4.5. Coloured legend shows voltage induced by bending. More elements were used for finer graphical representation.

Tab. 4.2: Summary of lowest eigenfrequencies for steel beam.

Elements	ω_1 [Hz]	ω_2 [Hz]	ω_3 [Hz]
1	8.39	82.71	-
2	8.36	52.81	178.60
4	8.36	52.42	147.74
8	8.36	52.37	146.70
16	8.36	52.36	146.61
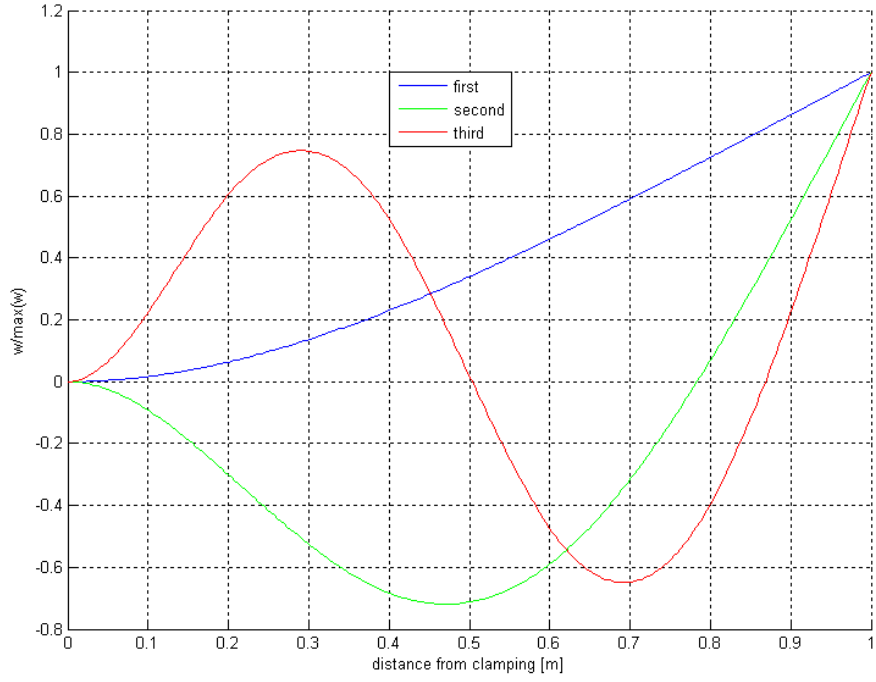
Fig. 4.2: First three normalized eigenmodes for beam made of 16 elements.

Tab. 4.3: Summary of lowest eigenfrequencies for hybrid steel/piezo beam.

Elements	ω_1 [Hz]	ω_2 [Hz]	ω_3 [Hz]
1	8.35	82.29	-
2	8.32	52.53	177.69
4	8.31	52.16	147.00
8	8.31	52.10	146.96
16	8.31	52.10	145.88
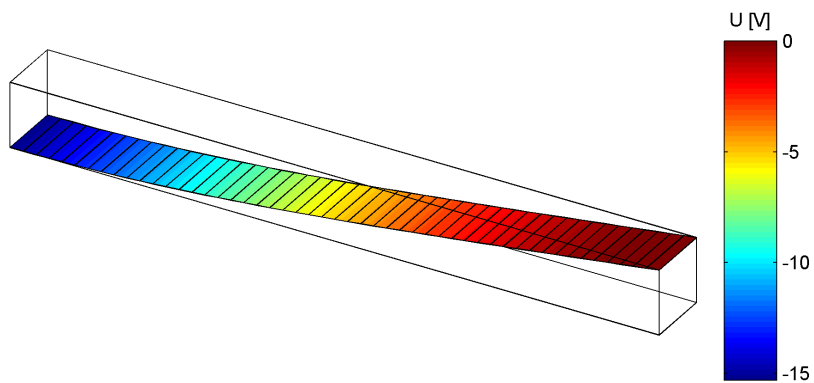
Fig. 4.3: First eigenmode with induced voltage.
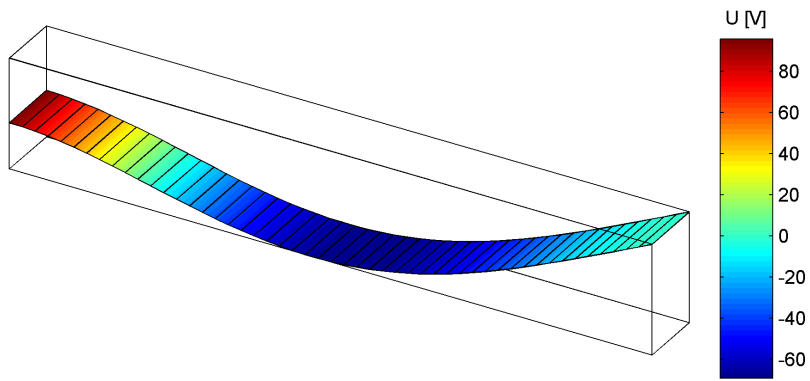
Fig. 4.4: Second eigenmode with induced voltage.
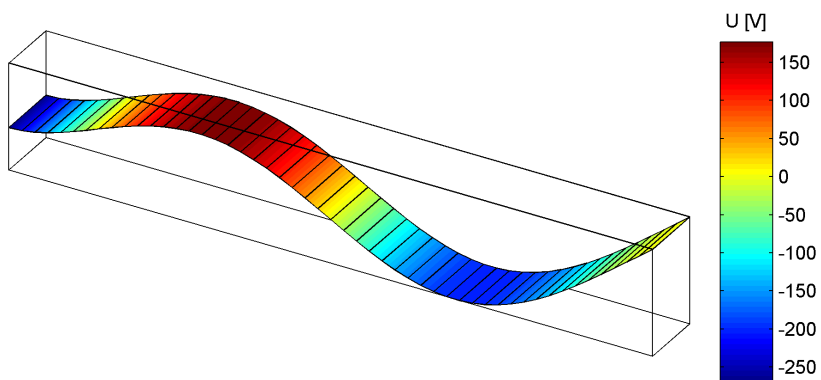
Fig. 4.5: Third eigenmode with induced voltage.

4.2 Static bimorph test

Two types of sensitivity analyses were carried out [21]. Both cases considered cantilever beam clamped at $x = 0$, which means $w(0) = 0$ and $\varphi(0) = 0$ as described above. Beam was made of two piezoelectric patches of same thickness $h = 0.0005\,\text{m}$ and width $b = 0.01\,\text{m}$. Total length was $l = 0.1\,\text{m}$. Other material properties were same as shown in tab. 4.1. PVDF (polyvynilidene fluorid) piezoelectric patch was used. As it was said in Introduction, when a piezomaterial is loaded with voltage, it extends or shortens itself depending on polarity. Bimorph in this test is composed of two layers with opposite polarity but parallel electrical circuit connection. The polarities are e_{31}^A for upper layer and e_{31}^B for lower layer, this means

$$e_{31}^A = -e_{31}^B. \tag{4.1}$$
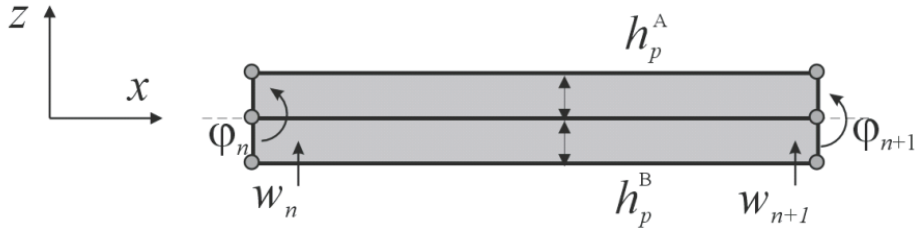
Fig. 4.6: Bimorph element geometry. Two coupled piezoelectric patches.

4.2.1 Actuator test

The bimorph actuator test (cantilever beam) with two piezoelectric layers (fig. 4.6) having opposite polarities is further analyzed. Two piezoelectric patches without external loads, with two grounded faces and two faces with applied voltage were modelled.

For graphical representation see fig. 4.7. Opposite polarity results in bending of the beam. (Similar principle can be found in temperature problem with a bimetallic beam.)

Using constant voltage $U = 1\,\text{V}$ ($\phi_i = 0$ and $\psi_i = U = 1\,\text{V}$) applied across the thickness the analysis yields tip displacement $w(l) = 3.30 \times 10^{-7}$ m (see fig. 4.8) for all number of elements used, whereas the corresponding simplified analytical solution using the Euler-Bernoulli theory is [18]

$$w(l) = \frac{3}{2}\frac{e_{31}Ul^2}{Eh^2} = 3.45 \times 10^{-7}\text{m}. \tag{4.2}$$
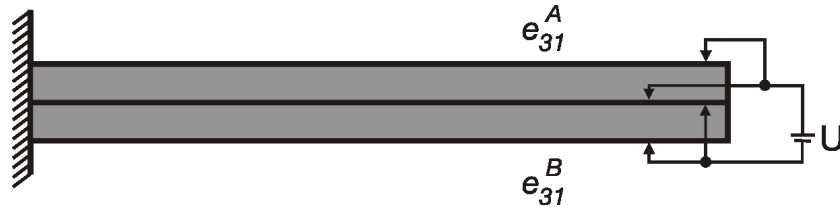
Fig. 4.7: Beam in actuator test made of two piezoelectric patches with opposite polarities.
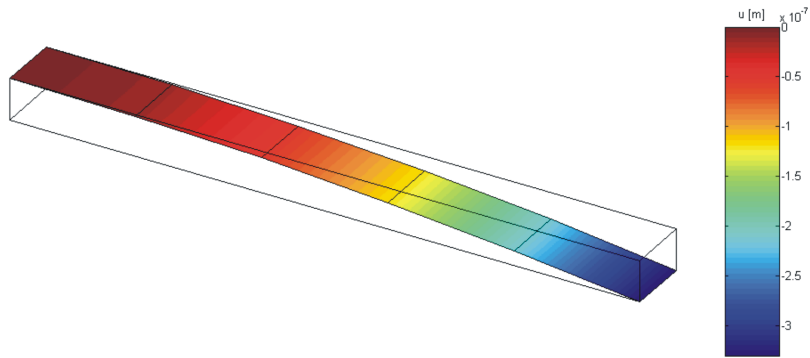
Fig. 4.8: Computed deflection.

As can be seen in tab. 4.4, model showed not only very good convergence but also results close to simplified analytical solution.

4.2.2 Sensor test

In the second case the free end of the hybrid beam was displaced of $w(l) = 0.01\,\mathrm{m}$. Sensitivity analysis was carried out to find out induced voltage. Highest voltage was induced at the clamped end (see fig. 4.10) because of highest bending moment. Sensitivity analysis was carried out for five models to see influence of number of elements on the result. As can be seen in tab. 4.5 the results are of a good convergence.

4.3 Aluminium beam with two piezoelectric patches

The results from previous element model (section 4.2) were used for creating a finite element model of an aluminium beam and two collocated piezoelectric

Tab. 4.4: Results of sensitivity analysis of actuator test.

Number of elements	Deflection [m] $\times 10^{-7}$
1	3.30
2	3.30
4	3.30
8	3.30
16	3.30
Analytical	3.45
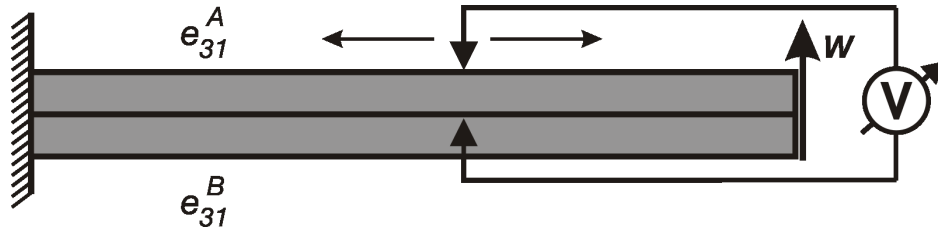
Fig. 4.9: Beam in sensor test. Curvature causes voltage altering along the beam.

patches [22]. The beam was clamped on one end (see fig. 4.11) with total length $l_b = 500$ mm, width $b_b = 30$ mm and thickness $h_b = 3$ mm. The dimensions of the piezoelectric patches were of a length $l = 50$ mm, same width as the beam and thickness $h = 0.3$ mm. Model of beam was made of 50 element of which 10 were considered to be covered with piezoelectric patches. Loading of the piezoelectric patches causes contraction (or extension - depending on polarization of loading) of the patches. As they are rigidly fixed to the aluminium beam, the patches force the beam to deform. For mentioned case of opposite polarity the beam bends up and down.

Three types of analyses of aluminium beam were carried out. The first test was modal analysis. The other two were based on loading the piezo-

Tab. 4.5: Results of sensitivity analysis of sensor test.

Number of elements	Maximum induced voltage [V]
1	155.3595
2	155.3595
4	155.3496
8	155.3317
16	155.2968
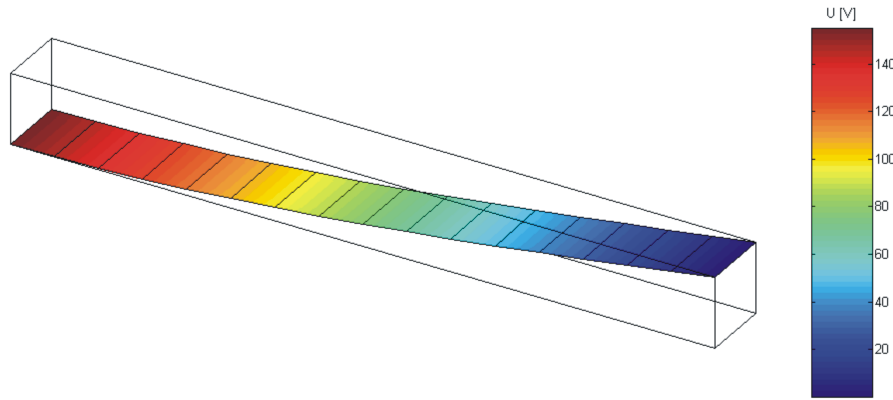
Fig. 4.10: Displaced free end and induced voltage.
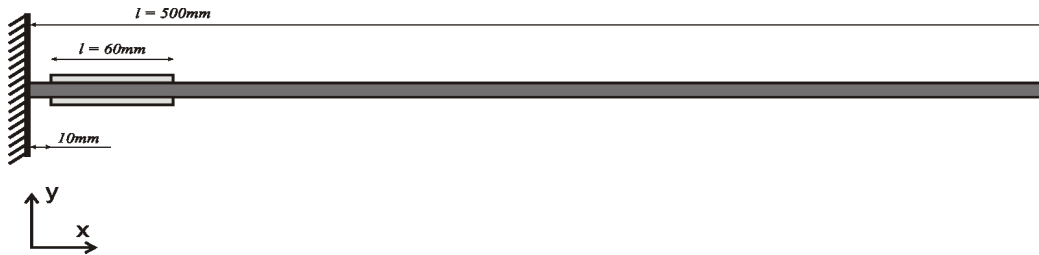
Fig. 4.11: Schema of location of piezoelectric patches on the beam.

electric patches with voltage. Firstly with statical loading and then with harmonic waveform.

An experiment was carried out previously by Plundrich [18] with an aluminium beam and two collocated piezoelectric patches. Plundrich in his work also created a numerical model in MSC.Marc software, based on analogy with thermal expansion. Geometry and material properties of following analysis correspond to model examined by Plundrich, the beam was of sam geometry. The dimensions of the piezoelectric patches were length $l = 61\,\mathrm{mm}$, width $b = 35\,\mathrm{mm}$ and thickness $h = 0.3\,\mathrm{m}$. From the total length of the piezoelectric patch only 50 mm may be considered as active (see fig. 4.12). This corresponds to the Matlab model created. Materials used also correspond with materials used for Matlab simulation.

The material properties considered for piezoelectric patch P-876.A12 (fig. 4.12) and aluminium beam are shown in tab. 4.6.

The patches were loaded by an electric signal $\phi = \Phi \sin(\omega t)$, where Φ is voltage amplitude.

This caused deformation of the piezo actuators and consequently this in-

Fig. 4.12: Two piezoelectric patches P-876.A12 used in experiment.

Tab. 4.6: Properties of used materials.

Property	E [GPa]	μ [-]	ρ [kg/m^3]	e_{31} [Cm^{-2}]
Aluminium	70.0	0.33	2670	-
P-876.A12	61.8	0.30	7760	5.6

duced oscillation of the free end. Deflection magnitude was measured through a laser equipment (fig. 4.13). Plundrich compared his results with finite elements method in MSC.Marc. He was also searching for eigenfrequencies. The two lowest eigenfrequencies measured were f_1=9.5 Hz and f_2=59 Hz.

4.3.1 Modal analysis

The first test was the modal analysis. Equation (3.23) was used again as in one of the previous chapters (section 4.1). But this time the two piezoelectric patches were taken into account. The two lowest eigenfrequencies found were $f_1 = 9.9256$ Hz and $f_2 = 62.2024$ Hz. As Plundrich in his work mentions only two lowest eigenfrequencies of the beam, higher frequencies were not searched for. As can be seen close parity was found to results obtained by Plundrich.
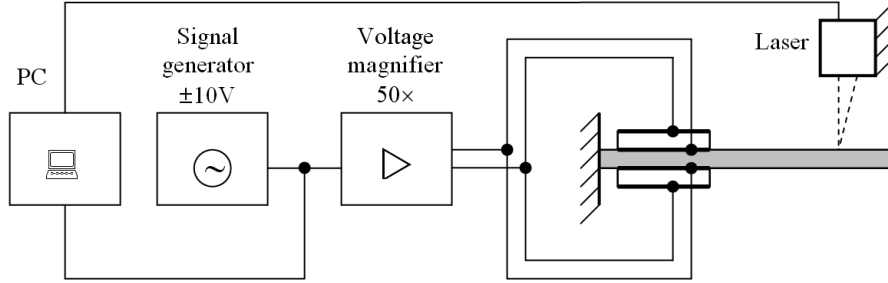
Fig. 4.13: Diagram of experiment arrangement [18].

4.3.2 Statical loading

The second test in Matlab focused on verifying the model with static loading. The beam was loaded and the deflection of the free end was found. Voltage of magnitude of $\phi = 0.7\,\mathrm{V}$ magnified 50 times was considered. Computation of the deflection uses relation from equation (3.30). Mentioned loading resulted in deflection (see fig. 4.14) of the free end of

$$w(l) = 6.6 \times 10^{-5}\mathrm{m}. \tag{4.3}$$
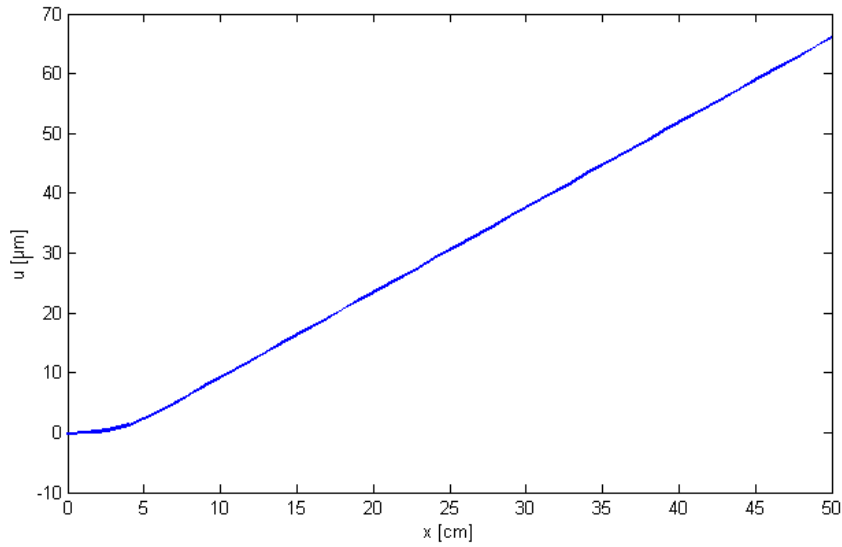
Fig. 4.14: Deflection of the beam with static loading.

4.3.3 Harmonic loading

The experiment realized by Plundrich was compared with the numerical solution in Matlab. The model of the beam was separately loaded by harmonic waveforms close to first eigenfrequency. Twenty tests with different voltage (see tab. 4.7) were performed in the same way as in experiment. The deviation between the frequencies corresponded to a deviation of about 1Hz.

Central differences in the time domain were used. Material damping was neglected. For graphical interpretation see fig. 4.15 and fig. 4.16.
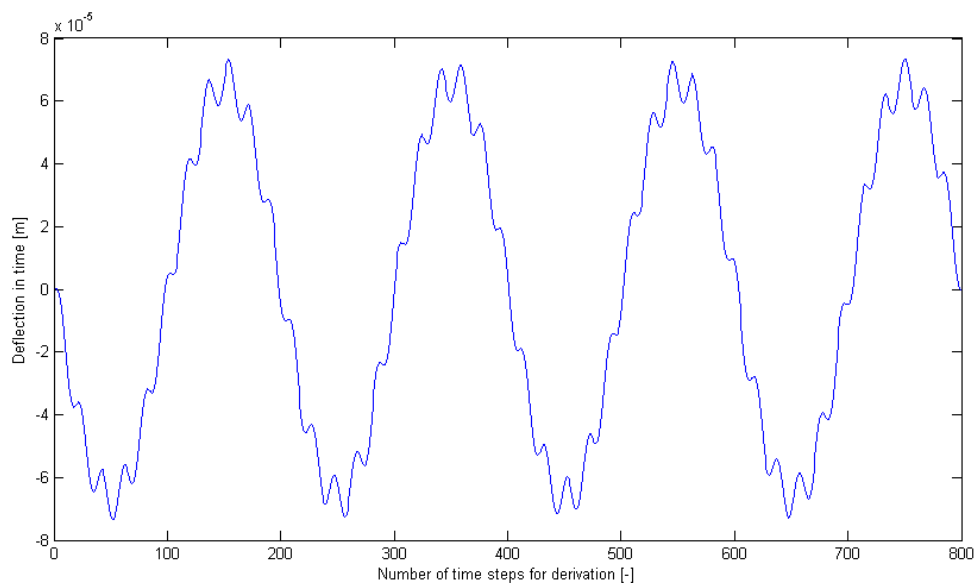
Fig. 4.15: Free end oscillation in time for frequency 0.97 Hz.

Comparison of Matlab results to experiment and results from MSC.Marc can be found in tab. 4.7. The results show similarity in most cases. Difference may be seen around eigenfrequency, as slightly different eigenfrequencies were already gained for Matlab model and in experiment. There may be several causes for the difference between results and the experiment. Besides inaccurate material properties corresponding to the beam used and integration method used, material damping was not taken into account and also preciseness of piezolayer may be impeached as Matlab model used only one dimensional model. It is also to notice, that the quasi static frequency of 0.97 Hz corresponds with result of equation 4.3.

Tab. 4.7: Comparison of aluminium beam amplitudes induced by harmonic waveform.

Frequency [Hz]	Voltage Φ [V]	Experiment [mm]	MSC.Marc [mm]	Matlab [mm]
0.97	35.0	0.10	0.06	0.07
1.95	42.5	0.10	0.07	0.10
2.81	31.0	0.11	0.05	0.08
4.02	43.5	0.13	0.09	0.14
4.88	41.0	0.16	0.09	0.15
5.85	43.5	0.17	0.11	0.20
6.96	40.5	0.19	0.13	0.24
7.93	34.5	0.21	0.16	0.30
8.67	35.5	0.30	0.22	0.43
9.76	41.5	5.50	0.64	1.40
10.74	36.5	0.41	1.31	1.00
11.59	33.5	0.28	0.29	0.64
12.45	29.0	0.18	0.14	0.32
13.55	30.0	0.12	0.09	0.22
14.52	40.5	0.10	0.09	0.22
15.62	32.0	0.07	0.05	0.14
16.60	29.0	0.06	0.04	0.11
17.70	33.5	0.05	0.04	0.11
18.43	33.0	0.04	0.04	0.10
19.77	38.0	0.06	0.39	0.10
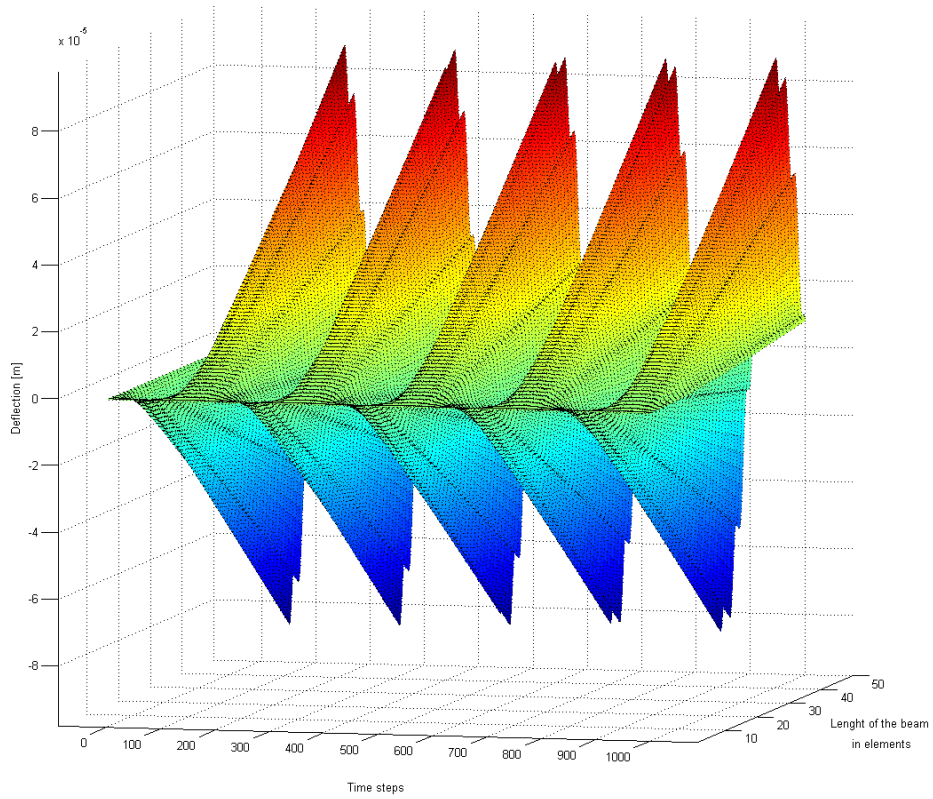
Fig. 4.16: Oscillation in time for frequency 5.85 Hz.
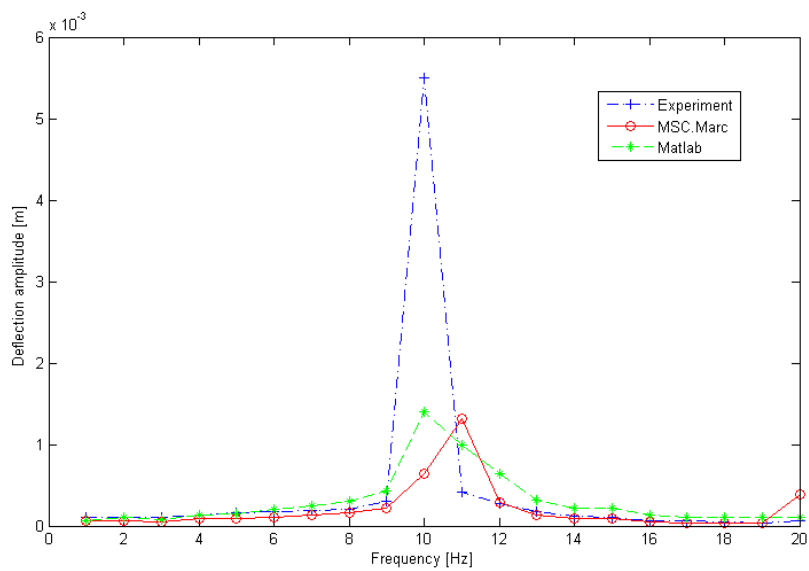
Fig. 4.17: Graphical comparison of maximal displacement tip at end induced by harmonic loading.

Chapter 5

Structural health monitoring of aluminium structure

As mentioned in introduction, piezoelectric patches can be used not only for sensing a structure, but also for excitation. With these means, shifts of eigenfrequencies can be then recognized using similar methodology. To understand a behavior of damaged structures and change of modal characteristics (e.g. shift of eigenfrequencies) an extended research was necessary.

Following work therefore focused on a more complex structure (see fig. 5.1). This structure was meant to be a ground for further investigation with a possible change to a more or less complicated build, depending on focus of the research. A structure made of aluminium was used for the first experiments, as an isotropic material was desirable for simplicity and eventual recheck. Used material also fulfilled requirements of easy possible rework.

Aluminium beams with thickness of 3 mm and width of 20 mm were prepared. As distance between connecting parts of 200 mm was desired, beams with total length of 220 mm were cut. To define the correct distance of 200 mm, beams were marked (see fig. 5.4). Aluminium connectors, steel screws and steel nuts were used for connecting. Connection part (see fig. 5.3) was designed to avoid shifts and rotation of the beams. The geometry of the connector was also designed in this way to allow creating different shaped structures in case a simpler or more complex design was desirable. The connecting part was also designed in this shape in order to fulfill requirements for using composite beams and their connecting without the need of gluing the structure.

The structure was loose hanged on a frame and slightly damped with rubber lines (see fig. 5.1). Two different configurations were examined, a symmetrical one with 17 beams and an asymmetrical one with 16 beams. Both configurations were examined with several approaches.
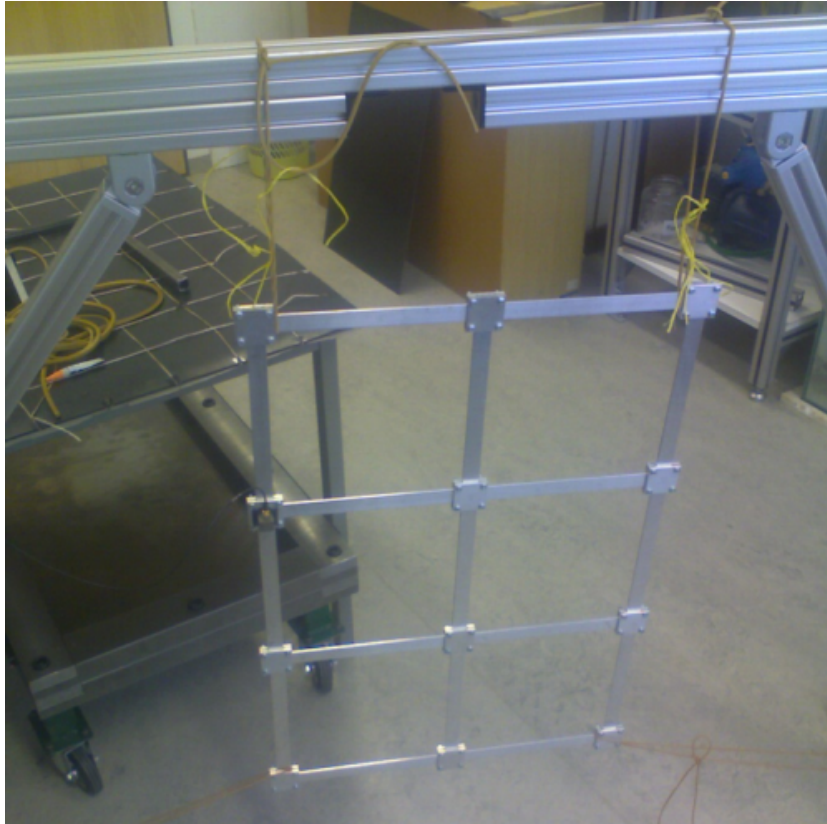
Fig. 5.1: Experiment arrangement in symmetrical configuration.

After the results were gained and compared a damage was simulated on the symmetrical structure and changes in eigenfrequencies were investigated using only two out of the three previous methods.

5.1 Modal characteristics of undamaged aluminium structure

As mentioned before, different approaches were used for finding eigenfrequencies of the structure. Firstly a finite element model was created in commercial software MSC Marc/Mentat that corresponded to the structure mentioned above in this chapter. Consequently two experiments were carried out to find out eigenfrequencies, one using an impact hammer and a second one using piezoelectric patches for excitation as well as for sensing the structure. Two different configurations were examined, a symmetrical one with 17 beams and an asymmetrical one with 16 beams, that represented the same structure only
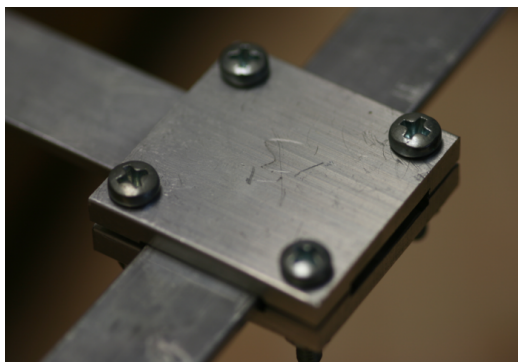
Fig. 5.2: Connecting part detail.
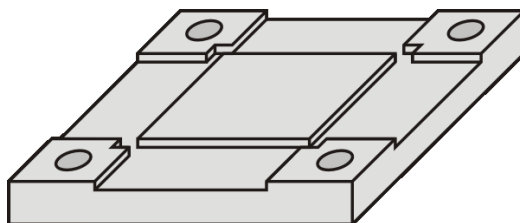
Fig. 5.3: Connecting part geometry (recesses for beams and holes for screws are visible).

with a missing beam.

All parts were weighted to define the correct mass for finite element model. The masses of selected parts were: connector $m_c = 18.455\,\text{g}$, screw and nut $m_s = 2.991\,\text{g}$, beam $m_b = 35.007\,\text{g}$ and accelerometer $m_a = 15.000\,\text{g}$. This makes the final configuration to have mass of $m_f = 12 \times m_c + (4 \times 12) \times m_s + 17 \times m_b + m_a = 1.18\,\text{kg}$. The final assembly was weighed with real mass of $m_r = 1.19\,\text{kg}$. The difference was caused by imperfection of sizing the parts. The difference of 1% was for purposes of experiment negligible, masses m_c, m_s, m_b and m_a were therefore used for definition of the FEM model in MSC.Marc.

5.1.1 Experimental analysis using impact hammer

Analysis of modal characteristics of the structure was performed. The measurement was carried out on both configurations, symmetrical and asymmetrical, to demonstrate the change of the characteristics such as the shift of eigenfrequencies and change of eigenshapes from the frequencies and eigenshapes of the symmetrical structure and to evaluate finite element modelling. First five eigenfrequencies found in experiments with impact hammer are rep-
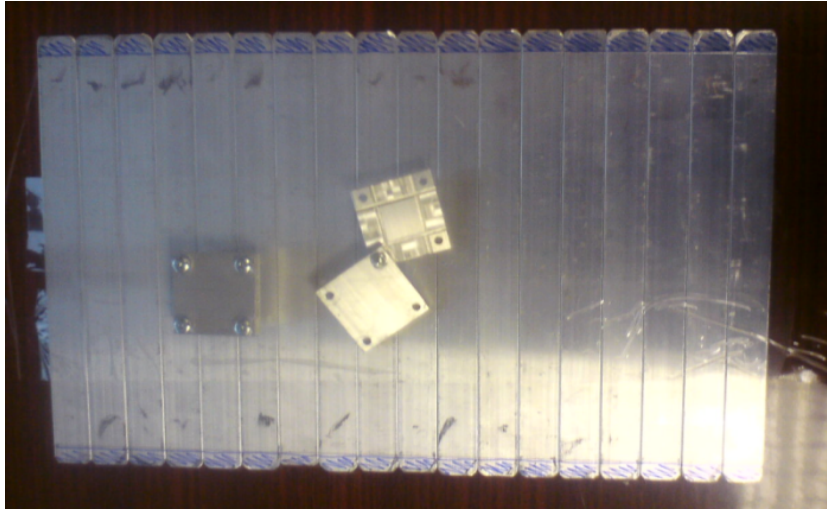
Fig. 5.4: Unassembled parts.

resented in fig. 5.9 – 5.11.

An impact hammer and a Brüel&Kjær accelerometer (see Fig. 5.5) bonded to one of the connectors were used. The eigenfrequencies and eigenmodes were determined using Pulse software.

It was difficult to distinguish between the higher eigenfrequencies that were close to each other and collapsed in one peak in the graph of dependency of amplitude on frequency. As can be seen in fig. 5.6 – 5.8 two lowest eigenfrequencies under frequency of 15 Hz were not found. Therefore the frequency of 25.33 Hz is noted as the first one. The results are compared with results from other methods in tab. 5.2 and tab. 5.3.
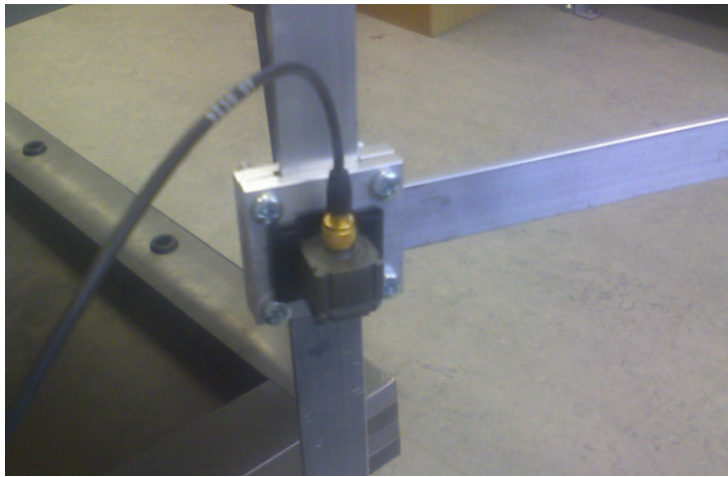
Fig. 5.5: Detail of accelerometer with attached cable.
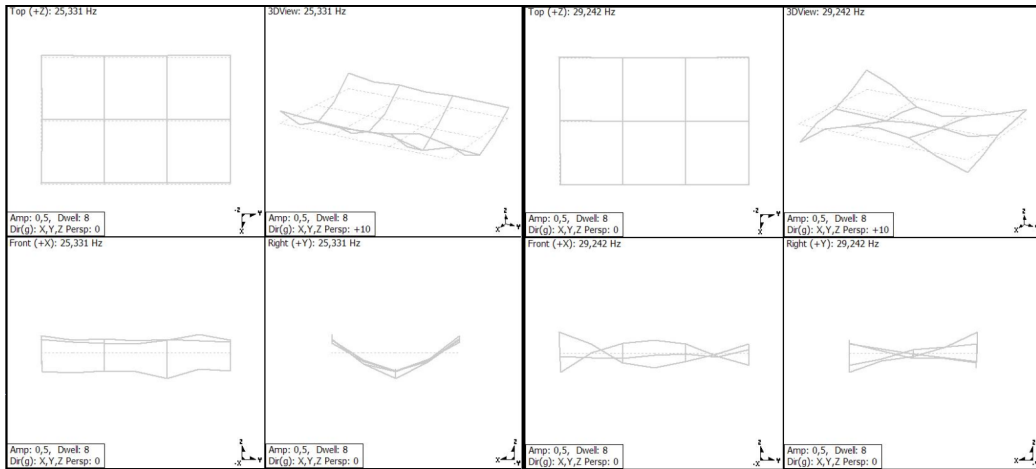
Fig. 5.6: First two eigenfrequencies from the experiment with symmetrical configuration.
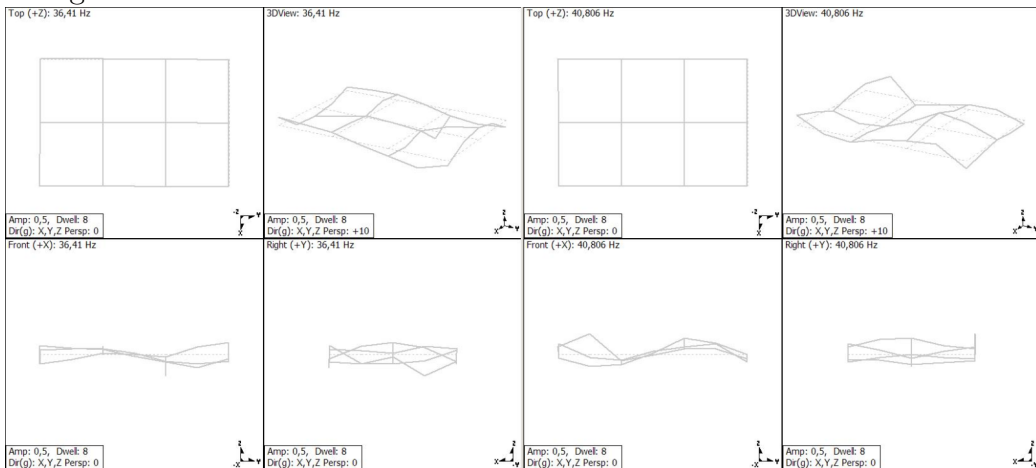
Fig. 5.7: Third and fourth eigenfrequency from the experiment with symmetrical configuration.
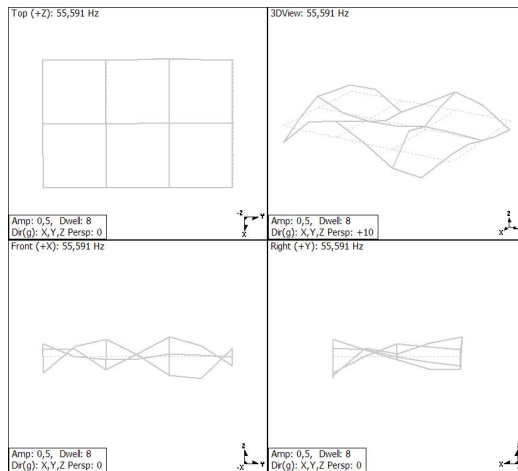
Fig. 5.8: Fifth eigenfrequency from the experiment with symmetrical configuration.
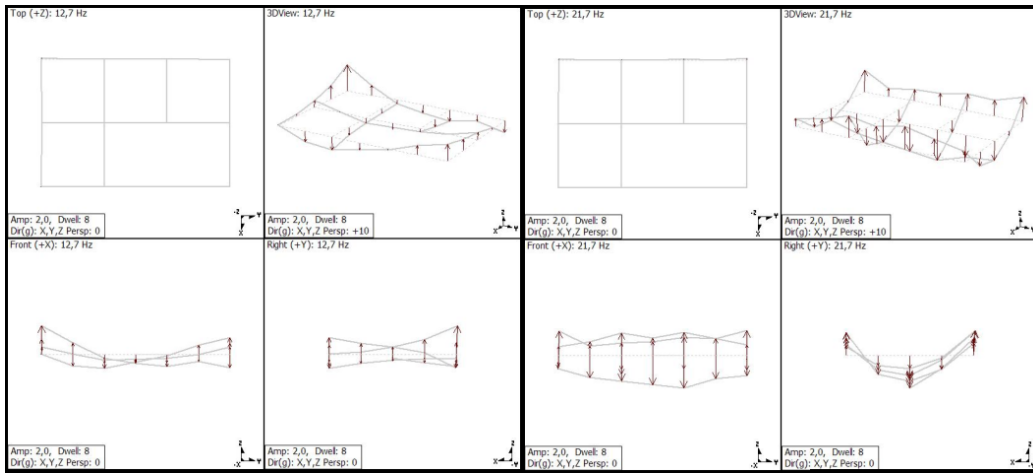
Fig. 5.9: First two eigenfrequencies from the experiment with asymmetrical configuration.
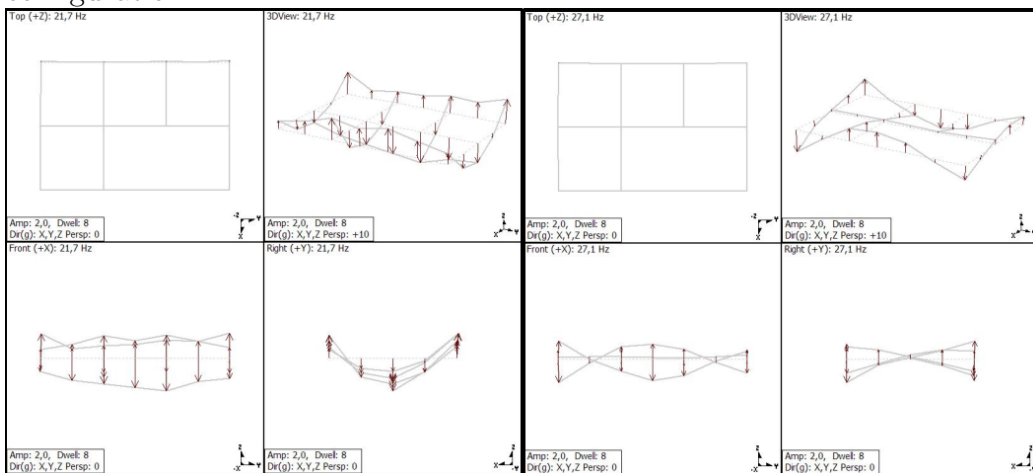
Fig. 5.10: Third and fourth eigenfrequency from the experiment with asymmetrical configuration.
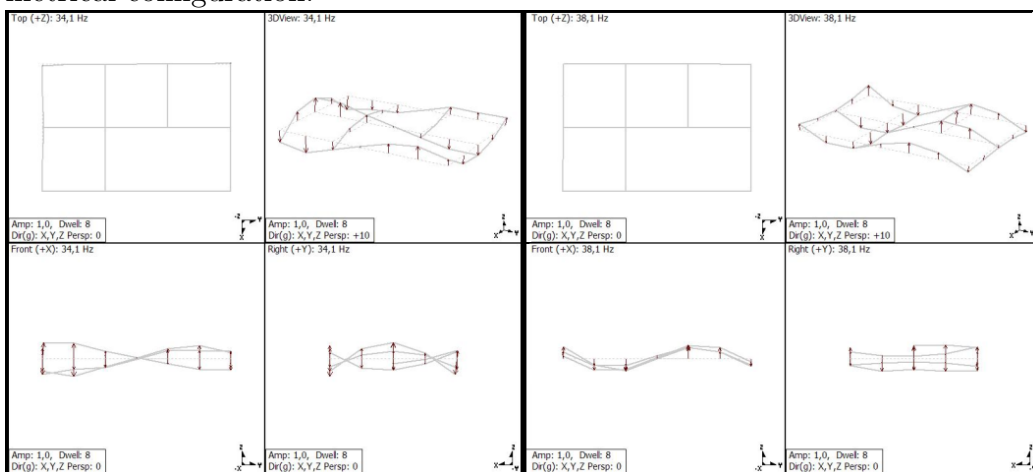
Fig. 5.11: Fifth and sixth eigenfrequency from the experiment with asymmetrical configuration.

5.1.2 Experimental analysis using piezoelectric patches

Consequently, another method for finding eigenfrequencies was undertaken. This time with a piezoelectric patches. The original symmetrical structure with 17 beams, that was previously examined with an impact hammer, was hanged loose and examined using two piezoelectric patches of the same type P-876.SP1 (see fig. 5.12).
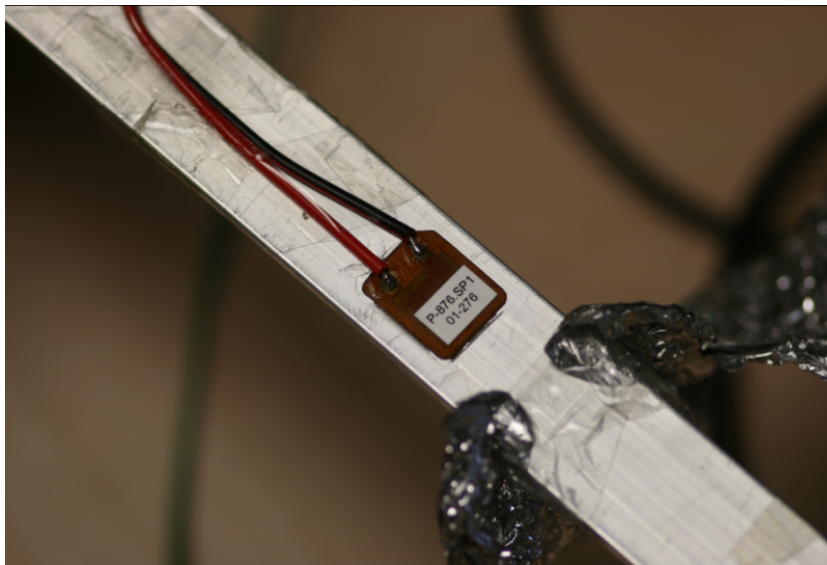
Fig. 5.12: Piezoelectric patch detail.

This is the smallest standard DuraAct patch transducer (fig. 5.13) where active area of a piezomaterial is a square with a side of 10 mm.

Both patches, one as a sensor and the latter as an actuator, were glued to the central beam of the original configuration with 17 beams. Since the patches are very sensitive, shielding with an aluminium foil (Fig. 5.12) was needed to suppress the unwanted electric 50 Hz hum from the power line.

Arrangement of the experiment is shown in Fig. 5.14. The experiment was controlled by a computer, connected to National Instruments CompactDAQ unit with 9263 output module and 9215 input module and using driver and charge amplifier. The output module converts the digital signal generated to an analog signal. This signal is amplified by the driver 50 times. The amplified signal goes to the actuator glued to the beam. The applied voltage contracts and stretches the piezoelectric patch, which excites the beam. The oscillation is than captured by the second piezoelectric patch. The sensor sends the signal through a charge amplifier to the input module that converts analog signal $\mathbf{U}$ to a digital signal. This is recorded by the computer.
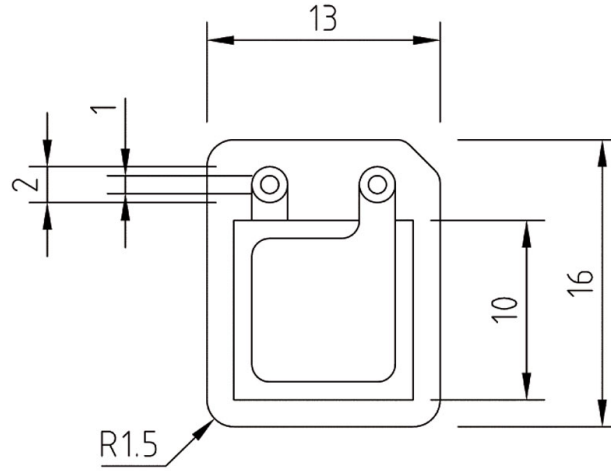
Fig. 5.13: Piezoelectric patch drawing. Dimensions are given in [mm]. [37]

The parameters of the charge amplifier type 2635 by Brüel & Kjær (see fig. 5.15) were set to 1 m/s^2 of unit output and 2 Hz lower frequency limit. Upper frequency limit was than set to 30 kHz. Unit output was set to 1 mV. Transducer sensitivity was set to 1 pC/m/s^2.

The experiment was carried out with a software in National Instruments LabView created by Jan Bartošek.[1] User has the possibility of choosing the type of excitation signal (such as sine wave, sawtooth, square or triangle wave). Excitation frequency and voltage has to be defined as well as sampling frequency (see fig. 5.16). All four types of exciting pulses were examined for different excitation frequencies. Different intervals of mentioned signals were used to excite the structure. Selected results are shown at fig. 5.18– 5.23. A whole period of chosen signal was tested in the first experiments, later mainly excitation with a section of square wave was used. Results did not differ significantly in dependency on the type of signal, but square wave showed clearer border between end of excitation signal and beginning of amplitudes of free end oscillation. Maximal possible sampling frequency of the module was used – 51.2 kHz. Lower of the two graphs for each excitation shows the response r of the piezoelectric patch that expresses strength of output signal O in dependency on input signal I. In our case this may be expressed by

$$r = 50\frac{O}{I}. \tag{5.1}$$

---

[1]Jan Bartošek is a PhD. candidate at Department of Mechanics at University of West Bohemia
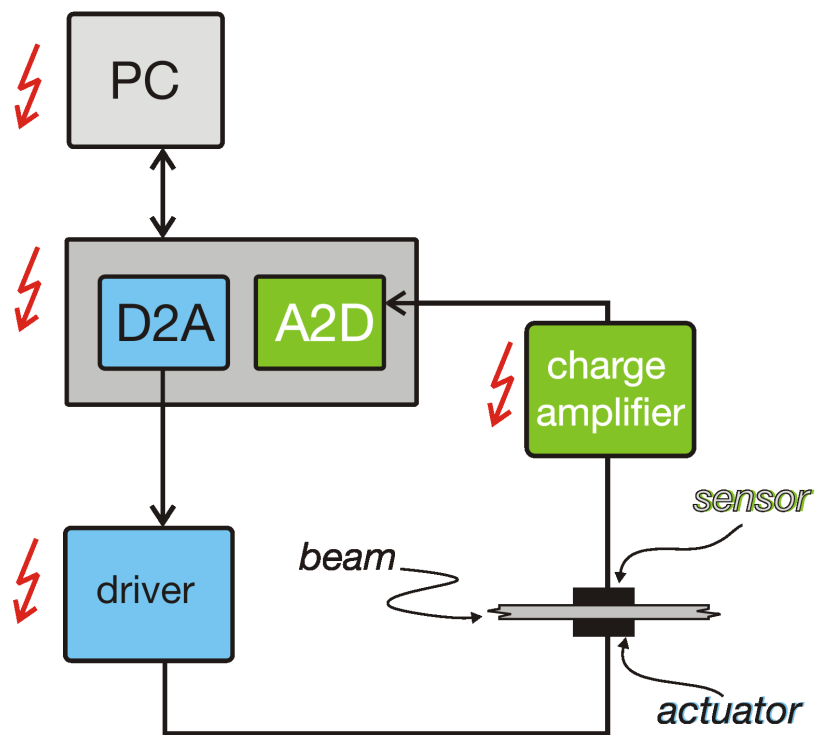
Fig. 5.14: Experiment arrangement.

Fig. 5.15: Detail of charge amplifier front panel with settings.
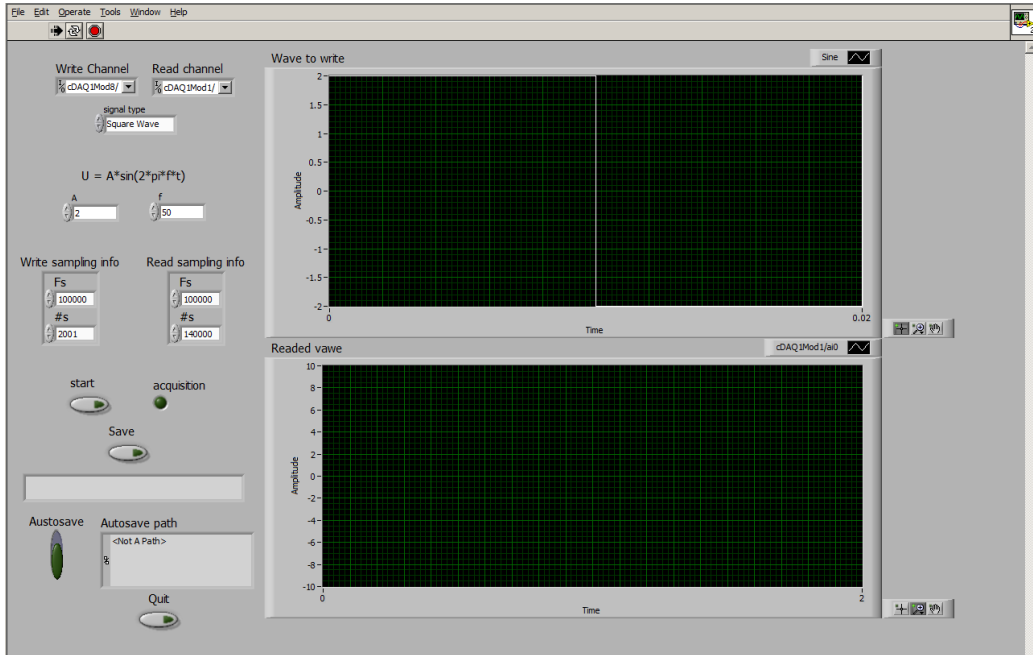
Fig. 5.16: Printscreen of program used.

5.1.3 Finite element analysis

Both cases (symmetrical and asymmetrical structure) were simulated in MSC.Marc software to validate material properties on simplified finite element model. 1132 hexahedral solids elements were used to create the model. All connections between beams and connectors (and screws) were defined as rigid, i.e. no contact was used. This approach was used to keep the model simple.

Firstly, an extra simulation was carried out to find influence of mass of the accelerometer. The effect of the accelerometer was defined by increased density of elements on the place, where the accelerometer was fixed (see fig. 5.17) according to results from weighting the parts (mentioned above). This resulted in higher mass of the region. This was sufficient for our case as the glued accelerometer had negligible effect on strength of the region. Eigenfrequencies were then compared and the maximal difference was found to be 1% between the model with and without accelerometer in the tracked values. Mass m_a (as mentioned in section 5.1) was therefore neglected as it made no substantial difference. Material properties used for the model of structure are shown in tab. 5.1.

Tab. 5.1: Material properties of aluminium structure.

	ρ [kg/m^3]	E [GPa]	ν [-]
Beam	2679	63	0.35
Connector	3050	70	0.30
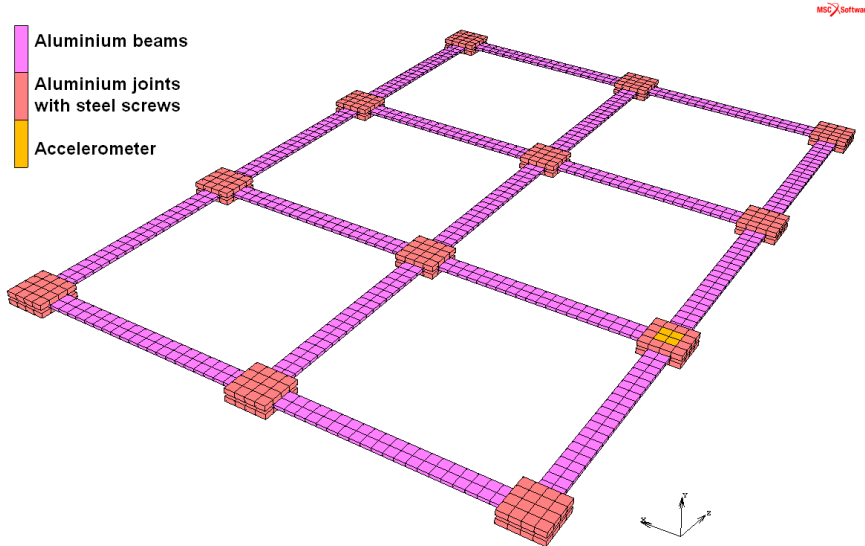
Fig. 5.17: Initial model of the aluminium structure in MSC.Marc, when influence of accelerometer was investigated – definition of materials used.

5.1.4 Discussion of results

When the results from the first experiment are compared to those from finite element analysis, it can be seen that the finite element model revealed additional lower eigenfrequencies that were not obvious from the experiments. Values of corresponding eigenfrequencies from the experiments and FEA was less than 5% of the latter eigenfrequencies. Except the missing eigenfrequencies from the experiment a satisfactory similarity between the experiments and the model created in MSC.Marc was found as shown in tab. 5.2 and tab. 5.3.

For future work an optimal pulse was searched for. Thirty different experiments were performed (selected results shown in fig. 5.18– 5.23), but the results gained from different excitation pulses did not differ strongly, only in ratio of specific peaks from Fourier transform that expressed eigenfrequencies. A whole period of chosen signal was tested in the first experiments, later mainly a section of square wave was used, as it showed clearer border between the end of excitation signal and the beginning of free oscillations.

Tab. 5.2: Comparison of results form experiments with results from MSC.Marc.

Frequency	1	2	3	4	5	6	7
Experiment impact [Hz]	-	-	25.33	29.24	36.41	40.81	55.59
MSC.Marc [Hz]	13.04	13.26	25.30	28.69	36.40	38.07	52.55
Experiment piezo[Hz]	12.21	13.30	-	27.47	35.10	37.38	50.35

Tab. 5.3: Comparison of results from MSC.Marc with experiment with asymmetrical configuration.

Frequency	1	2	3	4	5	6	7
Experiment [Hz]	12.7	-	21.7	27.1	34.1	38.1	47.8
MSC.Marc [Hz]	12.5	13.2	22.0	27.7	34.9	39.1	48.8

There was no signal, that would show all eigenfrequencies better than the other excitation signal(see fig. 5.23). No rule or lead, that would define an appropriate excitation signal, was found. Therefore, only six basic excitation pulses (one peak of 1/100 s triangular wave, 1/10 s, 1/50 s, 1/100 s, 1/200 s, and 1/350 s square wave) were chosen as a reference. These six frequencies were used in further investigation, where a damage was simulated.
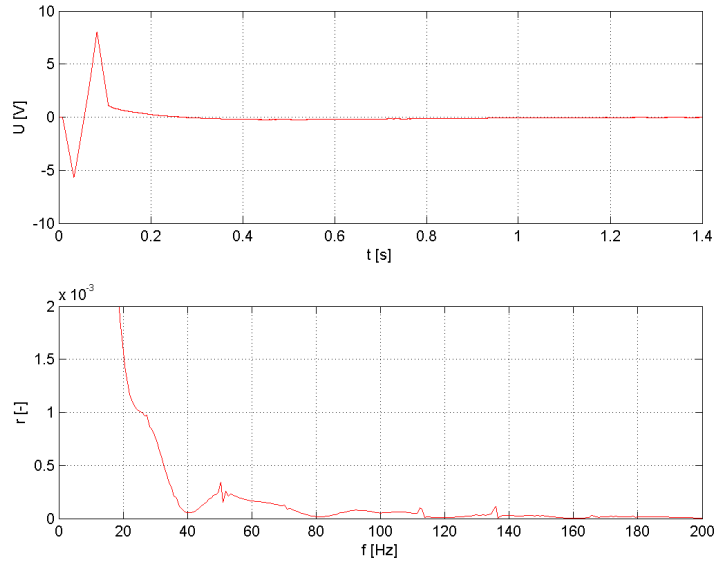
Fig. 5.18: Triangular wave excitation and frequency spectrum.
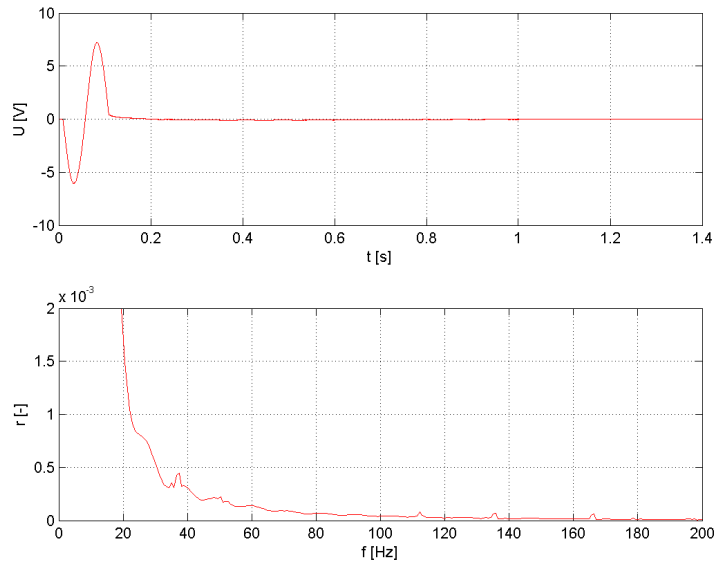
Fig. 5.19: Sine wave excitation and frequency spectrum.
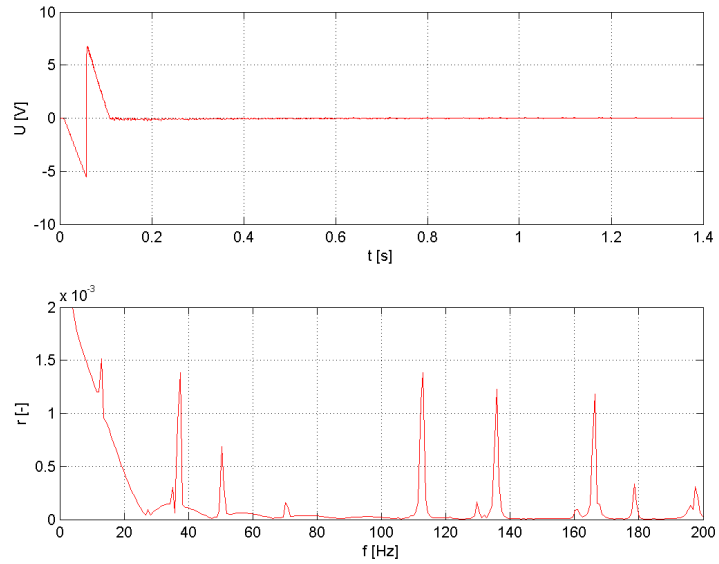
Fig. 5.20: Sawtooth wave excitation and frequency spectrum.
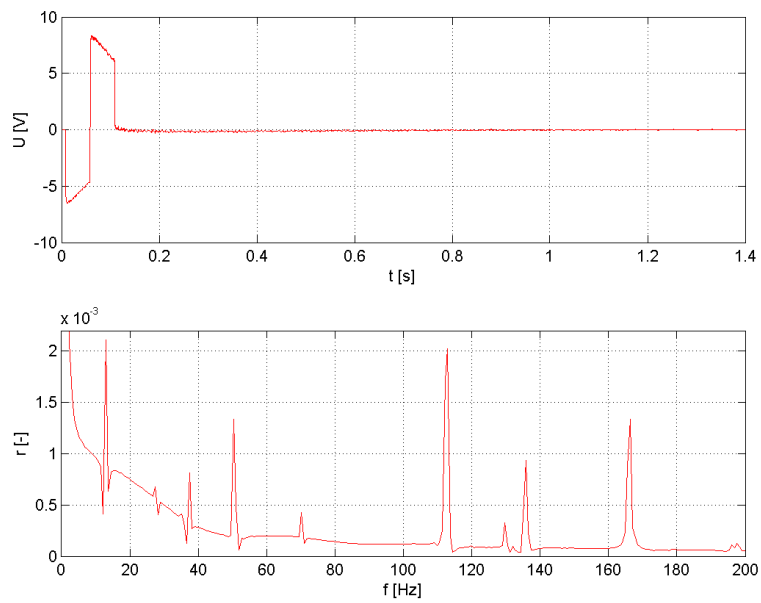
Fig. 5.21: Square wave excitation and frequency spectrum.
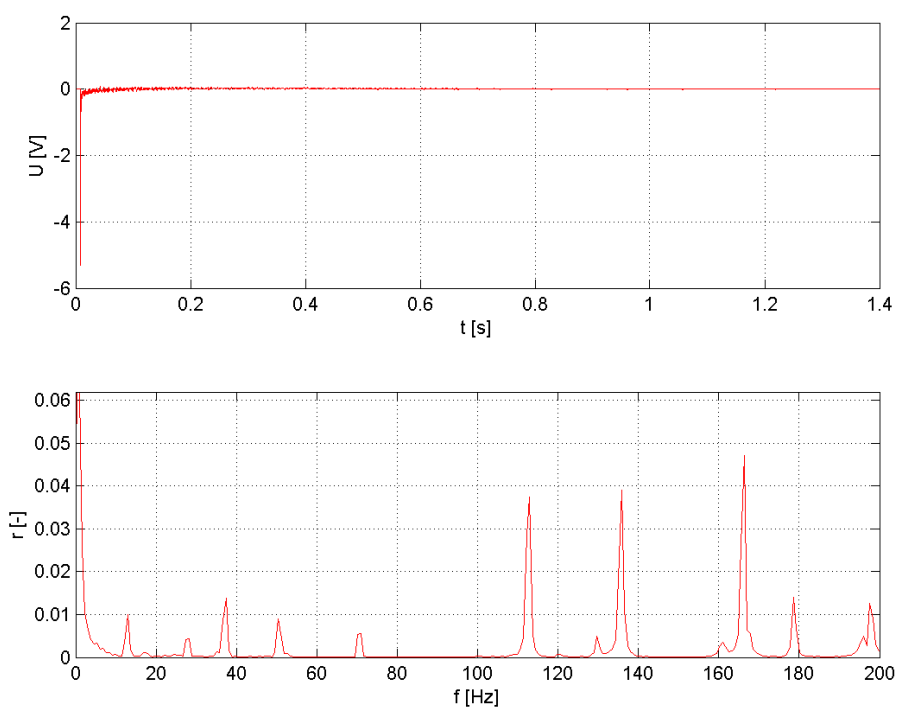
Fig. 5.22: Pulse excitation with duration of 1/200 s and frequency spectrum.
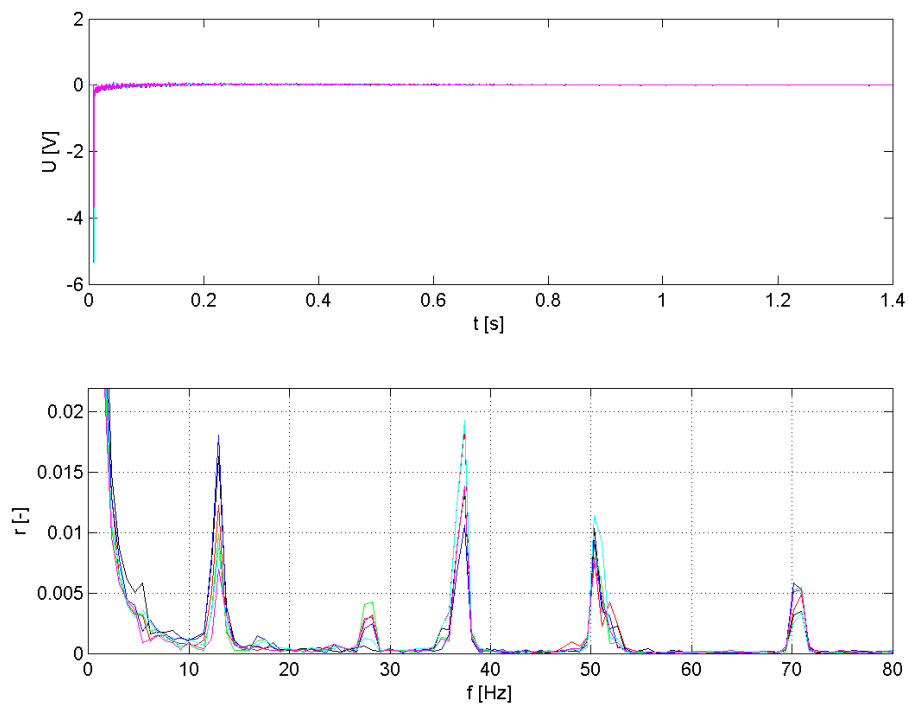
Fig. 5.23: Pulse excitations with different duration and their frequency spectra.

5.2 Experimental and FEM analysis of damaged aluminium structure

The symmetrical structure examined in previous sections was changed to investigate its behavior for purposes of SHM. A beam divided in half was chosen as a case of representative damage. There are six potential cases of such damage. Other 11 cases are only mirror types of mentioned six cases. In the fig. 5.24 are shown possible damages. Beams where the damage can happen are highlighted with a magenta line, mentioned symmetrical cases are expressed by grey lines.
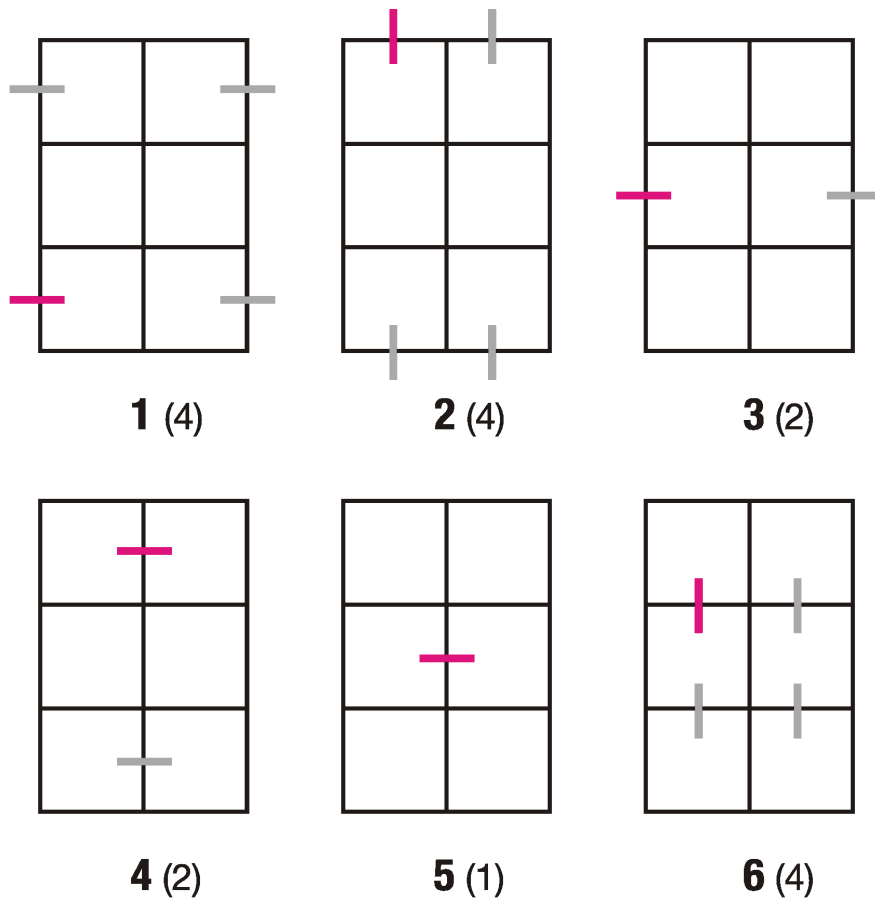
Fig. 5.24: Six cases of damaged structure with one damaged beam (magenta lines). Numbers in brackets denote the number of symmetrical cases (grey lines).
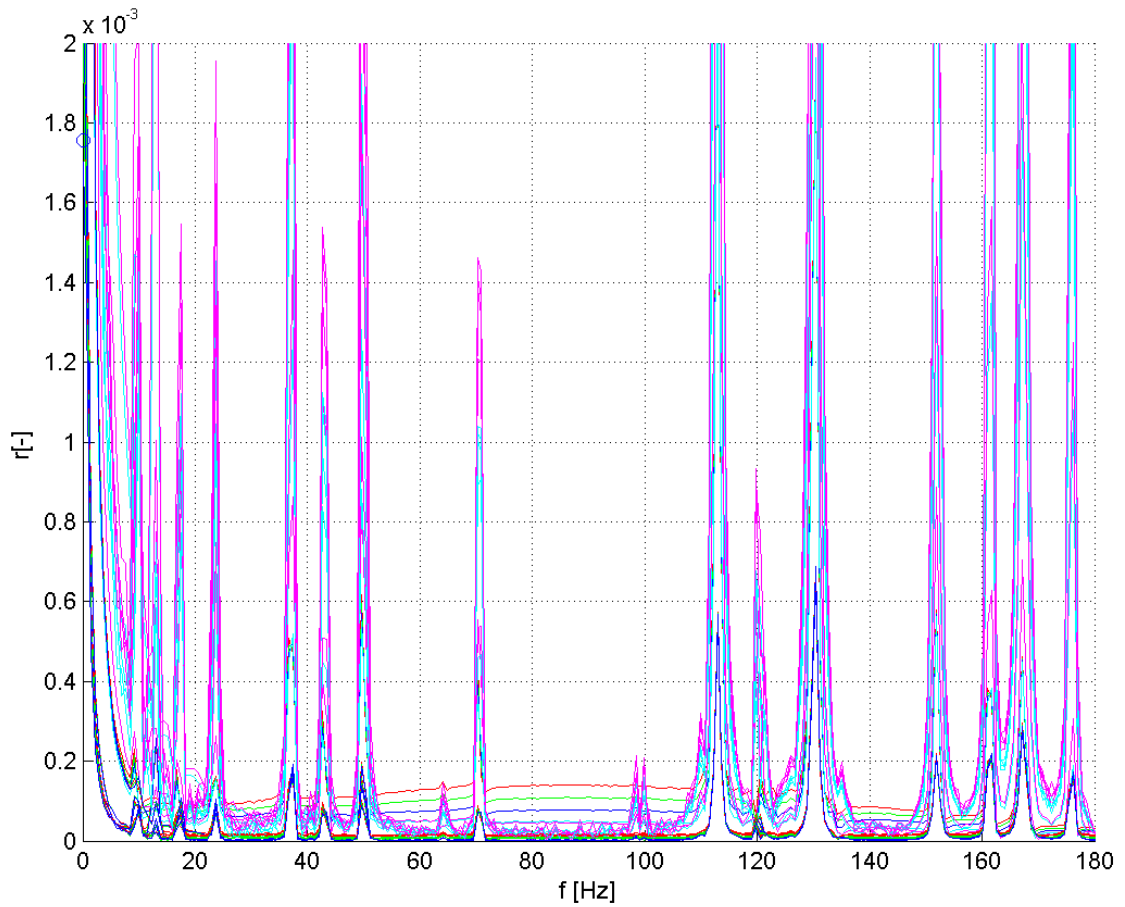
Fig. 5.25: Detail on results from different excitations with several trims - second type of damage.

All six cases with appropriate failures were modelled in MSC.Marc and all unconstrained structure models were submitted to modal analysis. Eigenfrequencies were found out for following confrontation with experiment.

The six above mentioned excitation signals were used (as in the previous section with undamaged structure) and all six cases of structure with artificial damage were examined accordingly. Eigenfrequencies were found in Matlab using Fourier transformation and subsequently compared to the results from software MSC.Marc (see tab. 5.4– 5.9). To suppress the noise induced in the beginning before the Fourier transformation certain number of input data had to be cut off. Variation of results with different amount of input data was also compared. Fourier transformation of all selected types of excitation signal with all different beginning trim are expressed in graphs in fig. 5.25 and

55
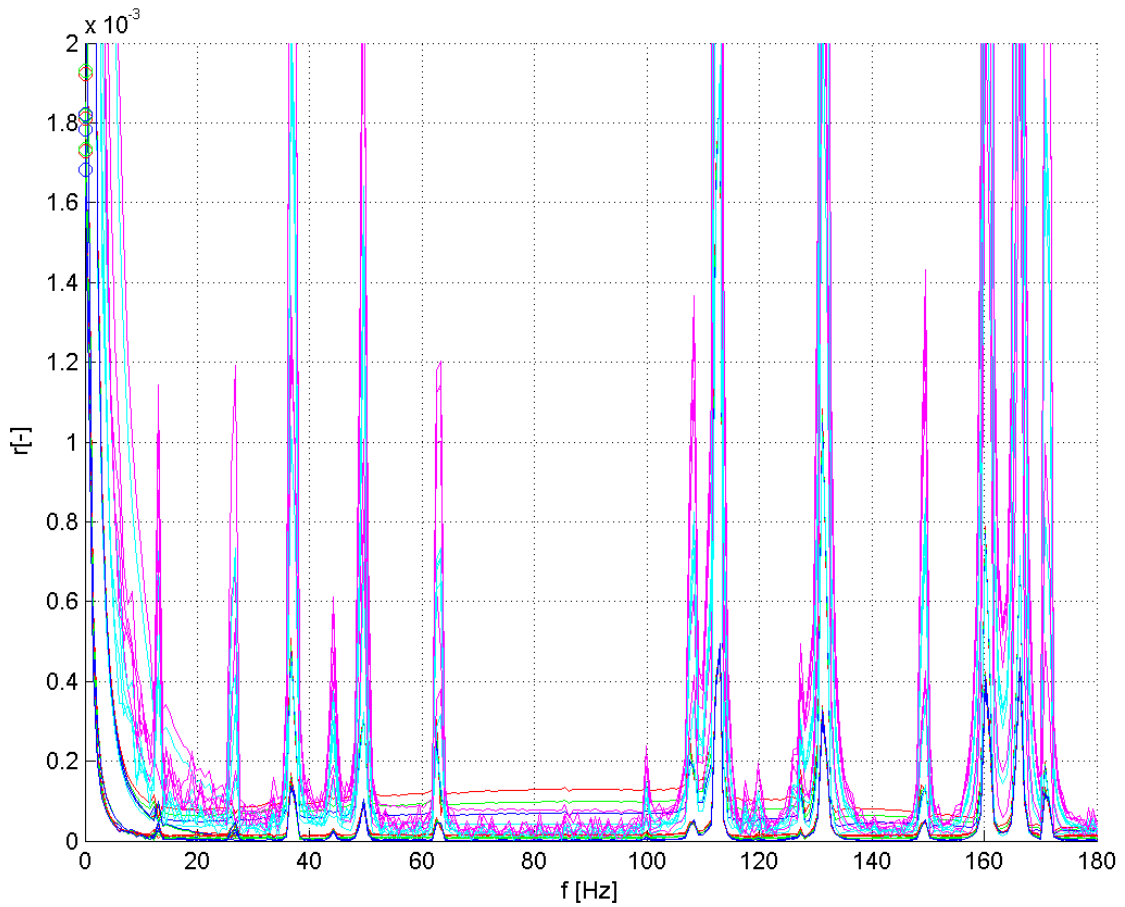
Fig. 5.26: Detail on results from different excitations with several trims - sixth type of damage.

fig. 5.26. As can be seen, all results lead to same eigenfrequencies. Largest difference can be seen by lower eigenfrequencies. Higher eigenfrequencies can be distinguished quite clearly. As the cropping was done in the same manner for all experiments and so was the assignment of a specific colour to this cropping done respectively, the graphical representation also shows how different experiment frequencies agree closely. Based on the comparison it can be concluded that the excitation signal does not have significant influence on the results.

As generally is not possible define, which eigenfrequencies will be affected by an undefined damage and it does not matter which spectrum of eigenfrequencies is monitored for SHM, a conclusion can be made, that higher frequencies may be used for comparison as well. Because when a shift of

eigenfrequencies happens due to a failure, this may affect higher eigenfrequencies as well as lower eigenfrequencies.

Fig. 5.27 shows progression of one of the excitation signals captured by sensor and its magnification for better representation.

Figs. 5.28 – 5.33 show the comparison of damaged and undamaged configuration for all 6 cases of damage and their corresponding Fourier spectra.
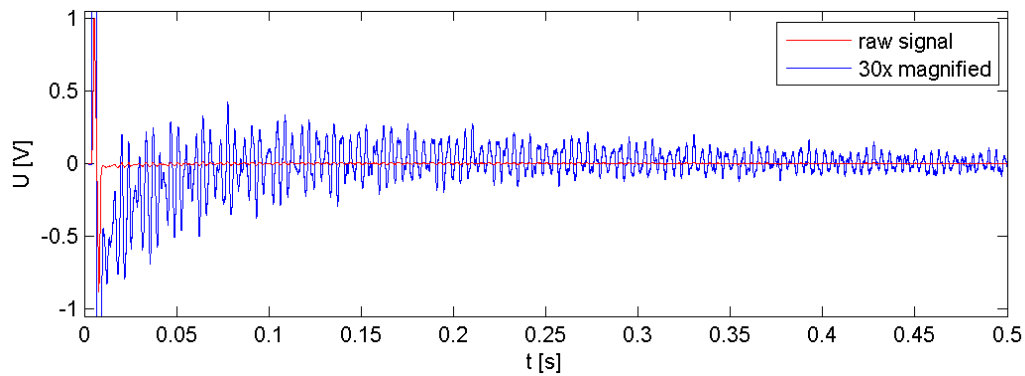
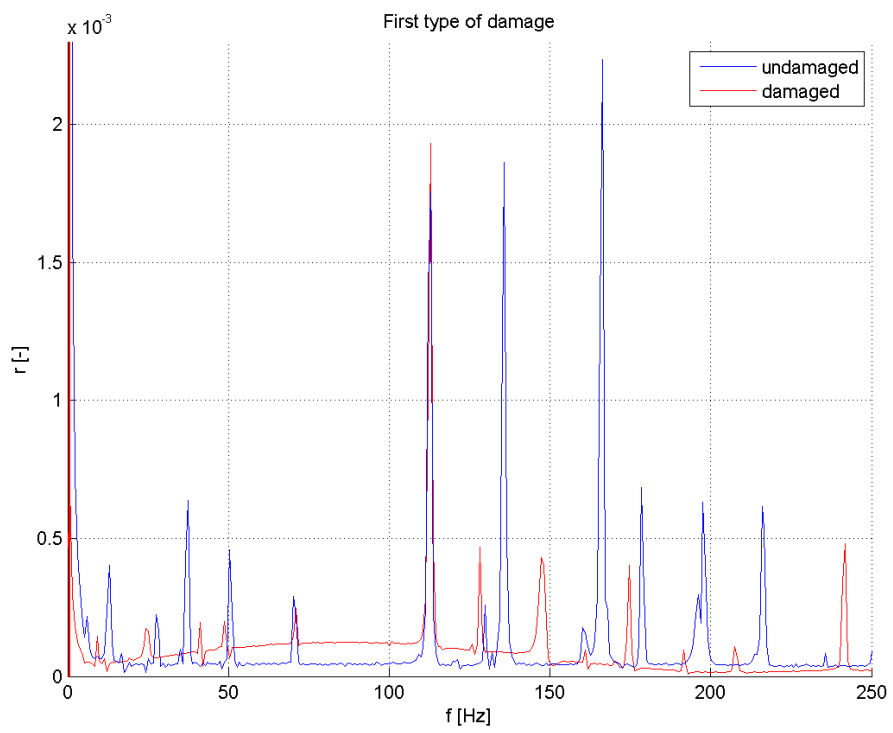Fig. 5.27: Signal from piezoelectric sensor.
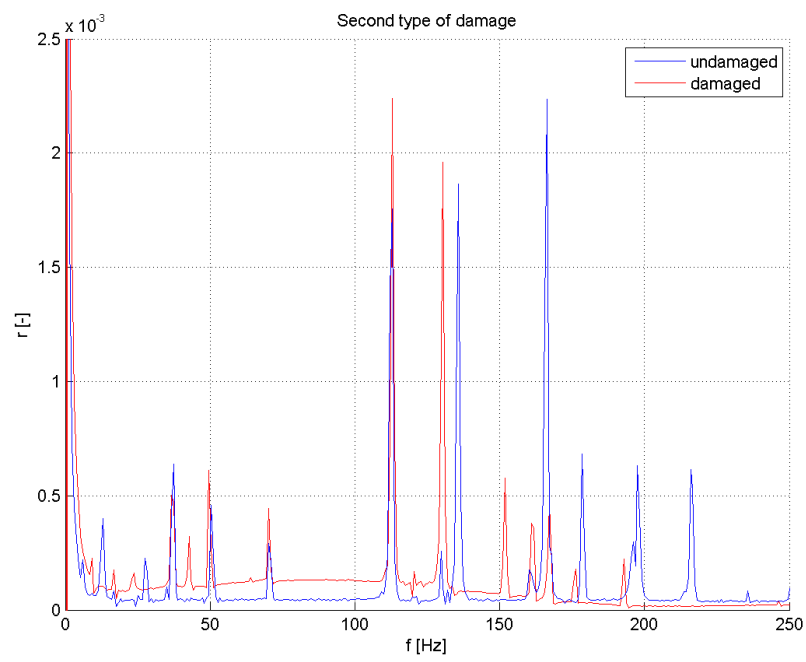
Fig. 5.28: Comparison of spectra of damaged (case 1) and undamaged structures.

Fig. 5.29: Comparison of spectra of damaged (case 2) and undamaged struc-
tures.
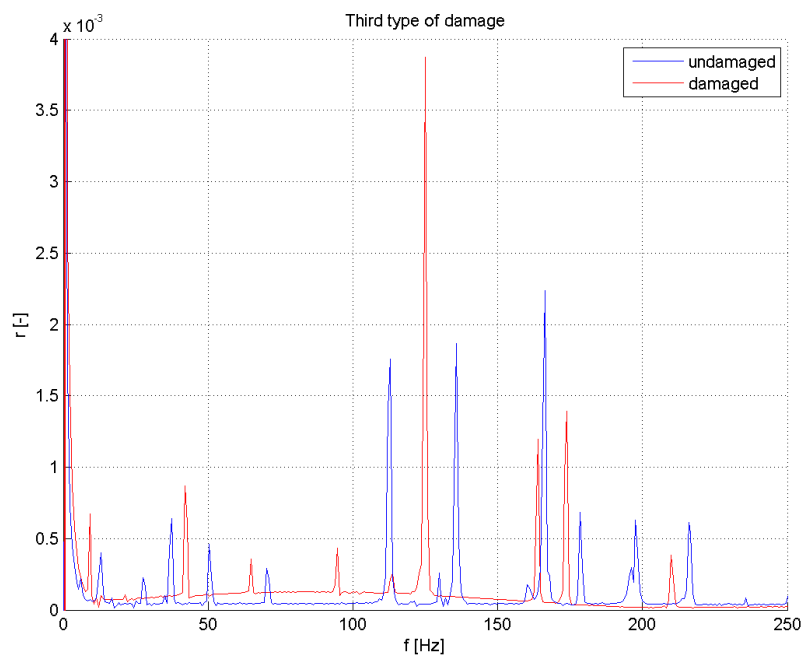
Fig. 5.30: Comparison of spectra of damaged (case 3) and undamaged structures.
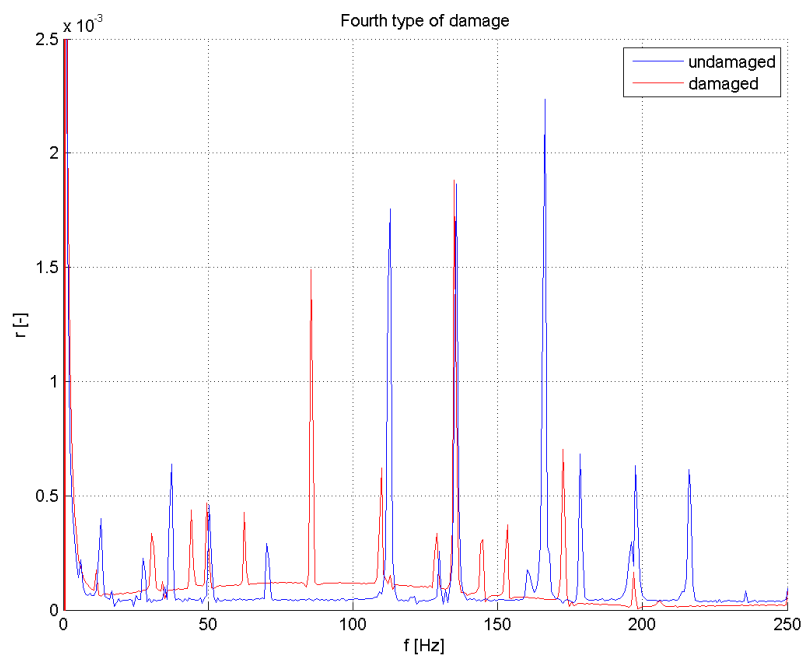
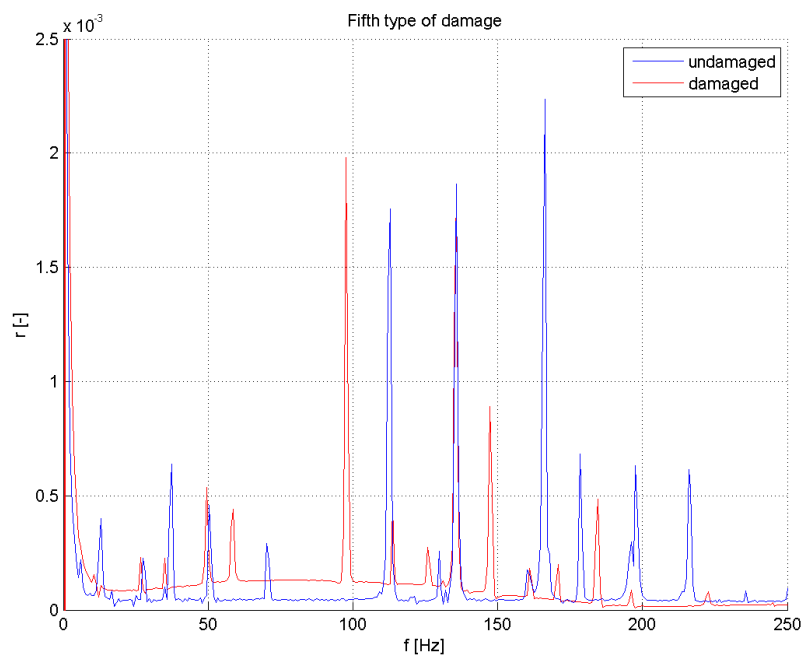Fig. 5.31: Comparison of spectra of damaged (case 4) and undamaged structures.

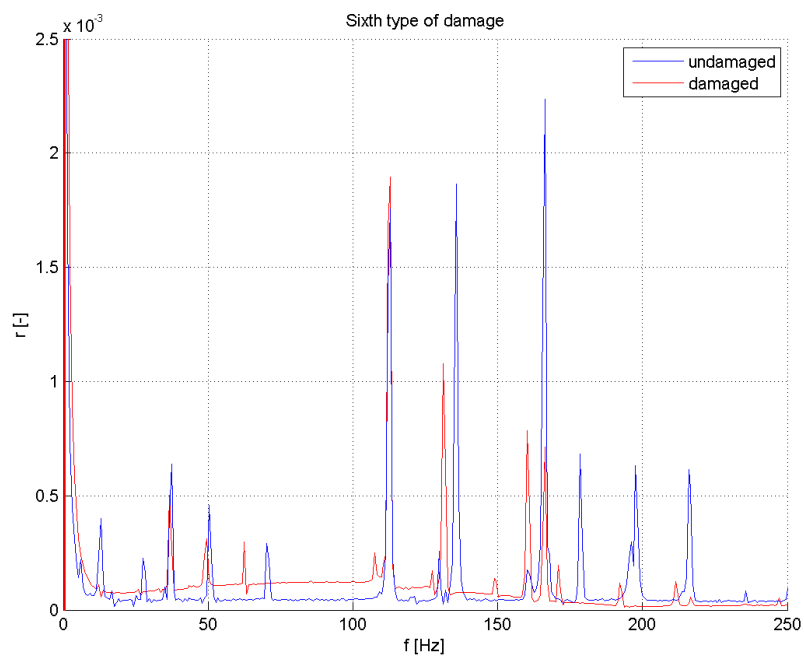Fig. 5.32: Comparison of spectra of damaged (case 5) and undamaged structures.

Fig. 5.33: Comparison of spectra of damaged (case 6) and undamaged structures.

Tab. 5.4: Comparison of eigenfrequencies from experiment with results from MSC.Marc – case 1.

Mode number	1	2	3	4	5	6	7	8	9	10
MSC.Marc [Hz]	9.42	12.08	19.77	25.29	32.54	34.79	42.74	50.86	66.37	73.64
Experiment [Hz]	9.16	12.21	19.84	25.18	-	-	41.20	49.59	64.09	70.95
Difference [%]	1.03	0.99	1.00	1.00	-	-	1.04	1.03	1.04	1.04

Tab. 5.5: Comparison of eigenfrequencies from experiment with results from MSC.Marc – case 2.

Mode number	1	2	3	4	5	6	7	8	9	10
MSC.Marc [Hz]	9.75	13.03	17.53	24.16	30.86	38.02	44.44	51.47	66.67	73.25
Experiment [Hz]	9.92	12.97	17.55	23.65	-	37.38	42.72	49.59	64.09	70.19
Difference [%]	0.98	1.00	1.00	1.02	-	1.02	1.04	1.04	1.04	1.04

Tab. 5.6: Comparison of eigenfrequencies from experiment with results from MSC.Marc – case 3.

Mode number	1	2	3	4	5	6	7	8	9	10
MSC.Marc [Hz]	9.06	10.52	22.09	25.30	26.92	34.48	43.50	52.56	67.44	96.29
Experiment [Hz]	-	10.68	21.36	-	26.70	34.33	41.96	49.59	64.85	94.60
Difference [%]	-	0.99	1.03	-	1.01	1.00	1.04	1.06	1.04	1.02

Tab. 5.7: Comparison of eigenfrequencies from experiment with results from MSC.Marc – case 4.

Mode number	1	2	3	4	5	6	7	8	9	10
MSC.Marc [Hz]	11.96	12.66	25.27	27.28	31.80	35.56	45.72	51.84	64.56	88.33
Experiment [Hz]	11.44	12.21	-	26.70	31.28	35.10	44.25	49.59	62.56	85.45
Difference [%]	1.05	1.04	-	1.02	1.02	1.01	1.03	1.05	1.03	1.03

Tab. 5.8: Comparison of eigenfrequencies from experiment with results from MSC.Marc – case 5.

Mode number	1	2	3	4	5	6	7	8	9	10
MSC.Marc [Hz]	10.89	12.36	25.29	27.57	28.69	36.50	51.51	52.09	60.25	98.74
Experiment [Hz]	10.68	12.21	-	26.70	-	35.10	49.59	-	58.75	97.66
Difference [%]	1.02	1.01	-	1.03	-	1.04	1.04	-	1.03	1.01

Tab. 5.9: Comparison of eigenfrequencies from experiment with results from MSC.Marc – case 6.

Mode number	1	2	3	4	5	6	7	8	9	10
MSC.Marc [Hz]	12.51	13.04	21.16	27.23	34.49	38.00	46.11	51.61	65.32	87.47
Experiment [Hz]	-	12.97	-	26.70	36.62	-	44.25	49.59	62.56	99.95
Difference [%]	-	1.01	-	1.02	0.94	-	1.04	1.04	1.04	0.88

Chapter 6

SHM of composite materials

As previous experiments with isotropic material led to results that corresponded with FEM results well, the effort was focused to structures made of composite materials. As research on composite plates is done on Department of mechanics, knowledge and structures from past investigation were used. Firstly, three plates were compared, out of which two were with different range of damage already. The undamaged plate was taken as a reference value to the others. During excitation tests major troubles were revealed, resolved and prevented in following experiments. Consequently new undamaged composite plate was investigated and subjected to several impacts. After experiments with unidirectional composite plate, more complex body was examined. A sandwich beam made of two outer composite layers and a foam core was investigated and subjected to several impacts. More bodies were impacted in the same manner to get comparable results.

6.1 Composite plates with different range of damage

Unidirectional long fiber composite plates from experiments realized by Mandys [14] were used. These specimens were made of four layers of unidirectional carbon-epoxy composite with dimensions of 270 mm × 15 mm × 1.15 mm 6.1. Two plates were with a crack already, created from impacts to the center of the plate. This crack was in direction of the fibers, parallel to edges, intersecting the center of the plate. The lengths of the cracks measured optically were 59 mm and 168.5 mm. As material properties can change in dependency on the production (for example by changing of material base supplier or technological process) they were verified experimentally [15] (tab. 6.1).

Tab. 6.1: Material properties of composite plate.

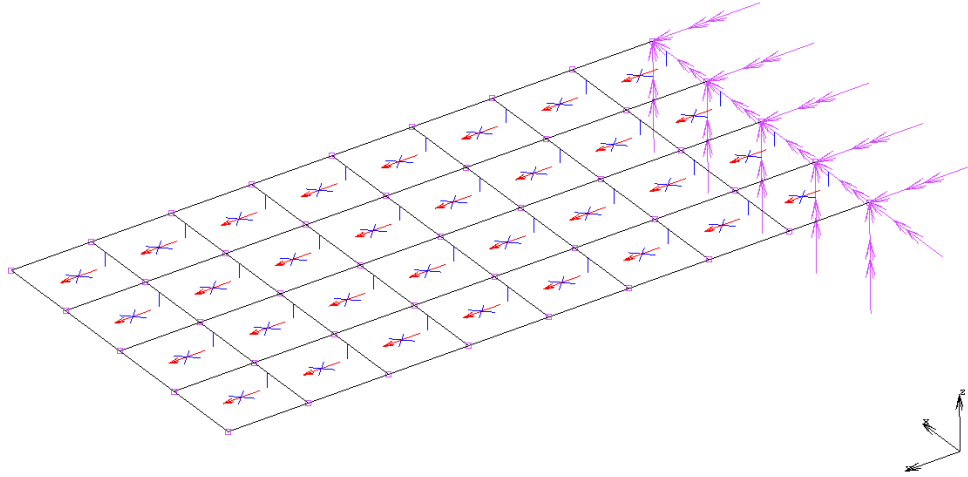| Material property	E_L[GPa]	E_T[GPa]	G_{LT}[GPa]	ν_{LT}[-]	ρ [kg.m^{-3}]
Value	153.4	7.8	4.5	0.28	1510

Fig. 6.1: Fiber orientation.

6.1.1 Impact excitation

In order to evaluate the upcoming results, several impact experiments on the plate with no damage were performed. Oscillation created by the impact was sensed using piezoelectric sensor and charge amplifier which sent the signal to National Instruments CompactDAQ unit with 9215 input module that converted this signal into a digital signal and this was recorded by a computer. Arrangement of the experiment is shown on fig. 6.2.

An impact created oscillation strong enough to last for a period of time sufficient enough to show eigenfrequencies clearly. This is visible on fig. 6.3. Delay between start of experimental measurement and impact itself is visible in the first half of the graph.

6.1.2 Finite element analysis

Material properties mentioned in tab. 6.1 were used for creating a finite element model in MSC.Marc. Two models in MSC.Marc were created. One model of a plate without a failure, second with a failure, that simulated a

crack in a damaged plate (see fig. 6.4). These two models corresponded to specimens from experiments undertaken by Mandys.

Results from finite element modelling were compared to results from the impact experiment and they corresponded well (compare with tab. 6.2). Values from the experiment and FEM analysis differ in maximum 10% in the tracked eigenfrequencies. This can be influenced by imperfection of the impact (double impact) or by variation of material properties after manufacture as well as by attached wires and patches that were neglected in the finite element model. Nevertheless, aim of the impact experiment was not to achieve a perfect match, but to verify, that the piezosensor and related equipment is connected correctly and able to fulfill its purpose.

Tab. 6.2: Results from experiment and MSC.Marc for undamaged plate.

Frequency	1	2	3	4	5
MSC.Marc [Hz]	59.23	156.4	167.6	200.8	205.6
Experiment [Hz]	57.81	140.6	168.0	185.7	198.4
Difference [%]	2.40	10.10	0.24	7.52	3.50

6.1.3 Pulse excitation with sensor

The undamaged plate, that was used in previous impact experiment (section 6.1.1) was connected into a circuit shown in fig. 6.5. This is similar to what was mentioned in chapter 5.1.2. The experiment was controlled by a computer, connected to National Instruments CompactDAQ unit with 9263 output module and 9215 input module. The output module converts the digital signal generated to an analog signal. This signal is amplified by a driver. The amplified signal goes to the actuator glued to the plate. The applied voltage contracts and stretches the piezoelectric patch, which excites the plate. The oscillation is than captured by the second piezoelectric patch. The sensor sends the signal through a charge amplifier to the input module, that converts analog signal $\mathbf{U}$ to a digital signal. This is saved by the computer.

Both patches were fixed to the same face of the composite plate, symmetrically to the centre of the plate. For better interpretation see fig. 6.6.

Series of experiments were carried out. Different types of shielding were put in action, but none of them was sufficient enough. As shielding of the piezoelectric patch was not successful, driver was taken out of the system and the patch was actuated with amplitude of 10 V only. This resulted in lower

noise as needed. The oscillation remained for a short period of time (0.3 sec). This made the accuracy of Fourier spectrum for finding peaks about 4 Hz.

Monitoring the signal for a longer period of time was also not sufficient, because the noise influenced the results and the eigenfrequencies were not visible either. The strongest frequency was the frequency of electrical power network – 50 Hz. Otherwise, no other stronger peak was to be clearly distinguished. This was examined on three different periods of time, with no better possibility of exact interpretation of eigenfrequencies. All three results can be seen on fig. 6.7. As can be seen, inaccuracy of the results causes, that it is almost impossible to tell apart the eigenfrequencies.

As the impact experiment in chapter 6.1.1proved the sensor to operate according to the expectations, actuator was determined as the source of previous unsuccess. A stronger excitation was necessary, therefore the driver was integrated into the circuit again with lower voltage for actuation. The excitation of the plate was stronger, but it also did not last for a time period sufficient enough to clearly tell apart the eigenfrequencies. The strongest response was induced by frequency of electrical power network. Other frequencies did not show much similarity among themselves when repeating the experiment (see fig. 6.8).

Shielding that was used by previous experiment with aluminium structure was not sufficient. Another method of efficient shielding was not found.
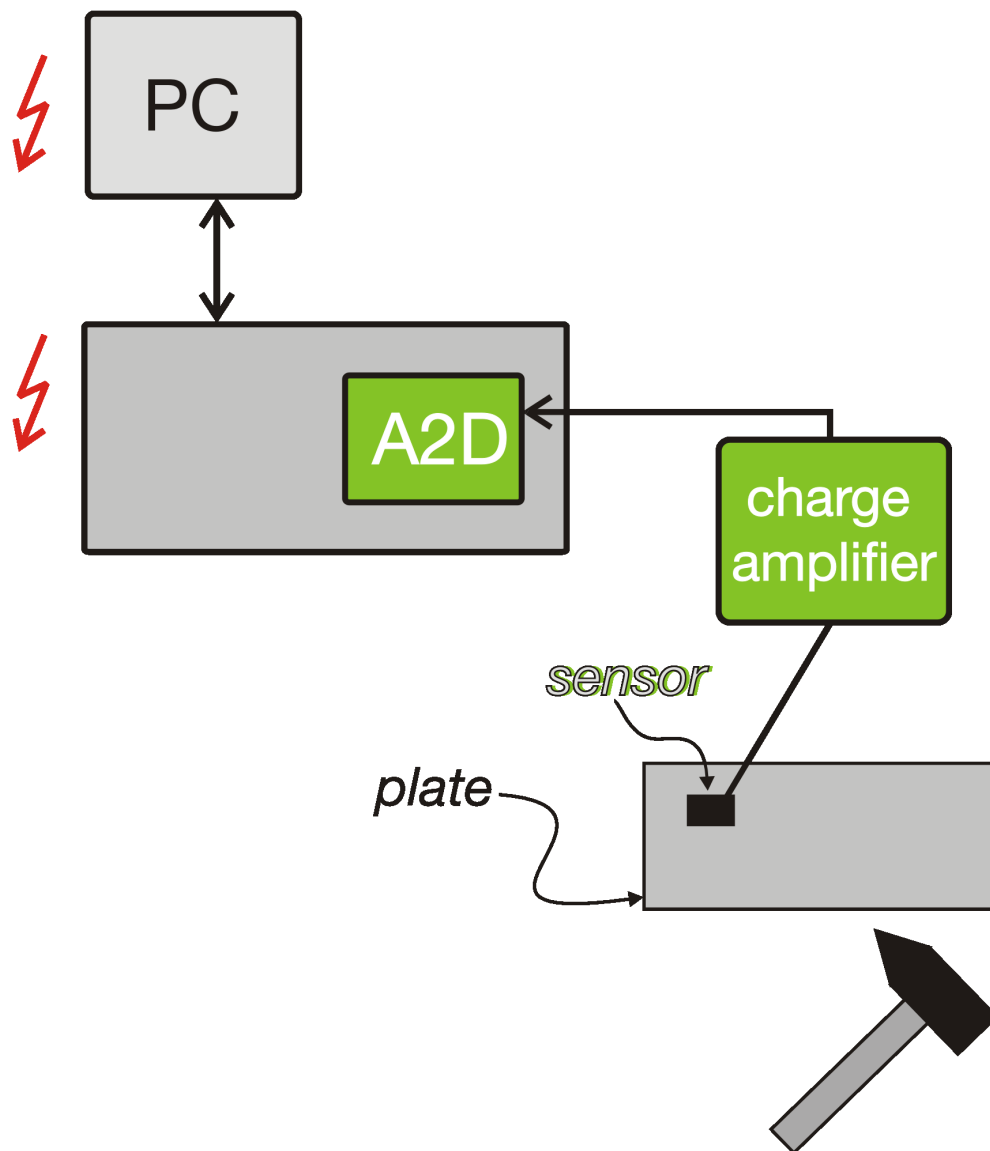
Fig. 6.2: Experimental arrangement.
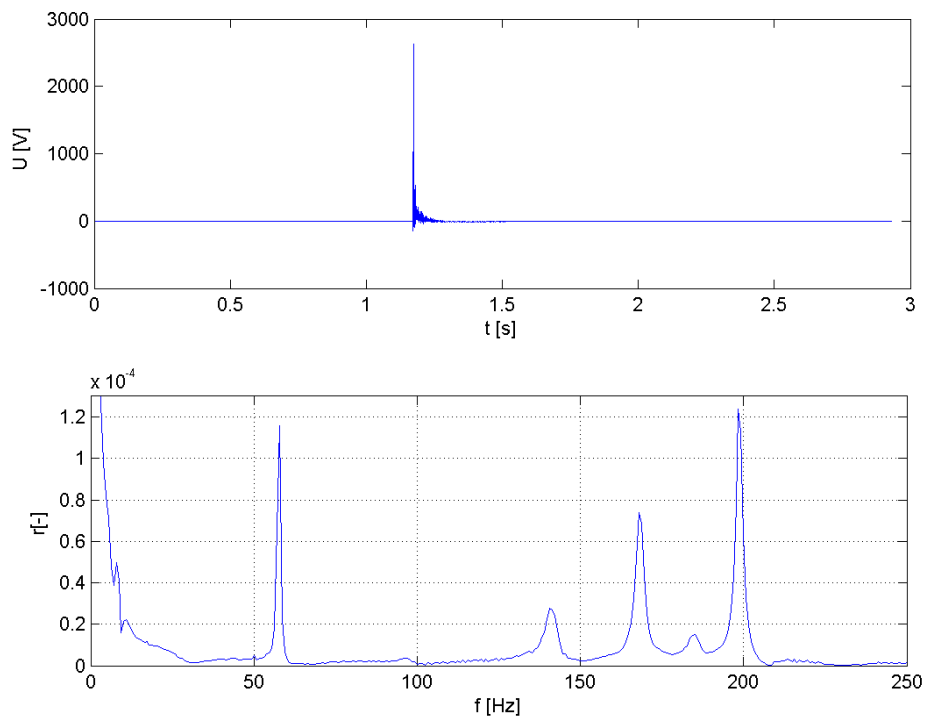
Fig. 6.3: Excitation with impact.
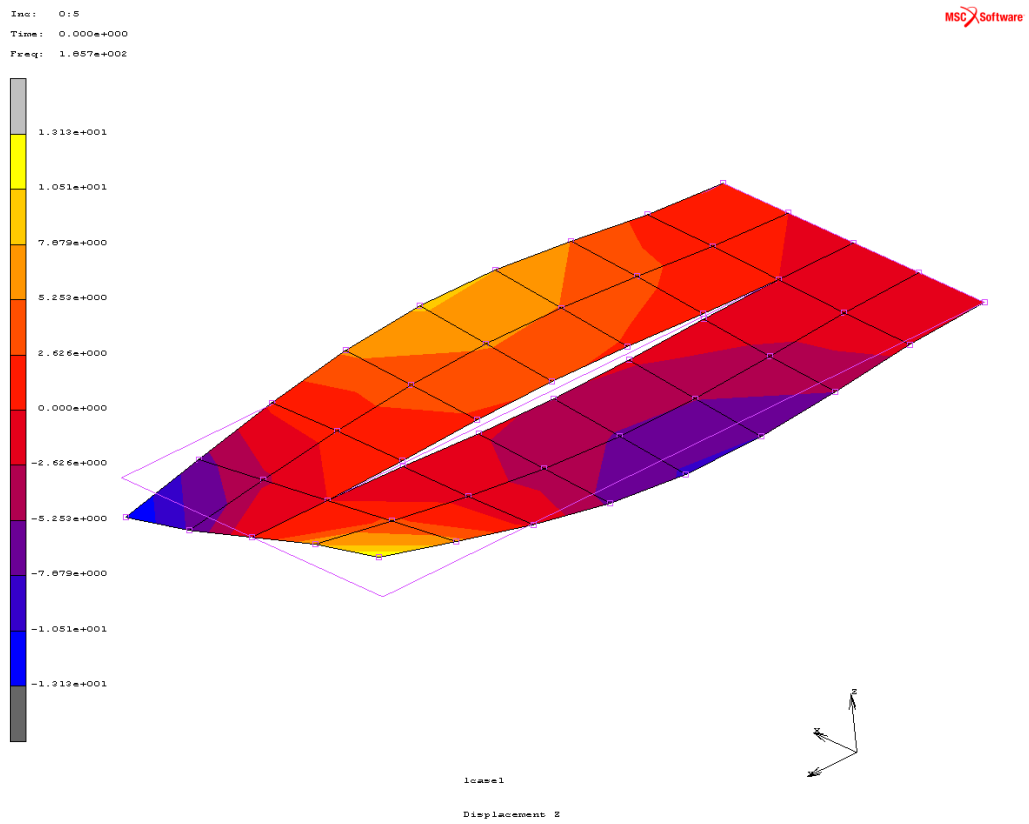
Fig. 6.4: The fifth lowest eigenfrequency of the damaged plate.
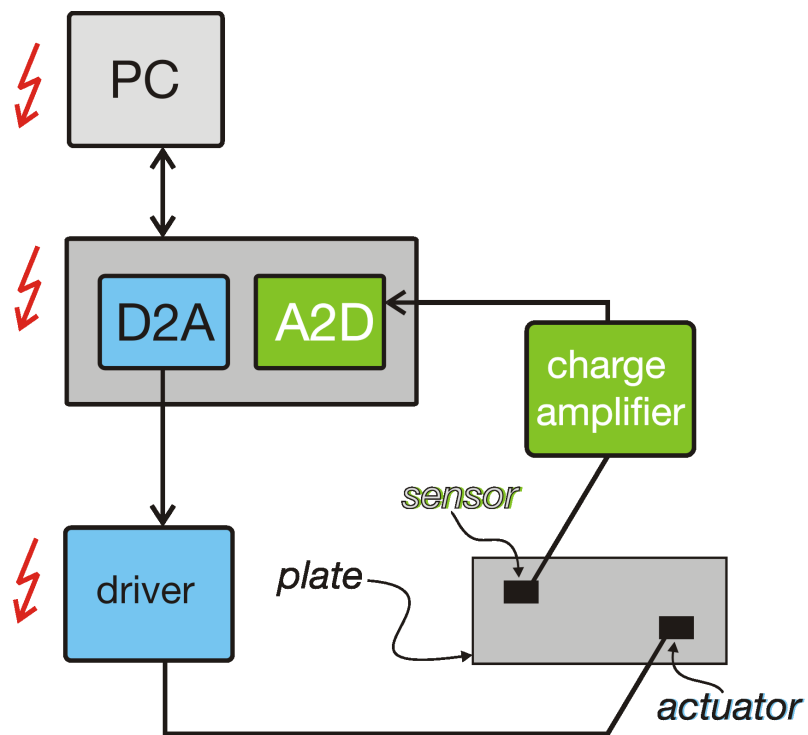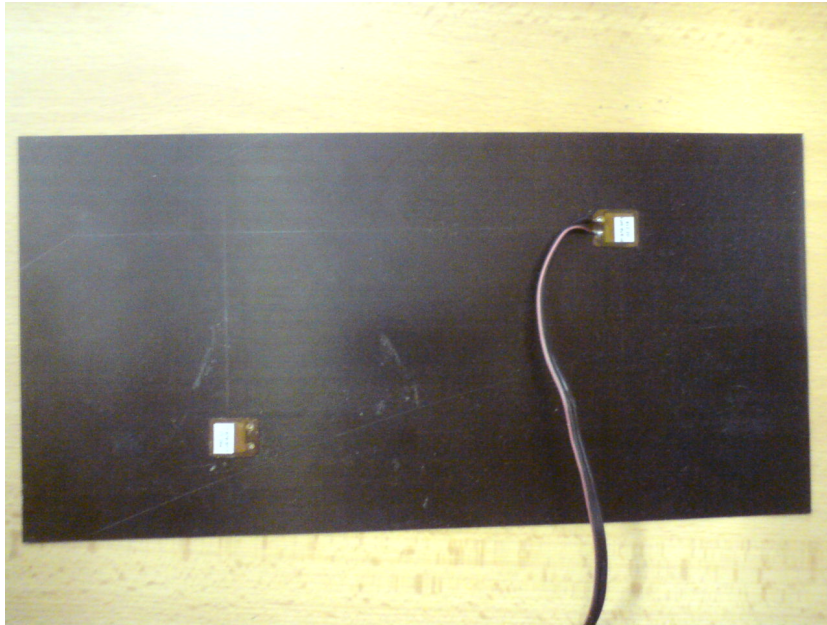
Fig. 6.5: Experimental arrangement.

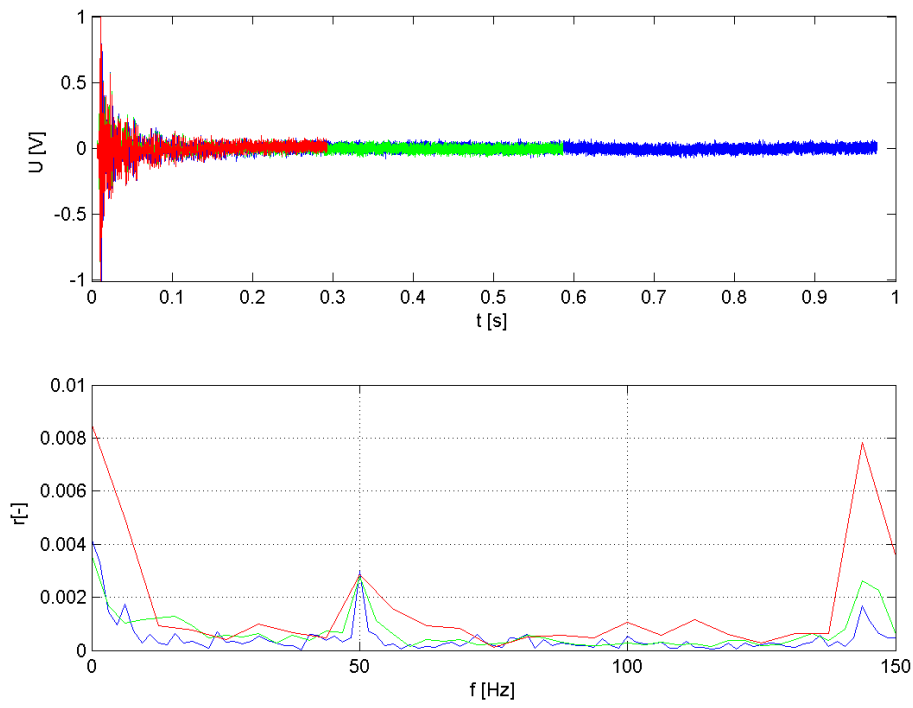Fig. 6.6: Location of piezoelectric patches on the composite plate.

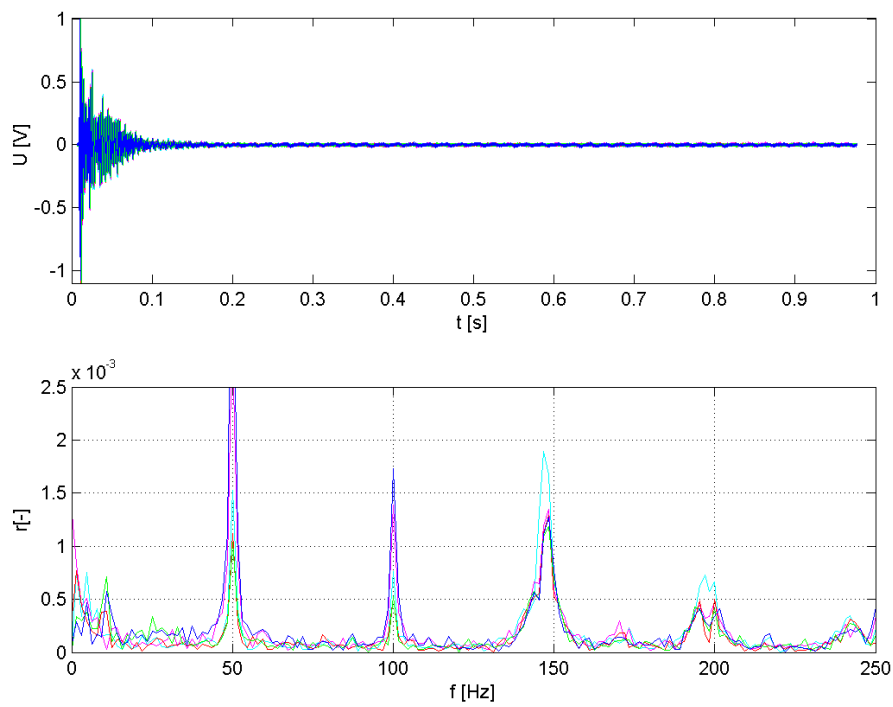Fig. 6.7: Same excitation signal with different length of monitored signal and corresponding frequency spectra.

Fig. 6.8: Frequency spectra from experiments with integrated driver.

6.1.4 Chirp signal using actuator

As previous excitation was not sufficient, different approach was chosen - excitation with chirp signal was performed. A chirp (or also sweep signal) is a signal in which the frequency increases or decreases with time. In this case an increasing frequency signal was used. The chirp signal is commonly used in sonar as well as in other applications, such as in spread spectrum communications or in optics, where ultrashort laser pulses also exhibit chirp. Two types of chirp signal are commonly used, linear chirp and exponential chirp. A linear chirp signal was used in presented case.

All three composite plates with different range of damage were excited with chirp signal from 0 Hz to 5000 Hz lasting for 10 s with sampling frequency of 51.2 kHz (for input signal as well as for output signal). This resulted in different responses r (eq. 5.1) as can be seen on fig. 6.12.

During the experiments another problem was found. As the patches were connected to the exciting and measuring equipment with cables, these influenced the results. The eigenfrequency changed according to the position of the free cables. Several experiments were performed to reveal the exact cause. Additional cable holder, that allowed to keep the cables and examined plate in constant position was then developed and used in the following experiments.

As the plate had no openings, an approach of realization of loose hanged body had to be contrived. Three different types were proposed and examined.

- A clincher that held the plate,

- tape stuck to the plate

- rubber tape, that created a loop, in which the plate was placed.

More experiments with the same plate and same type of hanging were carried out, to find the influence of approach used. The plate was loosen and then hung again. As can be seen on fig. 6.9 – fig. 6.11, the tape showed best similarity when stuck again compared to the other types of attachment of a loose hanged body when refixed.

After experiments the piezoelectric patches were removed (see fig. 6.13). The glued area was inspected to verify that the piezoelectric patches were glued properly. No problems were found.

Because the sensor was reused, there was a risk, that the attached amplifier will change its position and it will distort the results. The amplifier was therefore fixed into a stable position to the sensor (see fig. 6.21) and the same sensor was used in all experiments. Influence on results by using a different equipment was therefore minimalised.
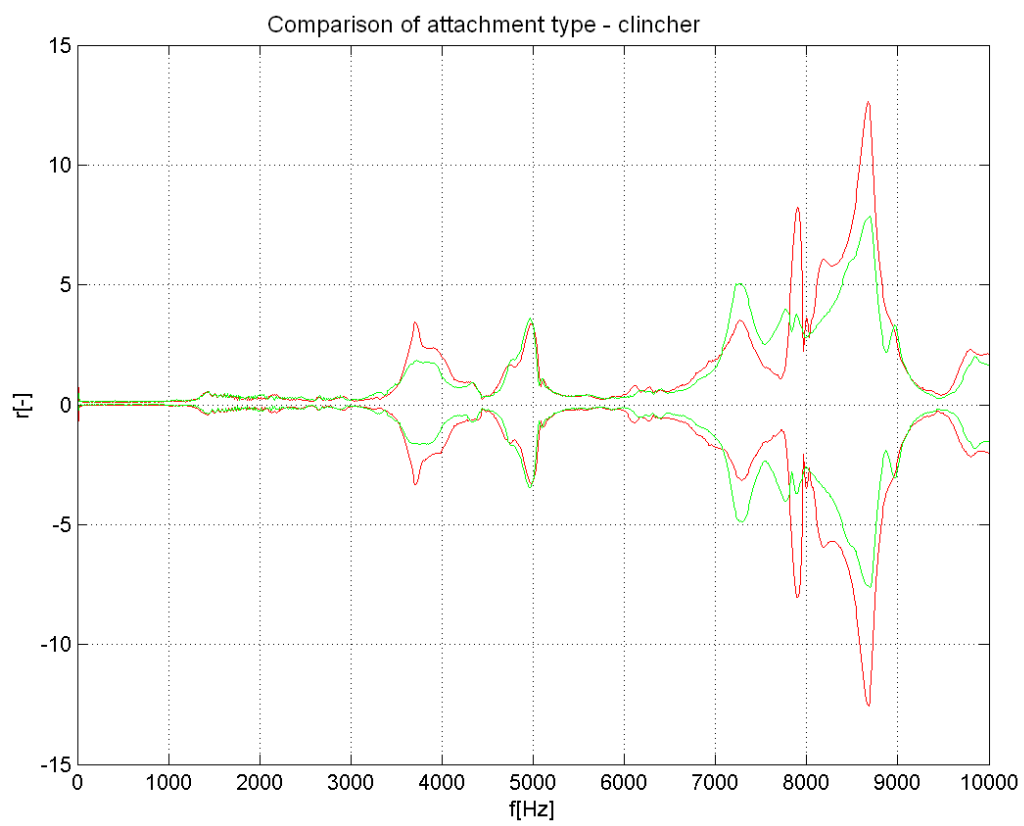
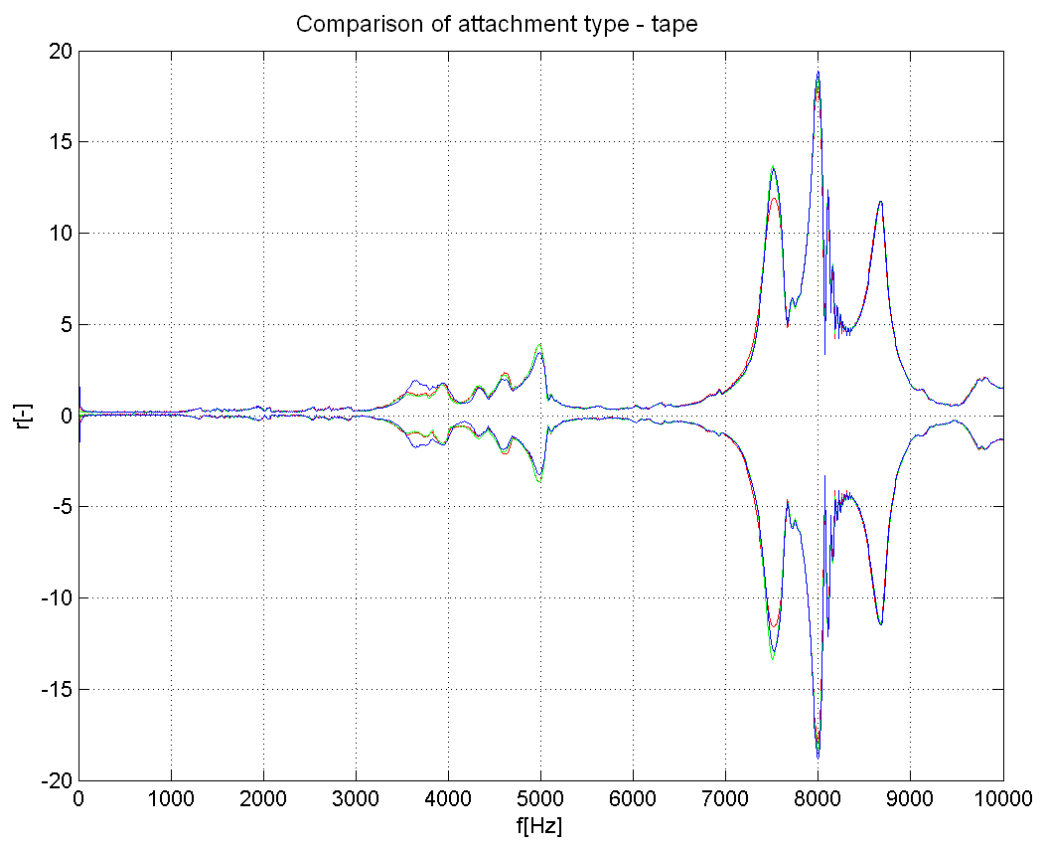Fig. 6.9: Free plate, held by a refixed clincher.
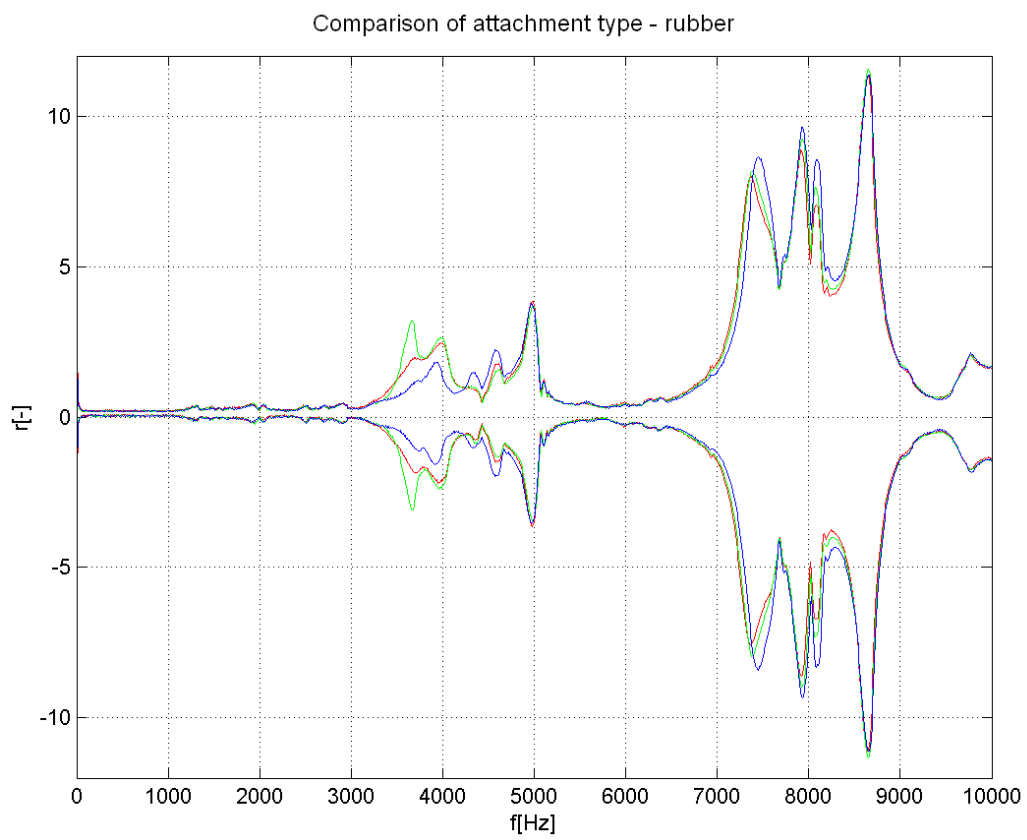
Fig. 6.10: Free plate, held by a restuck tape.

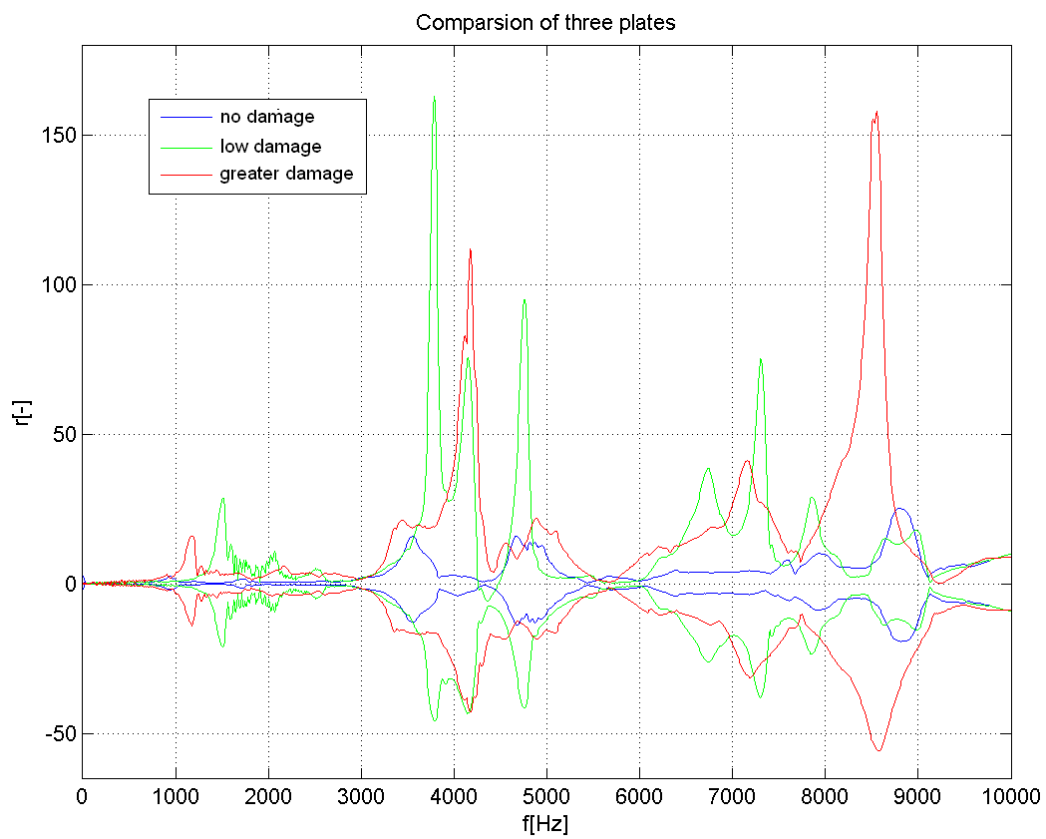Fig. 6.11: Free plate, held by a refixed rubber tape.

Fig. 6.12: Dependency of amplitude on frequency for a plate hanged on a tape.
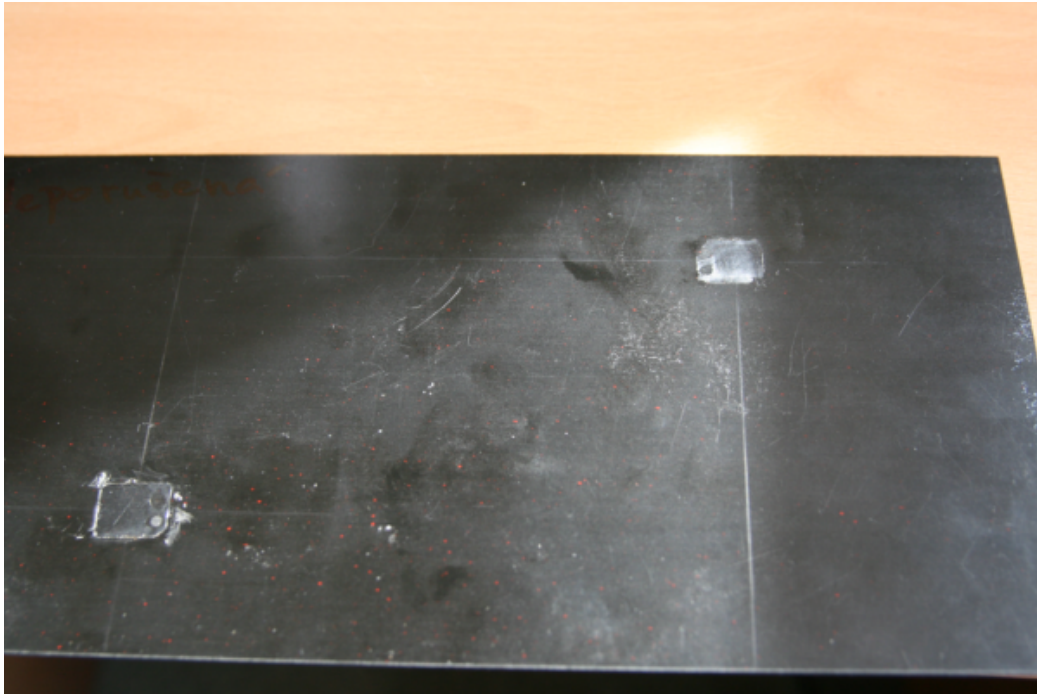
Fig. 6.13: Plate after patches were unglued.

Fig. 6.14: Detail of area of unglued patch.

6.2 Impact experiments

Previous experiments were performed on damaged plates to find out satisfactory SHM method. As excitation with chirp signal showed promising results, further investigation was performed. An undamaged composite specimens were examined. The spectra of eigenfrequencies of undamaged structures were found out using chirp and, in cooperation with Mandys, series of impact were performed on apparatus (see fig. 6.15) created by Mandys. This apparatus allows a free fall of a punch with different impact velocities and it catches the impactor after the impact, so that a double impact will not occur. After each impact the specimen was excited with chirp signal and the response signal was recorded in the same time. Firstly unidirectional composite plate was examined. The change of eigenfrequency started first with a visible crack. Following experiments were focused on a specimen where more different failures may happen - a sandwich beam. Four similar specimens of sandwich beam were examined in the same manner.
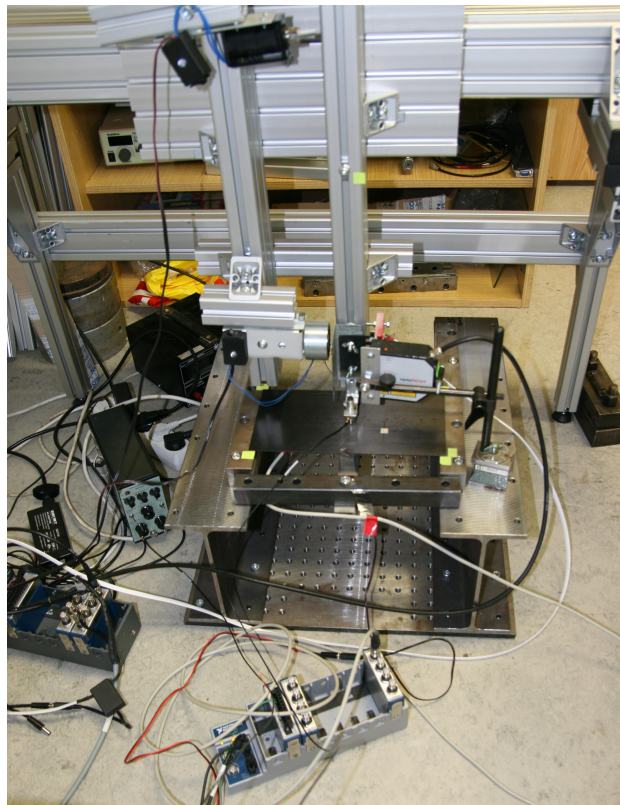

Fig. 6.15: Arrangement of the impact with impactor in the lowest position.

6.2.1 Gradually damaged composite plate

The composite plate was attached to a specially designed T-shaped holder. The holder was used for hanging the composite plate as well as for fixing the cables. On fig. 6.16 can be seen, how the cables leading to piezoelectric patches are fixed to the holder.
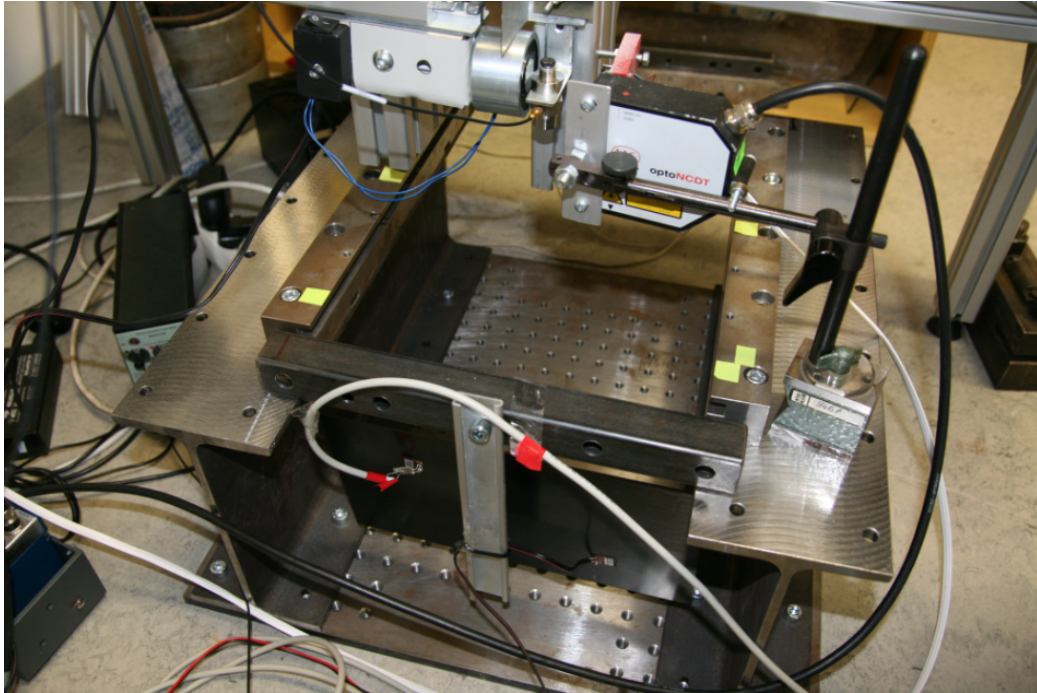

Fig. 6.16: Arrangement of the experiment for excitation.

The plate was examined with chirp signal beginning on 0 Hz and growing up to 5000 Hz with sampling frequency of 51.2 kHz. Three measurements were performed and recorded to evaluate the results. Afterwards the plate was placed in the apparatus constructed by Mandys [26]. The plate was moved together with the holder, needless to disconnect any parts of the apparatus. The composite plate was impacted by a 258 g impactor with velocities 1 m/s, 1.5 m/s, 2 m/s, 2.25 m/s, 2.4 m/s, 2.5 m/s, 2.75 m/s, 3 m/s and 3.25 m/s. Three measurements between each impact were carried out for verification of the results. No significant change was found until the first impact with 3.25 m/s. This was the point, where a visible damage happened.

After the first damage, the experiment continued with series of impact with velocity of 3.25 m/s. After each impact three chirp excitations were made, in the same manner as before the failure. In total, seven impacts with

velocity of 3.25 m/s were performed, until the matrix was damaged along the whole length.

Damaged plate was divided into two parts along the fibers by the series of impacts and stayed connected only with remaining fibers. Therefore, the curve representing spectrum of signal of damaged plate is significantly different to others. This can be seen on fig. 6.18, where the three measurements for each case are approximated by one curve. A detail of fig. 6.18 is shown on fig. 6.19. Three lines for each level of damage represent three independent measurements between each impact. As the crack was growing, the eigenfrequencies of the structure were shifting in the same manner to lower frequencies (see tab. 6.3). For better graphical representation see fig. 6.17.

Tab. 6.3: Length of crack and selected eigenfrequency.

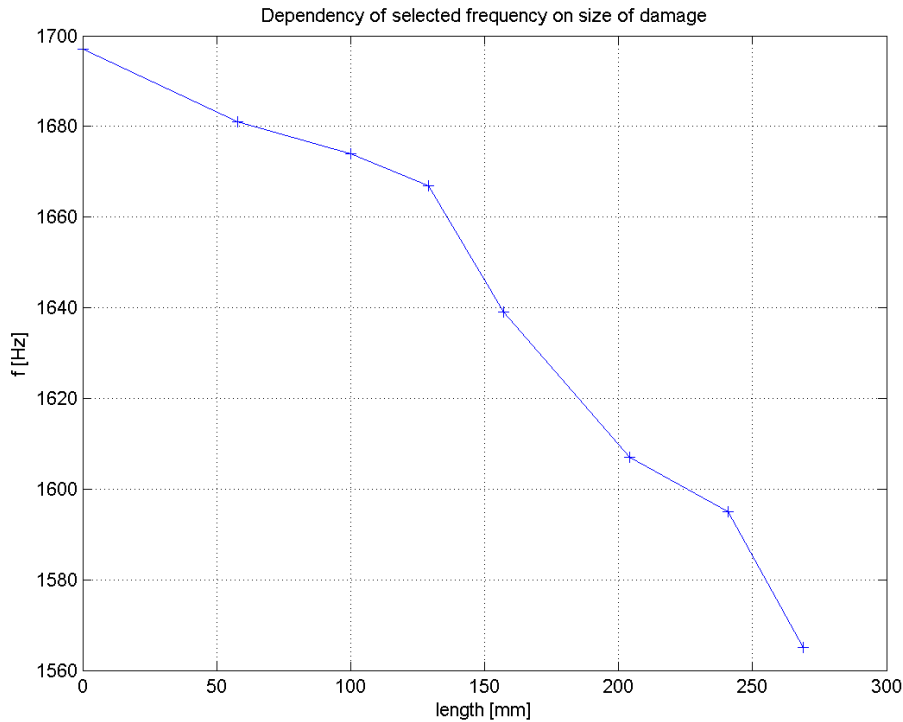| Length of crack [mm]	0	58	100	129	157	204	241	269
Eigenfrequency [Hz]	1697	1681	1674	1667	1639	1607	1595	1565

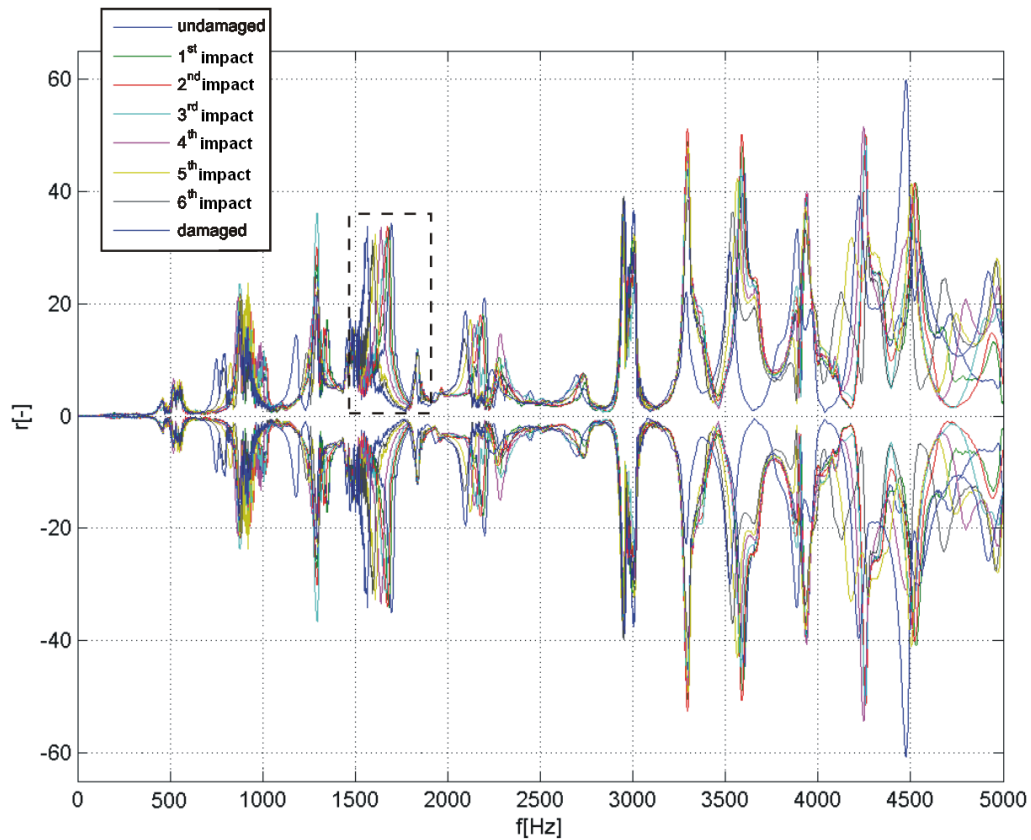Fig. 6.17: Decreasing selected frequency with growing damage.

Fig. 6.18: Spectrum of signal gained from chirp excitation.

On the picture of the damaged plate (fig. 6.20) it may be seen, how the crack was growing in linear manner in time. Numbers 1-6 describe where was the tip of the crack after each impact.

Identification of the crack using above mentioned method was possible first when the crack was visible to a human eye. Earlier identification of damage was expected, such as matrix cracking inside the plate. This did not happen, probably because the limit velocity before the unidirectional plate cracks in the whole thickness was exceeded. Nevertheless, identification with described method may be still an advantage in industry, because a failure may be identified earlier than by a regular visual inspection.

6.2.2 Gradually damaged sandwich beam

More complicated specimen was tested. A beam cut out of sandwich plate was examined. A sandwich is a special type of composite material that is made of two thin but stiff parallel outer skins and a thick but lightweight core.
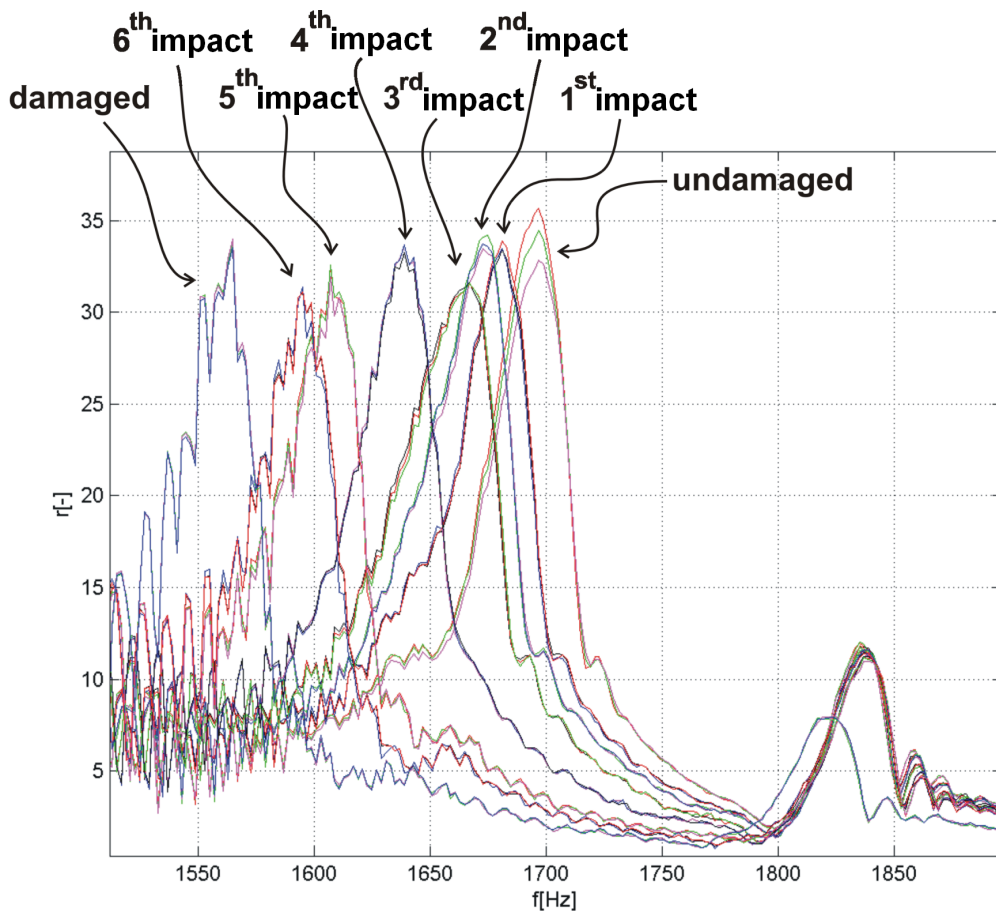
Fig. 6.19: Detail of shifting eigenfrequencies.

The core material is normally low strength material, but its higher thickness provides the sandwich composite with high bending stiffness with overall low density. In this case glass-epoxy laminate outer layers were attached to a PU foam core. Six specimens were examined, out of which four were examined in comparable manner by series of seven impacts. Impacts were performed with growing impact energy. Heavier impactor of 2.1 kg was used, because higher energy impact was desirable. Otherwise only low level of damage would appear with the apparatus available. The beam was simply supported on both ends and impacted into the centre of the glossy layer.

Exciting with actuator that was used in previous experiments was not very strong and the response was very weak as the beam had strong damping effect. Another piezoelectric patch (P-876.A12) was therefore used for exciting the beam. As the piezoelectric patch may be glued and than easily removed and used again, the same actuator was used in all experiments.
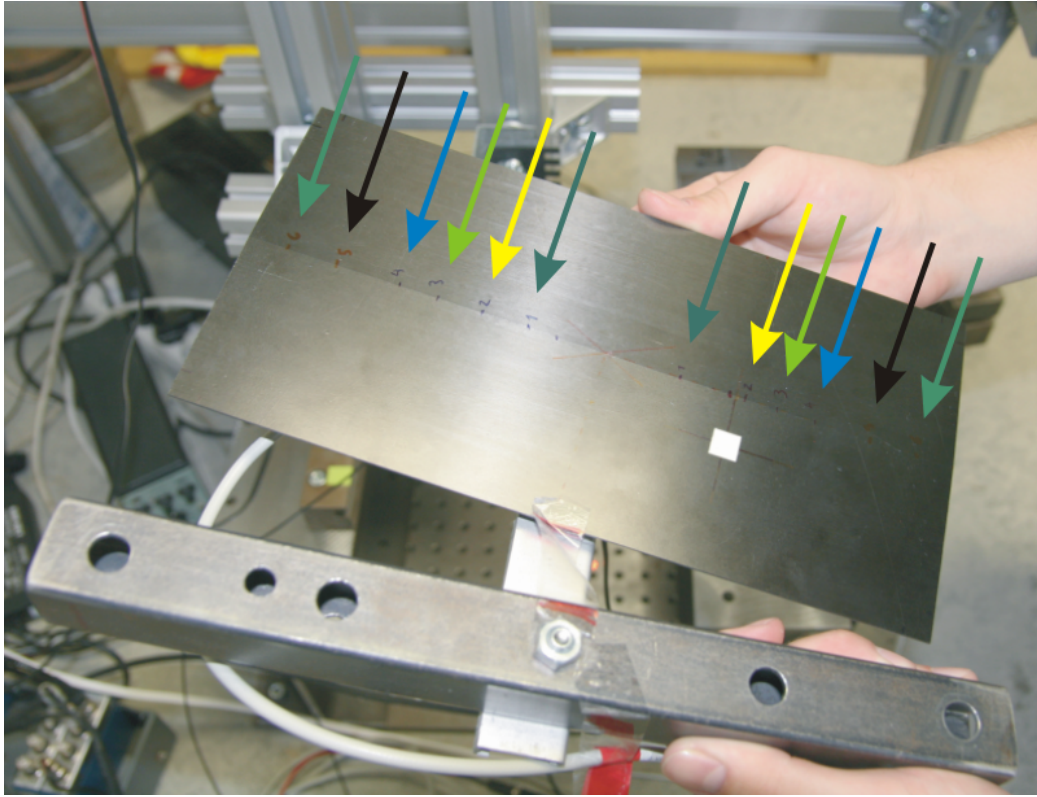
Fig. 6.20: Crack after six impacts.

Because the sensor was also reused, there was a risk, that the attached amplifier will change its position and it will distort the results. The amplifier was therefore fixed into a stable position to the sensor (see fig. 6.21) and the same sensor was used in all experiments. Affection of results that a usage of different equipment would cause was minimalised.

All the beams were weighted before the experiments, no significant difference in weight was found as can be seen in tab. 6.4.

Tab. 6.4: Weight of sandwich beam specimens.

Specimen nr.	1	2	3	4	5	6
Weight [g]	152.25	153.78	151.42	152.84	152.89	150.35

Because only samples 2-5 were subjected to the comparable experiments, the following statements are considering only results from these four samples.

As only specimens no. 2, 3, 4 and 5 were investigated under similar conditions, noted statements are considering only results from these four samples.
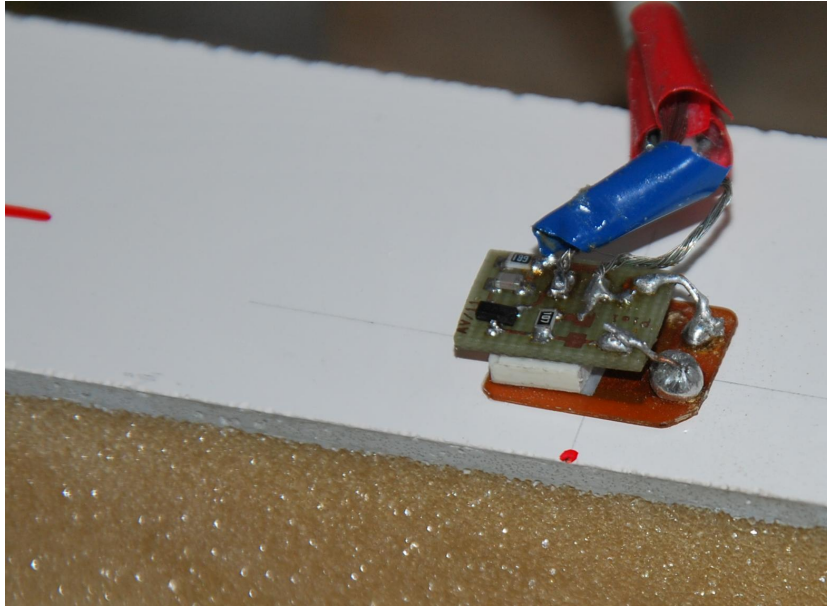
Fig. 6.21: Detail of amplifier fixed to the piezosensor.

Tab. 6.5: Overview of impact energies.

Impact nr.	1	2	3	4	5	6	7
Energy [J]	5	5	10	15	20	25	30
Height [m]	0.237	0.237	0.474	0.711	0.948	1.185	1.419

Main difference between the measurements was in location of actuators and sensors, that was modified to see how the results will be influenced. The sensor and the actuator were glued to the glossy upper (impact) skin of the specimens nr. 2, 3 and 4. Additional actuator was glued on the lower skin of the specimen nr. 4. Therefore, actuation from skin different to where the sensor was placed, was possible. This was examined to discover, if the actuator can reveal a damage on a different skin. On specimen nr. 5 were both piezoelectric patches glued to lower (non-impact) skin.

The progression of the experiment was similar for all the beams. After the first impact (tab. 6.5) only a small dot was visible on the glossy surface of the beam. After the second impact no change was found. After the third impact a crack appeared (see fig. 6.23). Not in the whole width, only partly in the upper layer. After the fourth impact a crack in the whole with of the layer appeared (see fig. 6.24). With the fifth impact a second crack across the beam appears (see fig. 6.25). The upper layer is divided into three parts.

The sixth impact deformed the impact area of the upper layer in a V-shape (see fig. 6.26). A crack in core also appeared, visible on both sides. The seventh impact does not change the damage of the structure rapidly, only a slight damage to the core happened (see fig. 6.27). This resulted only in low rise of the lower layer curvature. The damage was similar for all tested specimens as can be seen on fig. 6.36.

All examined specimens showed similar frequency spectra before the impacts. During the impact experiments the specimens were not damaged absolutely equally, difference in damage was clear from basic visual inspection. Change of frequency spectra proceeded in comparable manner for all examined specimens. When frequency spectra of all specimens after last impact are compared, strong similarity can be seen up to 2000 Hz and than around frequency of 4200 Hz (see fig. 6.35). Range of damage is not so easily predictable from the spectra as in the previous chapter when the composite plate was damaged. A growing damage can be predicted from the shift of eigenfrequencies, but to define the specific type of growing damage based on spectrum of eigenfrequencies a deeper research would be necessary.
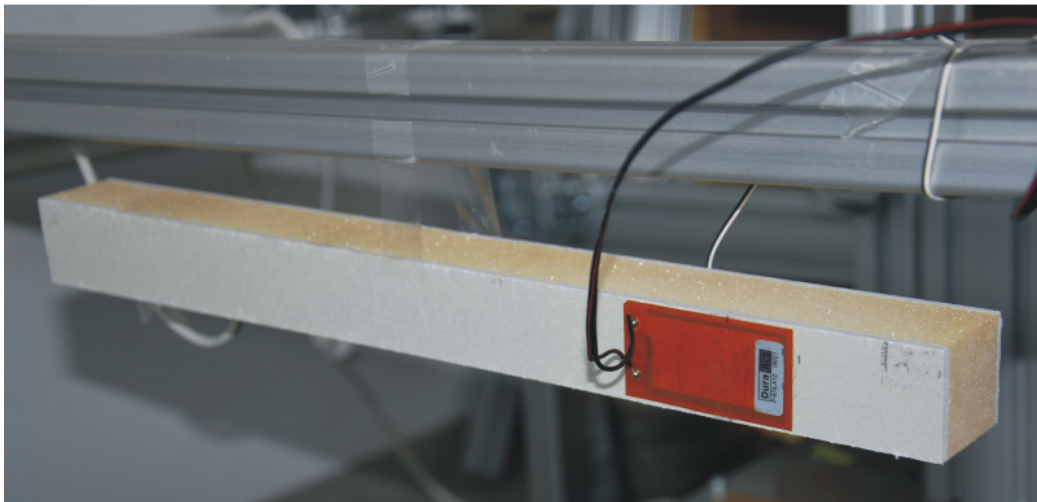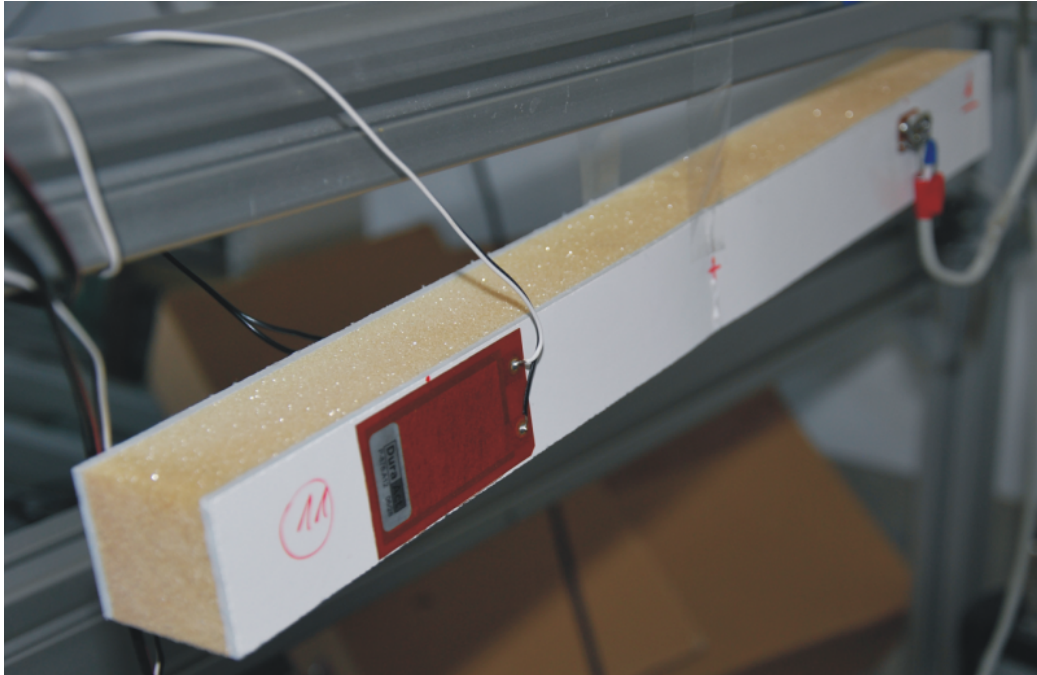
Fig. 6.22: Location of piezoelectric patches on specimen no. 4.
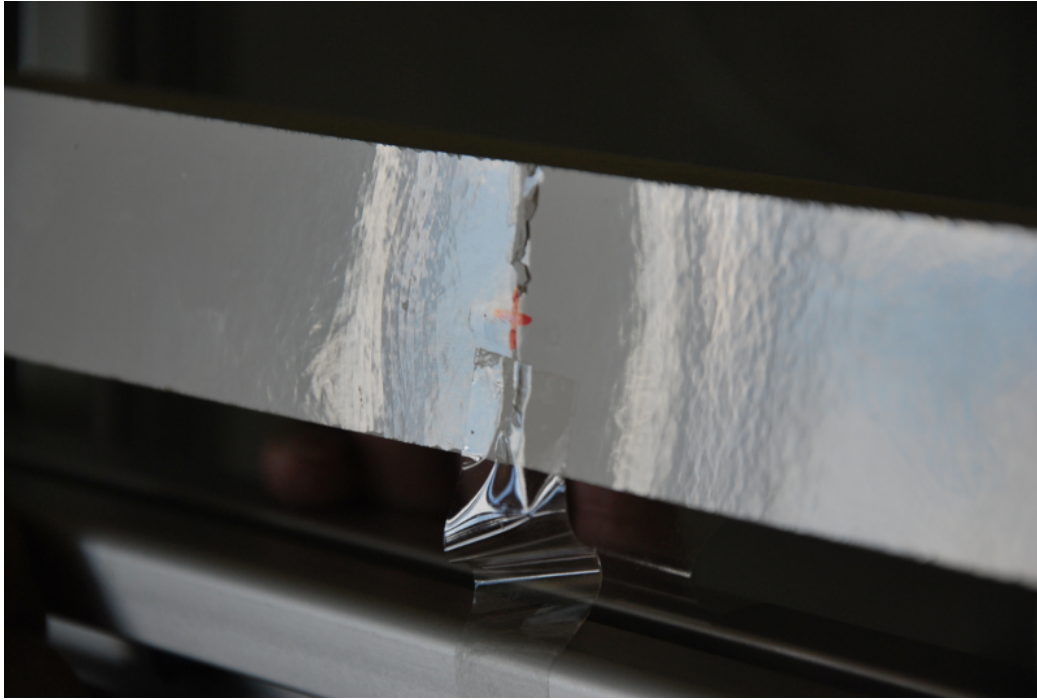
Fig. 6.23: Damage on the upper skin after the third impact on specimen no. 5.

Fig. 6.24: Damage on the upper skin after the fourth impact on specimen no. 5.
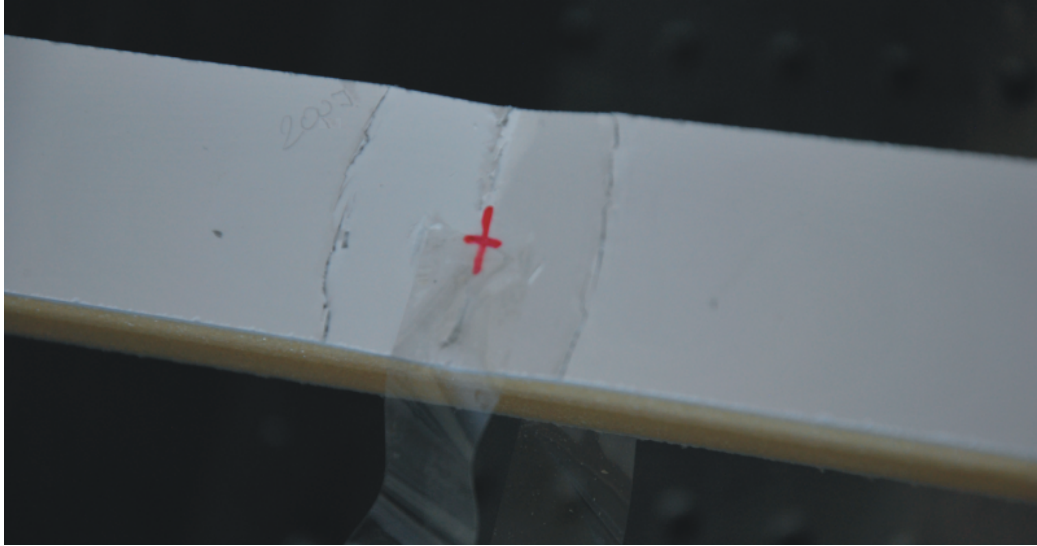
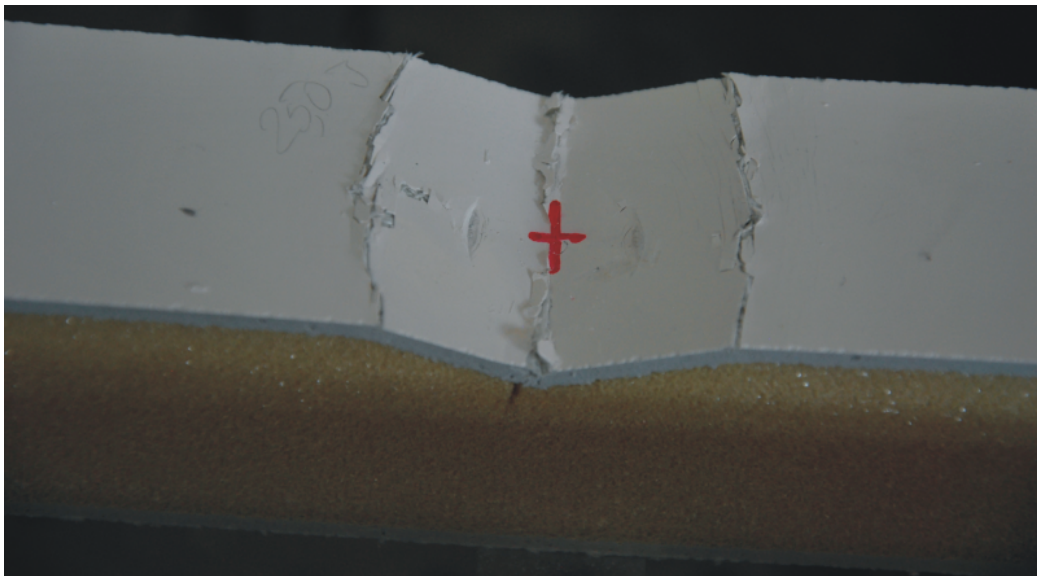Fig. 6.25: Damage on the beam after the fifth impact on specimen no. 5.

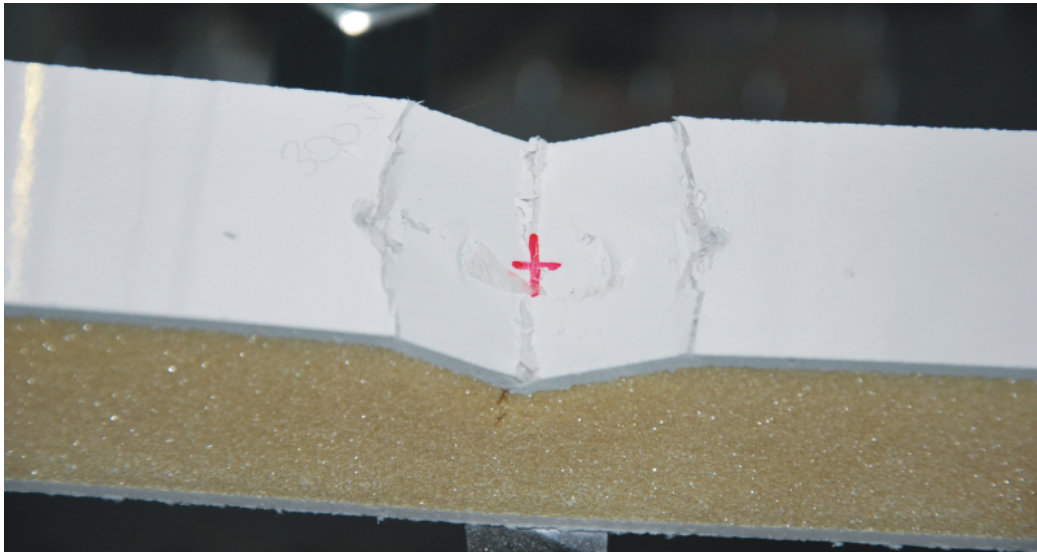Fig. 6.26: Damage on the beam after the sixth impact on specimen no. 5.

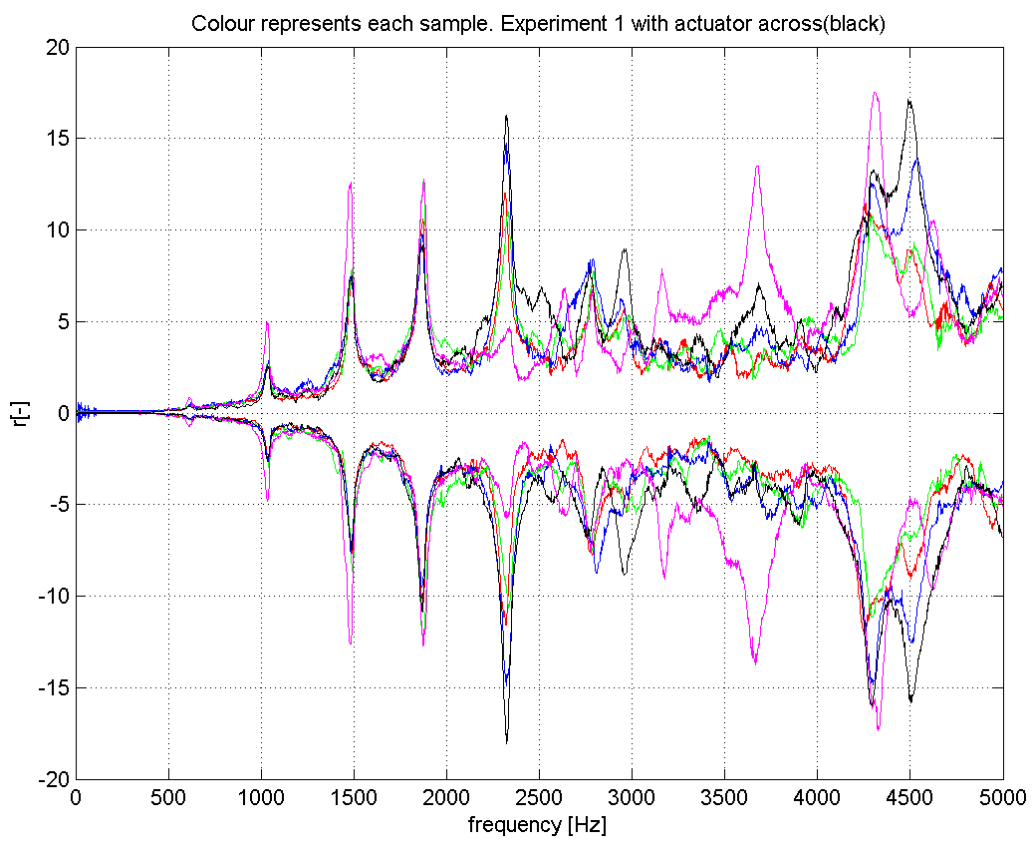Fig. 6.27: Damage on the beam after the seventh impact on specimen no. 5.

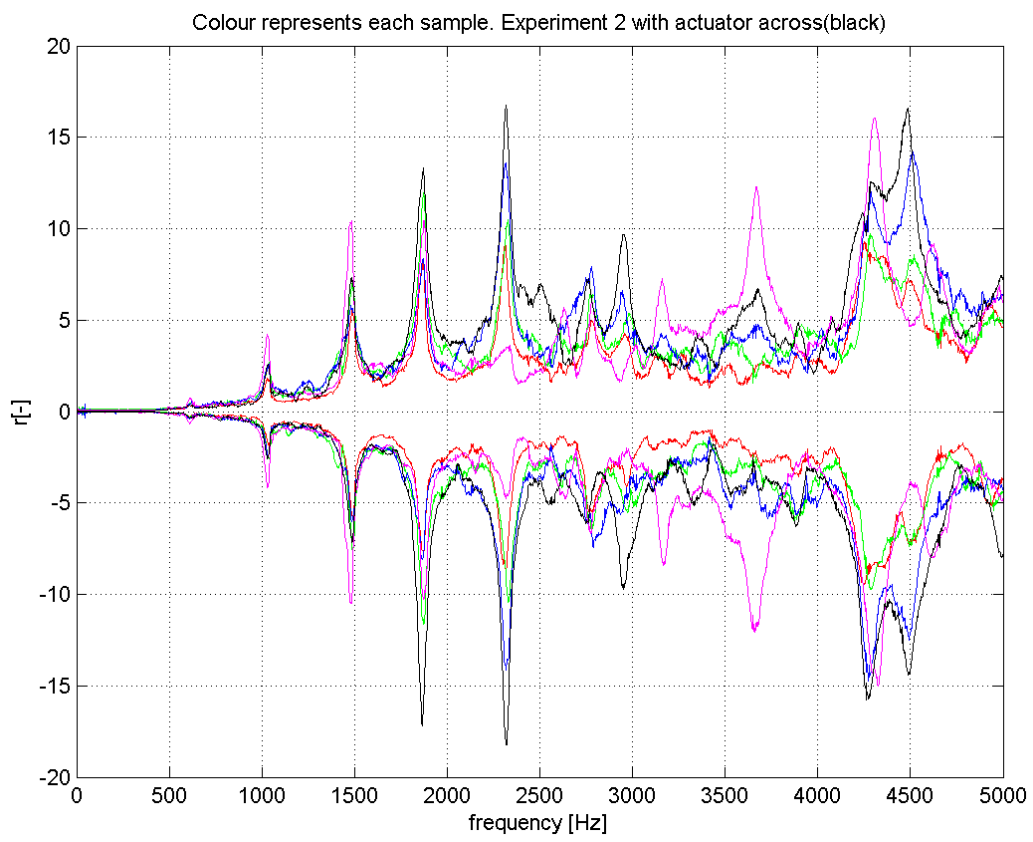Fig. 6.28: Excitation with chirp before the impacts.

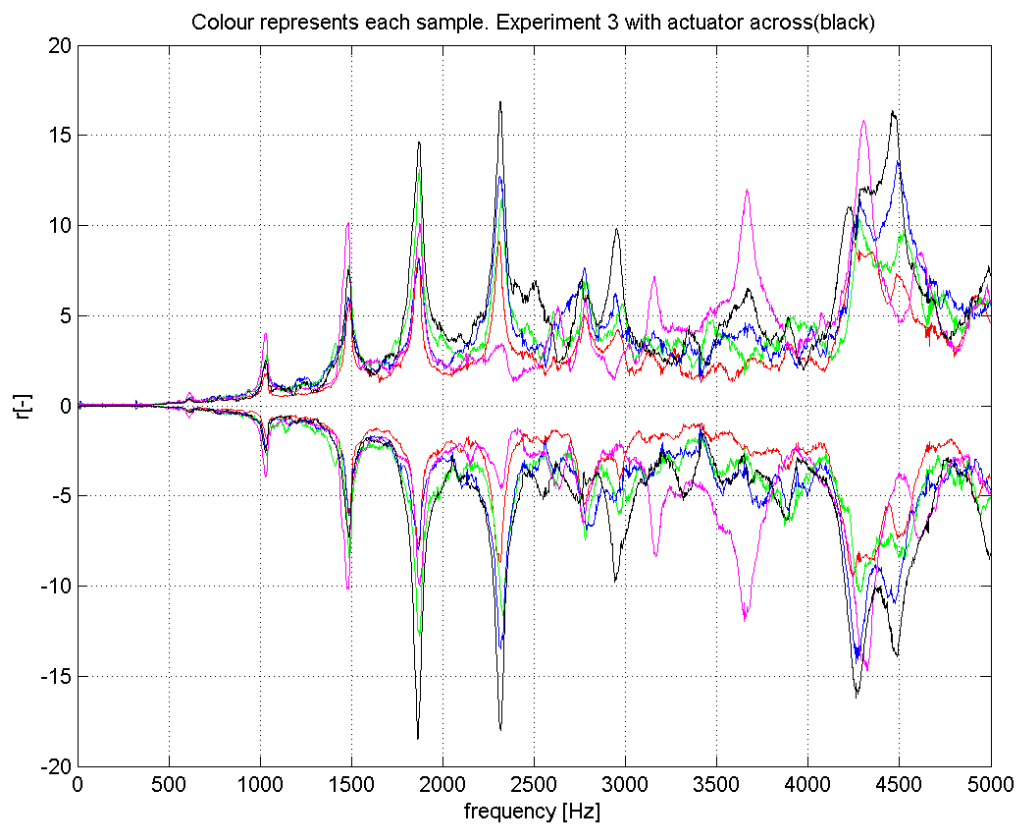Fig. 6.29: Excitation with chirp after first impact.

Fig. 6.30: Excitation with chirp after second impact.
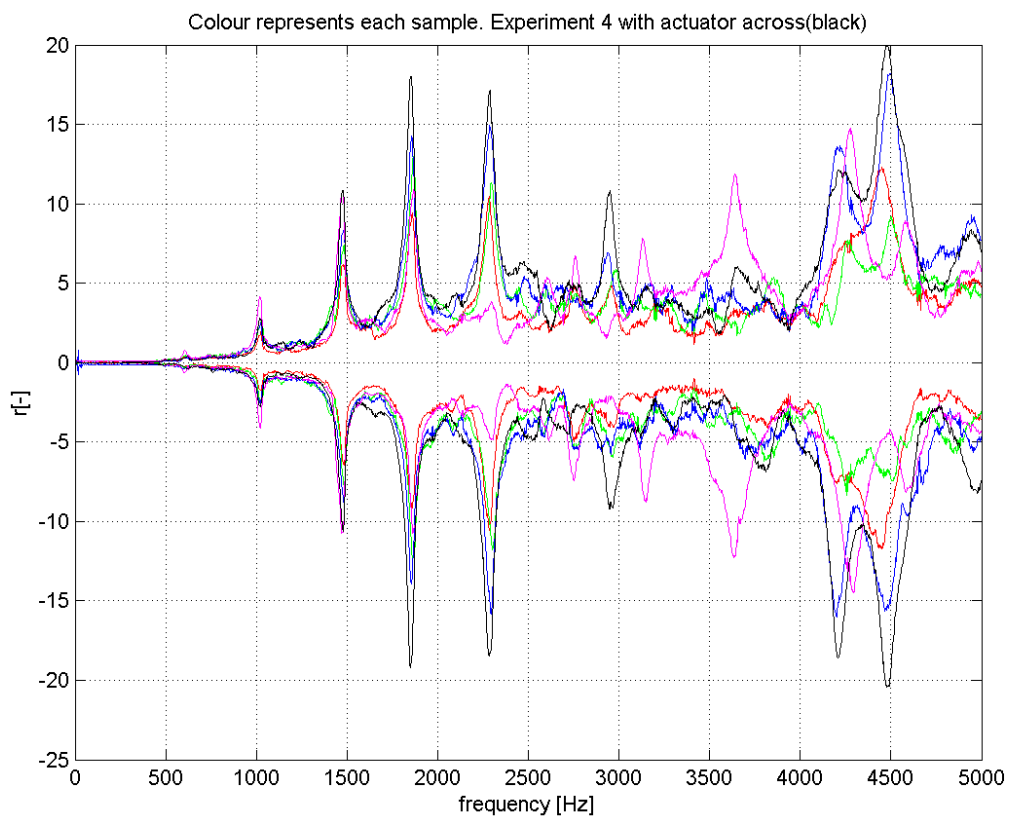
Fig. 6.31: Excitation with chirp after third impact.

Fig. 6.32: Excitation with chirp after fourth impact.

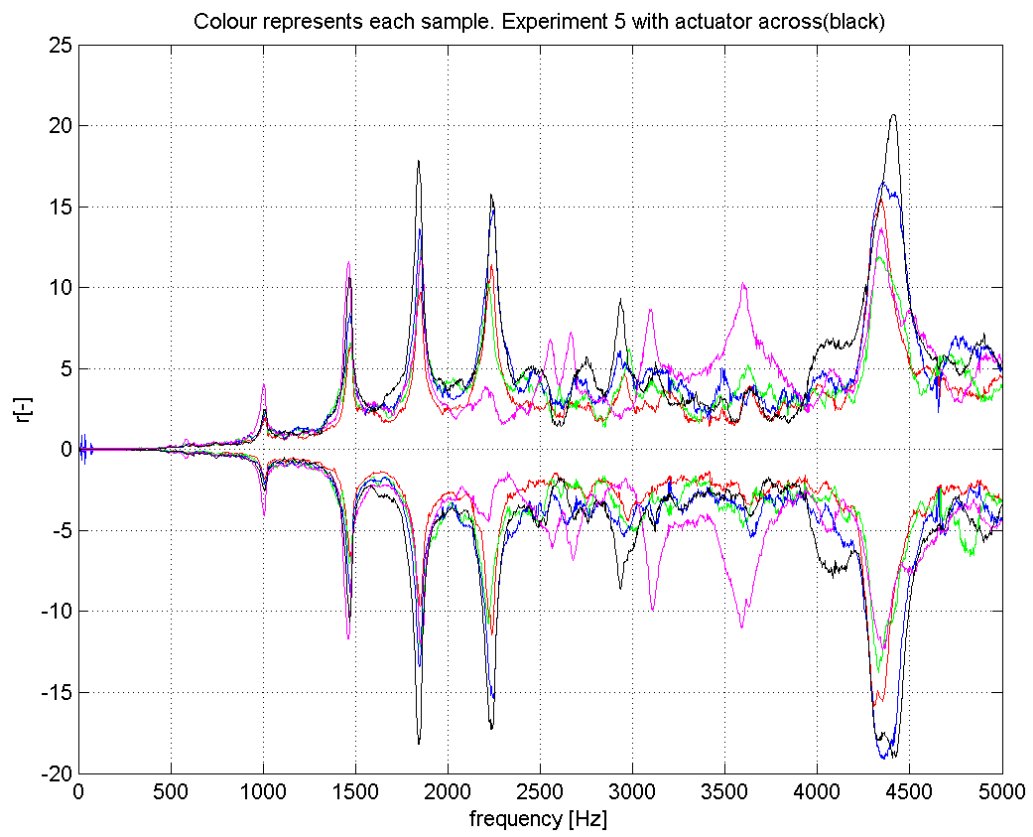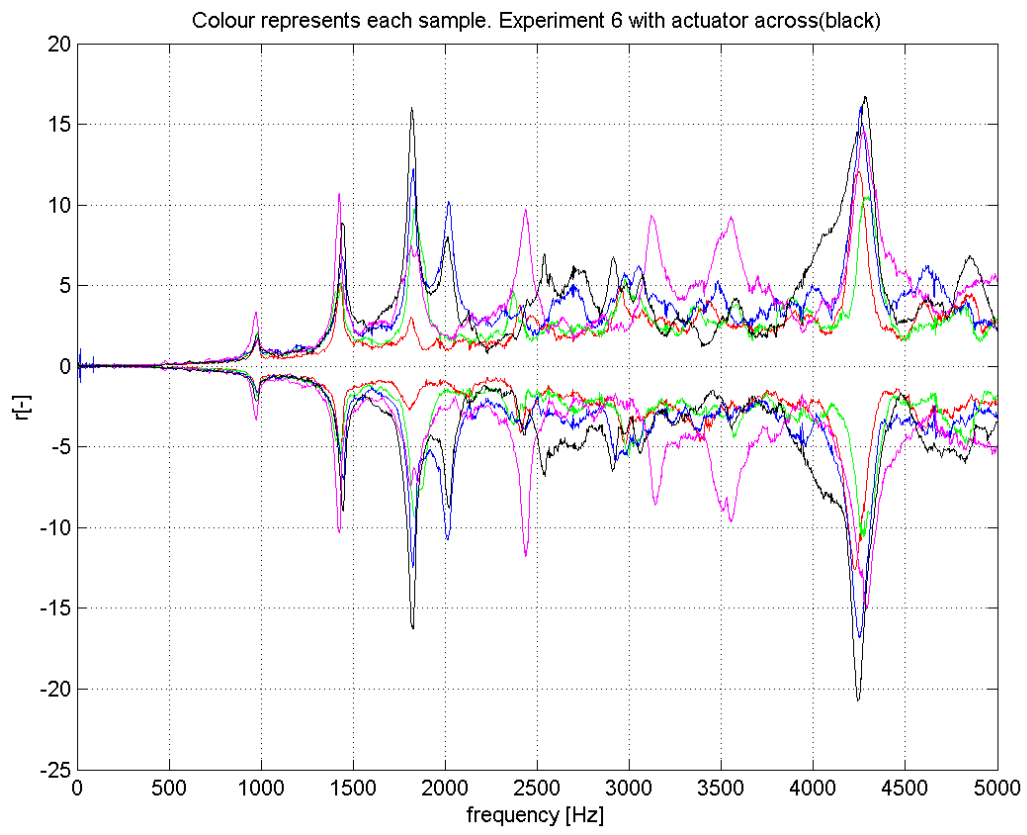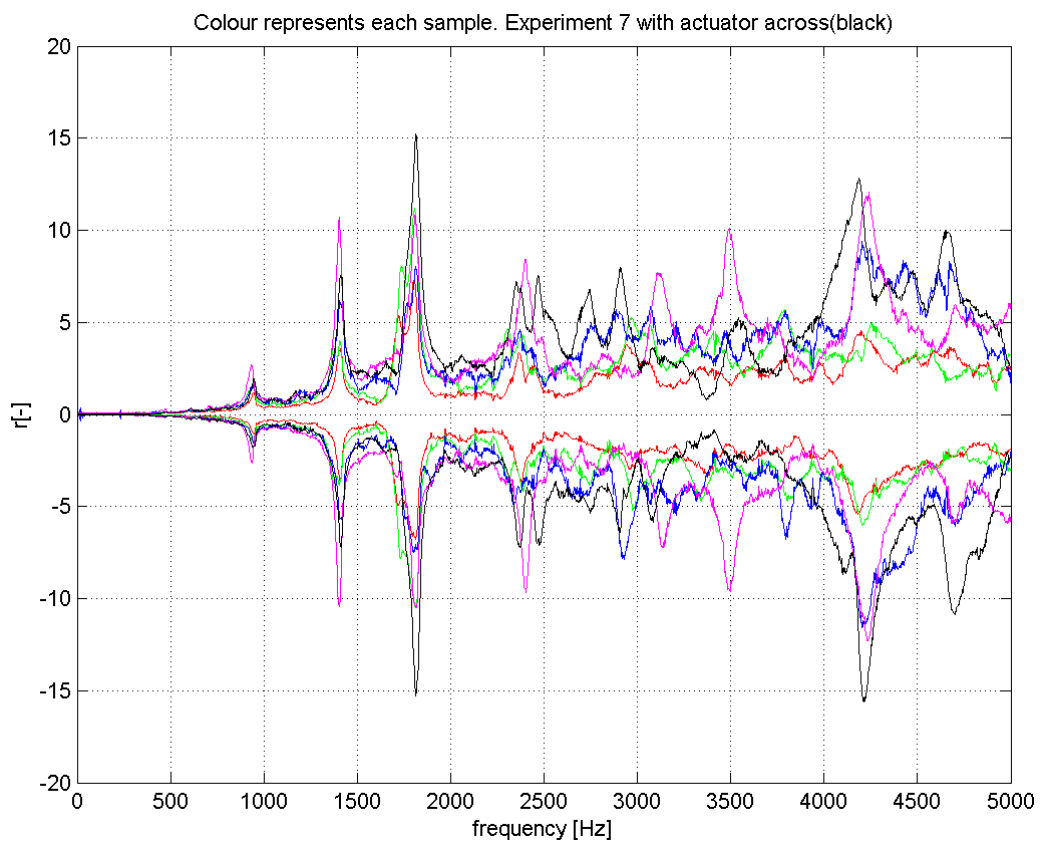Fig. 6.33: Excitation with chirp after fifth impact.

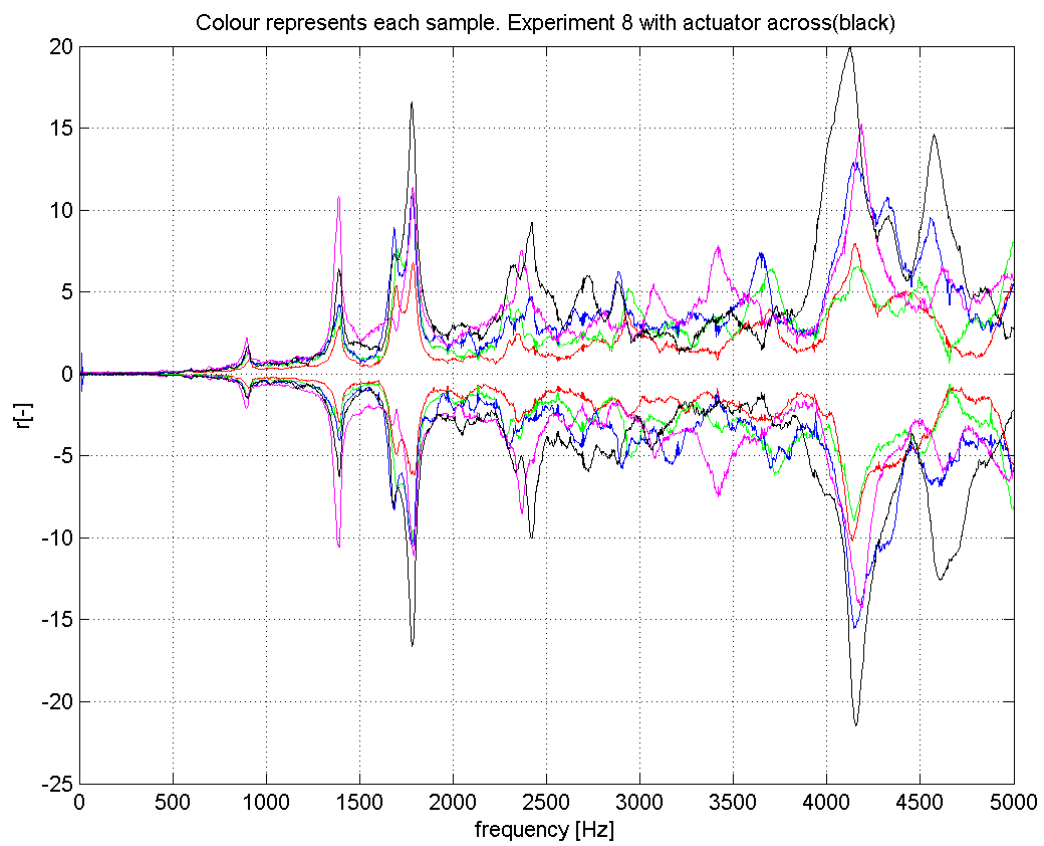Fig. 6.34: Excitation with chirp after sixth impact.

Fig. 6.35: Excitation with chirp after last impact.

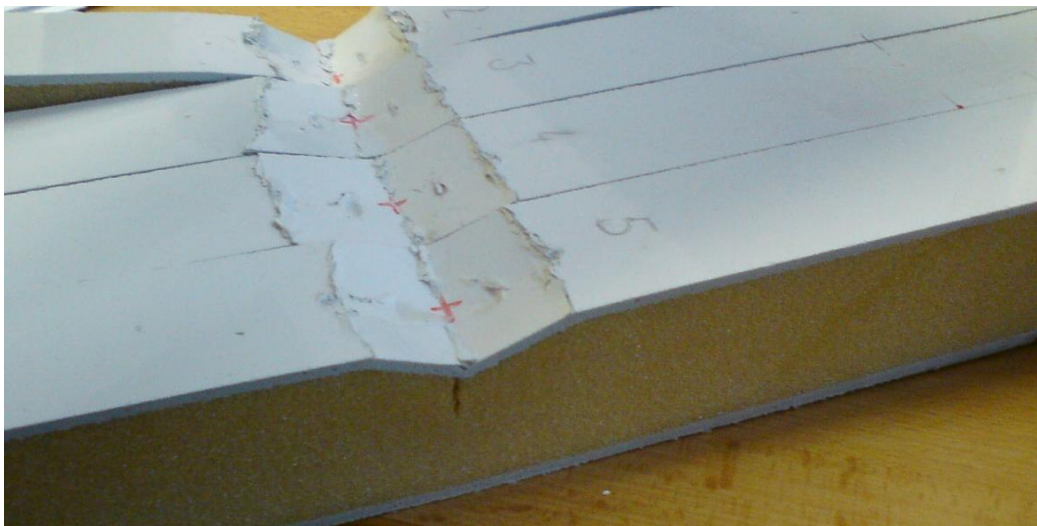Fig. 6.36: Impact area on specimens after experiments.

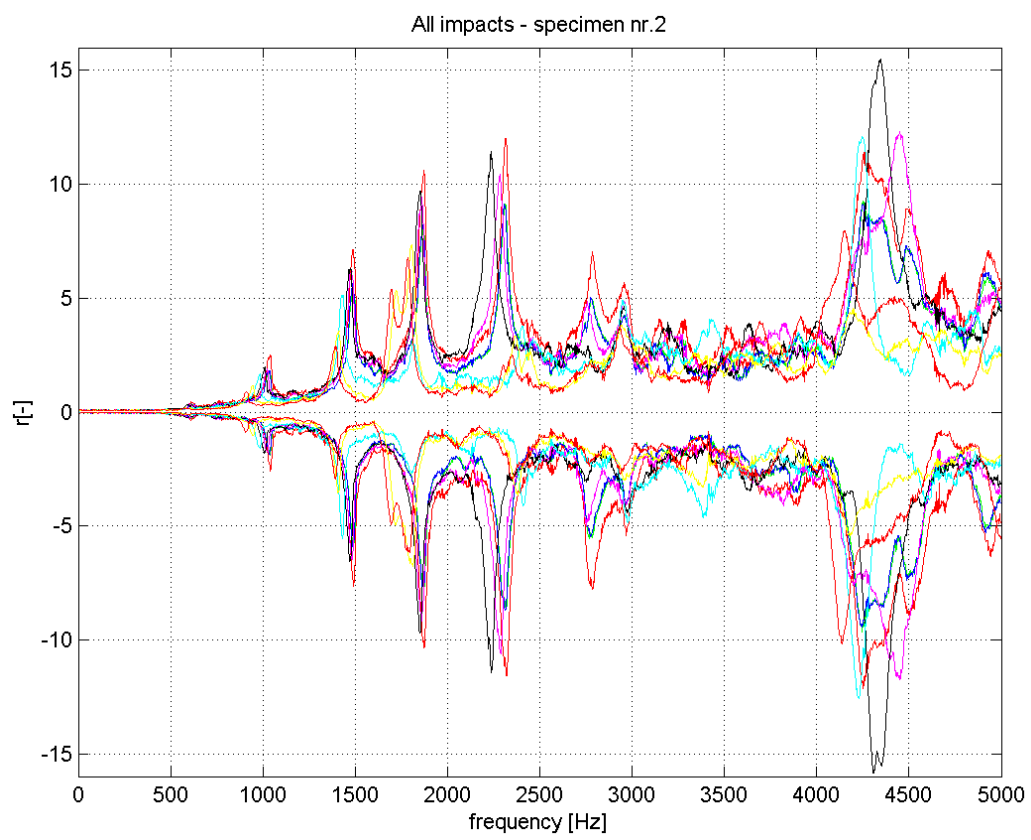Fig. 6.37: Impact area on specimens after experiments.

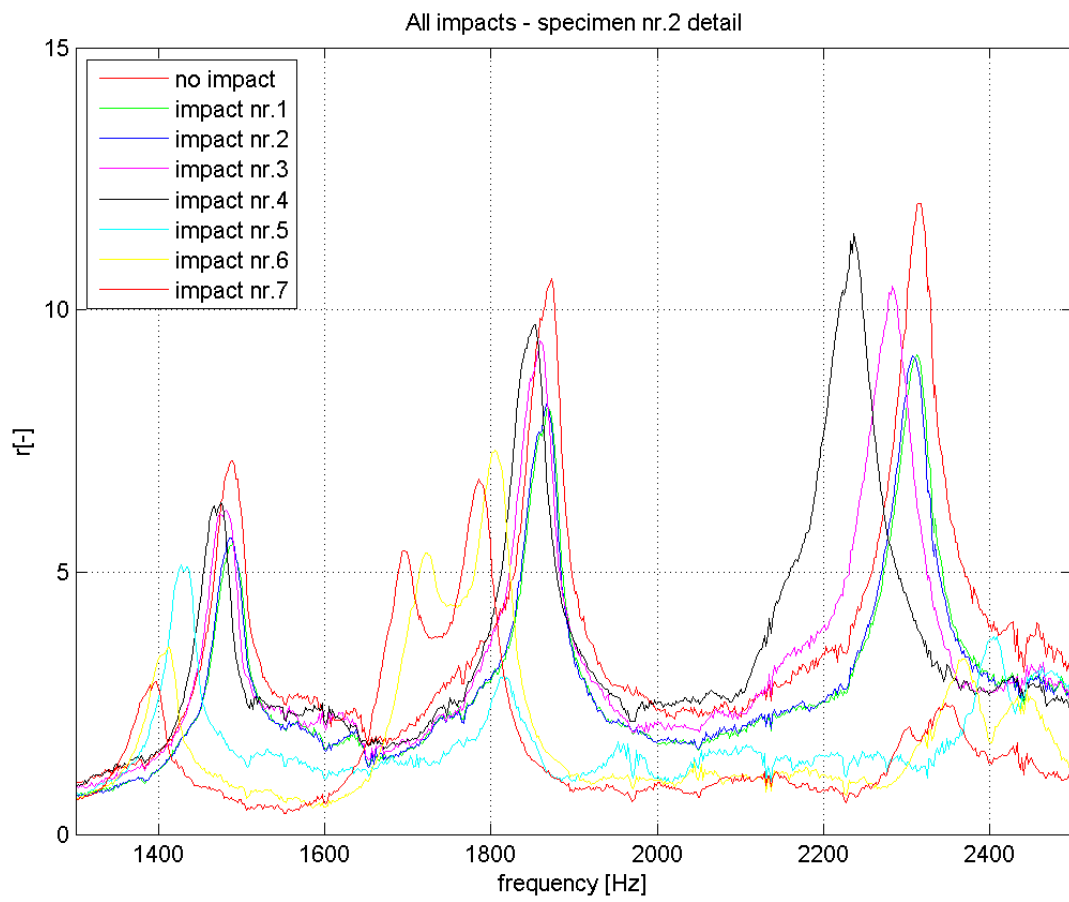Fig. 6.38: Excitation after each impact – specimen nr.2.

Fig. 6.39: Excitation after each impact – detail – specimen nr.2.

Chapter 7

Conclusion

The aim of this thesis is to propose a methodology that is able to identify a damage on a composite structure using change of spectral characteristics. Use of piezoelectric patches was chosen for this purpose.

Upon the study of the state-of-the-art it shows that piezoelectric materials may be well adapted for industrial SHM systems. One of the main advantages of SHM is, that it can reveal damage that may have occurred between scheduled intervals of inspections. Also an inspection is only visual, therefore forms of damage such as delamination of composites can be easily overlooked. With help of SHM system using piezoelectric sensors it is thus possible to detect and identify hidden defects in real time as well.

For deeper understanding of behavior of piezoelectric materials, one dimensional finite element with piezoelectric effect was developed. The mathematical model was implemented in MATLAB environment and compared on adequate mechanical problems to analytical solution. Sensitivity analysis was carried out for the case of modal analysis of the beam with and without piezo patches. Static and transient analysis for bimorph beam was also performed. A finite element model of an aluminium beam and two collocated piezoelectric patches was created and compared to finite element model from commercial software MSC.Marc and to an experiment. The results showed acceptable agreement.

After tests with piezoelectric finite element model, following steps were defined to create a suitable methodology for monitoring of a structure using piezoelectric patches:

- to experimentally compare eigenfrequency spectrum of the original body and a body with an artificial defect and

- to identify location and range of damage through combination of finite element method and optimization methods.

- to design a suitable distribution of piezoelectric patches for assessment of eigenfrequencies of given structure,

For comparing eigenfrequency spectrum of the original body and a body with an artificial defect an isotropic aluminium grid structure was designed and created. Eigenfrequencies were investigated using impact hammer and also by excitation and sensing with piezoelectric patches. Finite element model was also used for comparison of eigenfrequencies. Analysis with impact hammer did not reveal the two lowest eigenfrequencies found using piezoelectric patches and finite element modelling. Experiments with patches, on the other hand, did not reveal the third lowest eigenfrequency found using impact hammer and FEM. Values from the experiments and FEM analysis differed in maximum 10% in the tracked values.

Afterwards, different artificial defects were created on the previously investigated aluminium structure. Six different cases of damage were proposed and investigated. Tests with impact hammer were not performed, only eigenfrequencies from experiments with piezoelectric patches and FEM were compared. The results agreed well with corresponding results from commercial software MSC.Marc, values differed in maximum 1.06% in the tracked values. Some values found using FEM were not discovered during experiments using patches. Several excitation signals were used, to investigate suitability of specific signals. All tested signals yielded similar results. Presented research showed, that piezoelectric patches can be used for the excitation and measurement of response of an isotropic structure to detect damage.

Method of excitation with chirp signal was then used in combination with series of impacts causing gradual damage on intact specimens. Firstly, spectrum of eigenfrequencies was measured on one undamaged unidirectional composite plate and then after each impact event. As the plate was impacted a crack appeared by a certain level of impact energy. A change of the spectrum of eigenfrequencies was consequently found. With a growing crack the eigenfrequency spectrum was changing in the same gradual manner (not fully linear). This means, that in this case for this type of damage it would be possible to roughly identify the range (size) of the damage according to the shift of the spectrum of eigenfrequencies. Even though above mentioned damage does not cover all possible types of damage that can happen, several advantages can be concluded. Besides that a damage can be detected without a need of visual inspection, a range of damage may be monitored, or in other words the speed of growth of the damage. This may be done during operation or on a hardly accessible places, where visual inspection is not possible. Method for finding location of defect was not developed rather, more complicated specimens were examined instead.

Series of impacts were carried out on set of sandwich beams. Stronger piezoelectric actuator was implemented as the sandwich beam damped the vibrations markedly. Four specimens were examined in comparable manner. Impactor impact energy was growing stepwise, damaging each specimen gradually. To fulfill one of the resolutions for this work, the same pair of piezoelectric patches was used on different specimens and patches were distributed on different locations. All used alternatives of different placements were able to reveal the induced damage, moreover eigenfrequency spectra measured among different locations agreed well up to certain frequency. Experiments showed gradual change of tracked spectrum of eigenfrequencies with a growing damage of beam, just as it did in previous experiment with the composite plate. The damage was not that predictable as in the case of the composite plate, because different types of damage occurred at once. Nevertheless, growth of a damage might be deduced from the shift of frequency spectrum when the methodology is used.

Most of the steps defined before the actual work were fulfilled. Identification of location using combination of finite element method and optimization methods was not performed however, three different distributions of patches were tested successfully.

Presented methodology may be used for monitoring change of eigenfrequency spectra. For additional more precise information about a damage (size or localization) deeper research of the specific structure is necessary.

Bibliography

[1] Ackers S., Adams D., Evans R., Zwink B., Crack Detection in an Embedded Spindle using Broadband Modal Excitation. Experimental Mechanic, 48, pp. 509 – 520, 2008.

[2] Allik H., Hughes T. J. R., Finite element method for piezoelectric vibration. International Journal for Numerical Methods in Engineering, 2, pp. 151–157, 1970.

[3] Benjeddou A., Advances in piezoelectric finite element modeling of adaptive structural elements: a survey. Computers and Structures, 76, pp. 347–363, 2000.

[4] Burianová L., Hána P., Panoš S., Furman E., Zhang S., Shrout T.R., Piezoelectric hydrostatic coefficient d_h of PZT ceramics, PZN-PT, and PYN-PT single crystals. Journal of Electroceramics, 13, pp. 443 – 448, 2004.

[5] Cen S., Soh A.-K., Long Y.-Q., Yao Z.-H., A new 4-node quadrilateral FE model with variable electrical degrees of freedom for the analysis of piezoelectric laminated composite plates. Composite Structures, 58, pp. 583–599, 2002.

[6] Diamanti K., Soutis C., Structural health monitoring techniques for aircraft composite structures. Progress in Aerospace Sciences, pp. 342–352, 2010.

[7] Heyliger P., A note on the static behavior of simply supported laminated piezoelectric cylinders. Int. J. Solids Structures, 34, No. 29, pp. 3781–3794, 1997.

[8] Heyliger P., Wu Y.-C., Electroelastic fields in layered piezoelectric spheres. International Journal of Engineering Science, 37, pp. 143–161, 1999.

[9] Ko J.M.,Ni Y.Q., Technology developments in structural health monitoring of large-scale bridges, Engineering Structures, 12, pp. 1715–1725, 2005.

[10] Kovářová J., Dupal J., Vibration Control of Plate Structures. Engineering Mechanics, 14, pp. 23–37, 2007.

[11] Kögl M., Bucalem M. L., Analysis of smart laminates using piezoelectric MITC plate and shell elements. Computers and Structures, 83, pp. 1153–1163, 2005.

[12] Lee S., Goo N., Park H. C., Yoon K. J., Cho C., A nine-node assumed strain shell element for analysis of a coupled electro-mechanical system. Smart Mater. Struct., 12, pp. 355–362, 2003.

[13] Nichols J.M., Structural health monitoring of offshore structures using ambient excitation, Applied Ocean Research, 3, pp. 101–114, 2003.

[14] Mandys T., Kroupa T., Laš V., Zemčík R., Bartošek J., Finite Element Analysis of Failure of Composite Plate in LS-Dyna in Case of Low-velocity Impact. Proceedings of the 3rd ECCOMAS Conference on the Mechanical Response of Composites, pp. 145–152, 2011.

[15] Mandys T., Kroupa T., Laš V., Zemčík R., Bartošek J., Investigation of response of composite plate subjected to low-velocity impact, Experimental Stress Analysis, pp. 209–214, 2011.

[16] Piefort V., Finite Element Modelling of Piezoelectric Active Structures. PhD Thesis, ULB, Bruxelles, 2001.

[17] Piefort V., Preumont A.,Finite element modelling of smart piezoelectric shell structures. 5th National Congress on Theoretical and Applied Mechanics, Louvain-la-Neuve, 2000.

[18] Plundrich T., Zemčík R., Analýza kompozitového nosníku s aktivními prvky, Master thesis, University of West Bohemia, 2008.

[19] Reddy J. N., An evaluation of equivalent single-layer and layerwise theories of composite laminates. Composite Structures, 25, pp. 31–35, 1993.

[20] Sadílek P., Zemčík R., Mathematical model of beam with embedded piezoelectric sensors and actuators, The 1st Young Researchers Conference on Applied Sciences, pp.141–146, 2007.

[21] Sadílek P., Zemčík R., Model of Hybrid piezoelectric beam, The 7th Youth Symposium on Experimental Solid Mechanics, 2008.

[22] Sadílek P., Zemčík R., Frequency response analysis of hybrid piezoelectric cantilever beam, Computational Mechanics, 2008.

[23] Sadílek P., Zemčík R., Structural health monitoring of aluminium structure with piezopatches, Proceedings of the 50th Annual Conference on Experimental Stress Analysis, pp. 407–414, 2012.

[24] Sadílek P., Zemčík R., Active structural health monitoring of composite plates and sandwiches, Computational Mechanics, 2012.

[25] Saravanos D. A., Heyliger P. R., Hopkins D. A., Layerwise mechanics and finite element for the dynamic analysis of piezoelectric composite plates. Int. J. Solids Structures, 34, No. 3, pp. 359–378, 1997.

[26] Mandys T., Kroupa T., Laš V., Determination of value of shear modulus for linear stress-strain relationship in case of impact on composite plate, Proceedings of the 50th Annual Conference on Experimental Stress Analysis, pp. 257-262, 2012.

[27] Nečas M., Valášek M., Innovative concept of increasing dynamic stiffness of compliant structures by mechatronic approach. Bulletin of Applied Mechanics, 4(16), pp. 129-137, 2008.

[28] Varadan V., Vinoy K. J., Gopalakrishnan S., Smart Material Systems and MEMS: Design and Development Methodologies. John Wiley & Sons, 2006.

[29] Ware R., Reams R., Woods A., Selder R., Sensor Reliability in Fielded C-17 Aircraft Strain Gauges. Proceedings of the 5th International Workshop on Structural Health Monitoring, pp. 478-486, 2005.

[30] Tzou H. S., Piezoelectric shells. Distributed sensing and control of continua. Kluwer Academic Publishers, 1993.

[31] Tzou H. S., Wang D. W., Chai W. K., Dynamics and distributed control of conical shells laminated with full and diagonal actuators. Journal of Sound and Vibration, 256(1), pp. 65–79, 2002.

[32] Zhou Y., Chen Y., Ding H., Analytical modelling and free vibration analysis of piezoelectric bimorphs. Journal of Zhejiang University Science, 6A(9), pp. 938–944, 2005.

[33] Zemčík R., Non-stationary progressive failure analysis of fiber-reinforced composites. Doctoral thesis, Univeristy of West Bohemia, Plzeň, 2005.

[34] Zemčík R., Rolfes R., Rose M., Tessmer J., High-performance four-node shell element with piezoelectric coupling for the analysis of smart laminated structures. Int. J. Numer. Meth. Engng., 70, pp. 934–961, 2007.

[35] Zemčík R., Sadílek P., Modal analysis of beam with piezoelectric sensors and actuators. Applied and Computational Mechanics, pp. 401–410, 2007.

[36] Zemčík R., Sadílek P., Identification of material properties of sandwich structure with piezo patches. Applied and Computational Mechanics, 2008.

[37] http://www.piceramic.com

Author's publications

[A1] ZEMČÍK, R., SADÍLEK, P. Modal analysis of beam with piezoelectric sensors and actuators. *Applied and Computational Mechanics,* 2007, vol. 1, nr. 2, p. 401-410. ISSN: 1802-680X.

[A2] SADÍLEK, P., ZEMČÍK, R. Mathematical model of beam with embedded piezoelectric sensors and actuators. In *The 1st Young Researchers Conference on Applied Sciences.* Pilsen: University of West Bohemia, 2007. p. 141-146. ISBN: 978-80-7043-574-8.

[A3] SADÍLEK, P., ZEMČÍK, R. Model of Hybrid piezoelectric beam. In *The 7th Youth Symposium on Experimental Solid Mechanics.* Wroclaw: Wroclaw University of Technology, 2008. p. 1-4. ISBN: 978-83-7493-386-5.

[A4] ZEMČÍK, R., SADÍLEK, P. Identification of material properties of sandwich structure with piezo patches. In *Computational Mechanics 2008.* Pilsen: University of West Bohemia, 2008. p. 1-2. ISBN: 978-80-7043-712-4.

[A5] SADÍLEK, P., ZEMČÍK, R. Frequency response analysis of hybrid piezoelectric cantilever beam. In *Computational Mechanics 2008.* Pilsen: University of West Bohemia, 2008. p. 1-2. ISBN: 978-80-7043-712-4.

[A6] ZEMČÍK, R., SADÍLEK, P. Identification of material properties of sandwich structure with piezo patches. *Applied and Computational Mechanics,* 2008, vol. 2, nr. 1, p. 199-206. ISSN: 1802-680X.

[A7] SADÍLEK, P., ZEMČÍK, R. Frequency response analysis of hybrid piezoelectric cantilever beam. *Engineering Mechanics,* 2010, vol. 17, nr. 2, p. 73-82. ISSN: 1802-1484.

[A8] SADÍLEK, P., ZEMČÍK, R., BARTOŠEK, J. Structural health monitoring of aluminium structure with piezopatches. In *Proceedings of the 50th Annual Conference on Experimental Stress Analysis.* Praha: Czech Technical Univerzity in Prague, 2012. p. 407-414. ISBN: 978-80-01-05060-6.
Awarded by Czech Society for Mechanics as the **third best paper** presented at the 50th Annual Conference of EAN 2012 by young researcher under 35 years of age.

[A9] SADÍLEK, P., ZEMČÍK, R., BARTOŠEK, J. Active structural health monitoring of composite plates and sandwiches. In *28th conference with international participation Computational Mechanics 2012.* Pilsen: University of West Bohemia, 2012. p. 1-2. ISBN: 978-80-261-0157-4.